10-24-2023 2:00 PM

Development of an EMG-informed neuromusculoskeletal modelling framework to measure knee joint contact forces during walking in patients with medial dominant knee osteoarthritis and varus alignment

Dominique Cava, *Western University*

Supervisor: Birmingham, Trevor B., *The University of Western Ontario*
Co-Supervisor: Willing, Ryan, *The University of Western Ontario*
A thesis submitted in partial fulfillment of the requirements for the Doctor of Philosophy degree in Health and Rehabilitation Sciences

Abstract

Knee OA is a complex disease where aberrant gait biomechanics may contribute substantially to progression of structural joint damage and symptoms. Medial opening wedge high tibial osteotomy (MOWHTO) is a limb realignment surgery intended to lessen loads on the medial compartment of the tibiofemoral joint in patients with medial dominant knee OA and varus alignment. As it is difficult to directly measure knee joint contact forces (KJCF) the effect of MOWHTO on joint loading remains unclear. Neuromusculoskeletal (NMSK) modelling can estimate these forces. Therefore, purposes of this thesis were to: 1) develop an electromyography (EMG)-informed NMSK modelling framework to predict tibiofemoral medial and lateral compartment KJCF during walking in patients with medial dominant knee OA and varus alignment, and 2) evaluate the effect of MOWHTO on KJCFs during walking.

Chapters 2 and 3 sought to better understand the effects of adjusting patient-specific model parameters. Chapter 2 evaluated results from patient-specific NMSK models using two control modes. Results indicated the EMG-assisted control mode, compared to the EMG-driven control mode, provided greater consistency between knee flexion/extension torques and KJCFs were better aligned with previous studies. Chapter 3 compared patient-specific EMG-assisted models with a neutral varus angle (0º) and a patient-specific varus angle. No statistically significant differences occurred in the KJCFs between models after adjusting this parameter. Chapter 4 investigated: 1) the effect of medial opening wedge HTO on medial and lateral tibiofemoral compartment KJCFs during walking, using the established patient-specific EMG-assisted modelling framework, 2) changes in the external knee adduction moment (EKAM) and muscle co-contraction indices (CCIs), and 3) associations between the changes in medial compartment KJCF and EKAM and CCIs. There were moderate

improvements in medial KJCFs (standardized response mean, SRM>0.60) and small-to-large reductions in the EKAM (SRM>0.90) and CCIs (SRM>0.20). Correlations between changes in medial KJFCs and EKAM and muscle CCI were low-to-moderate (r<0.5).

Results from this thesis contribute to the development of a patient-specific EMG-assisted modelling framework to predict KJCF during walking in patients with medial dominant knee OA and varus alignment. The EMG-assisted NMSK modeling framework suggests medial opening wedge HTO substantially decreases knee medial compartment load during walking.

Keywords

knee osteoarthritis, computational modelling, medial opening wedge high tibial osteotomy, EMG-assisted NMSK modelling, EMG-driven NMSK modelling, gait

Summary for Lay Audience

Knee osteoarthritis (OA) is a complex disease, for which “bowed legs” and altered activity from muscles can contribute to inappropriate loads on the knee during walking. Conducting a gait analysis to simulate the patient’s walking patterns may provide an estimate of these loads acting on the knee joint with patient-specific computer models. Therefore, purposes of this thesis were to: 1) develop a computer modelling framework to predict knee loads during walking in patients with medial dominant knee OA and bow-legged alignment, and 2) evaluate the effect of an alignment surgery on knee loads during walking.

Chapters 2 and 3 sought to better understand the effects of adjusting computer model parameters on its’ predictions. Chapter 2 evaluated and compared results that were simulated using a model that utilized muscle activity that was obtained as the patient was walking. The second model uses the same muscle activity patterns but also incorporates external forces that act on the joints. Joint loads calculated using the modified muscle activation model more closely resembled joint loads that were reported in other studies. Chapter 3 also evaluated and compared results that were simulated using two separate models. The first model was scaled to have neutral lower limb alignment and the second model was scaled to match the patient’s bow-legged alignment. Results were similar using both models regardless of the adjusted parameter.

Chapter 4 investigated 1) the effect of the alignment surgery on knee loads during walking using patient-specific computer models, 2) changes in measures associated with knee loads, and 3) explored associations with change in knee loads. There were moderate improvements in knee loads. Large reductions also occurred in measures that are related to knee loads. Associations between changes in knee loads and parameters associated with knee loads were

low-to-moderate. Results from this thesis contribute to the development of a patient-specific computer modelling framework to predict knee loads during walking in patients with medial dominant knee OA and bow-legged alignment. The patient-specific computer model suggests the alignment surgery substantially decreases knee loading during walking.

Co-Authorship Statement

This thesis contains material from three manuscripts that are prepared to be submitted for publication following the thesis defense. D. S. Cava is the primary author of all chapters within this thesis with contributions from the following:

Chapter 1, Introduction, was written by D. S. Cava with the input from R. Willing, Professor, Mechanical and Materials Engineering, Western University Professor, Mechanical and Materials Engineering, Western University, and T.B. Birmingham, Professor, School of Physical Therapy, Western University.

Chapters 2-4 were co-authored by D.S. Cava, R. Willing, K.M. Leitch, and T.B. Birmingham. Chapters 2 and 3 are prepared for submission to the Journal of Biomechanics and Chapter 4 is prepared for submission to the American Journal of Sports Medicine.

Chapter 5, discussion, was written by D. S. Cava with the input from R. Willing and T.B. Birmingham.

Dominique Cava was responsible for data extraction and the modelling analysis. She also conducted the statistical analyses, interpreted the results and wrote the original draft of the thesis. Drs. Willing and Birmingham critically reviewed and revised drafts of the thesis.

Acknowledgments

Anything is possible when you have the right team cheering you on. For that, I sincerely thank my supervisors Dr. Willing and Dr. Birmingham, other mentors (past and current), and lab mates that became close friends (in WOBL and BERL). I would also like to specially thank my, mom, dad, and Scotty, as well as, other family members and friends (both furry and human) who have provided me with an immense amount of support throughout my journey. I would not have gotten here without any of you. Also, a special thank you to Dr. Diamond and her PhD student (Tamara Grant) for lending your time and support this past year as I completed my research.

Table of Contents

List of Tables

List of Figures

List of Abbreviations

In order of appearance.

OA	Osteoarthritis
MOWHTO	Medial opening wedge high tibial osteotomy
KJCF	Knee joint contact force
NMSK	Neuromusculoskeletal
EKAM	External knee adduction moment
CCI	Co-contraction index
EMG	Electromyography
MAA	Mechanical axis angle
KL	Kellgren Lawrence
MSK	Musculoskeletal
SO	Static optimization
CMC	Computed muscle control
BMI	Body mass index

SD	Standard deviation
Hz	Hertz
N	Newtons
RF	Rectus femoris
VM	Vastus medialis
VL	Vastus lateralis
MH	Medial hamstrings
LH	Lateral hamstrings
MG	Medial gastrocnemius
LG	Lateral gastrocnemius
TA	Tibialis anterior
MVIC	Maximum voluntary isometric contraction
DOF	Degree of freedom
ICD	Intercondylar distance
MTU	Muscle-tendon unit

RMSE	Root mean square error
BW	Body weight
Nm	Newton meters
PSV	Patient-specific varus
CI	Confidence interval
KOOS	Knee osteoarthritis outcome survey

Chapter 1

1 Introduction: Background and Rationale

1.1 Fundamentals of Osteoarthritis Related to this Thesis

Osteoarthritis (OA) is a leading cause of pain and disability worldwide (Hunter and Bierma-Zeinstra, 2019; Vos et al., 2016). OA is the most common degenerative joint disease, which was projected to exceed an economic burden of 800 billion Canadian dollars by 2030 (Bombardier et al., 2011). OA is often considered a whole joint disease where the knee joint is seen as an organ, meaning it is a collection of tissues that work together to perform a vital function that has the ability to return to normal homeostasis after injury (Chen et al., 2020; Loeser et al., 2012; Thomas and Neogi, 2020). Furthermore, OA is considered a dynamic process that affects several intra-articular and extra-articular structures of the knee and leads to substantial pain and disability. OA has a complex etiology that can include joint injury, malalignment, obesity, aging, and heredity that can further result in chronic pain, joint instability, stiffness, and radiographic joint space narrowing (Chen et al., 2017). As there are currently no disease modifying interventions, research has focused on understanding risk factors that may lead to new treatments.

The knee is the joint that is most commonly affected by OA and accounts for approximately 85% of the burden of OA worldwide (Felson, 2006; Hunter and Bierma-Zeinstra, 2019). The pathogenesis of knee OA involves a complex interplay of

mechanical, inflammatory, and metabolic factors that contribute to joint damage (Hunter and Bierma-Zeinstra, 2019). To obtain a better understanding of the pathogenesis of knee OA, a basic understanding of the joint and knee joint mechanics is imperative. The knee joint is made up of articulations between the distal femur, proximal tibia, and posterior patella (Felson, 2006). The primary motion of the knee joint is flexion/extension, although this joint has the ability to move within 3 planes of motion including flexion/extension, abduction/adduction, and internal/external rotations and anterior/posterior, superior/inferior, and medial/lateral translations (Marques Luís and Varatojo, 2021). These motions are accomplished through two main articulations. One articulation of the knee that will be described in brief, the patellofemoral joint, is a diarthrodial joint between the posterior aspect of the patella and the trochlear surface of the distal anterior femur that is presented in Figure 1.1 (Loudon, 2016). The function of this articulation will not be described in detail within this thesis. The other articulation, the tibiofemoral joint, is a synovial hinge joint between the distal portion of the femoral condyle and the proximal portion of the tibial plateau. Furthermore, the tibiofemoral joint is comprised of two main compartments, medial and lateral, that are separated by the joint center (Felson, 2006). This articulation is the focus of this thesis. Healthy joint alignment results in knee loads that are shared by the medial and lateral compartments during cyclic tasks such as walking or stair climbing (Felson, 2006). These loads are transmitted through the femoral condyles to the contact locations of the tibial plateau and, within a healthy joint during walking, the medial compartment bears approximately 60-70% of the weight compared to the lateral compartment (30-40%) (Kutzner et al., 2010). Musculature surrounding the knee joint includes the quadriceps, hamstrings, and

gastrocnemius muscle groups and additional components of the knee joint also facilitate normal gait and proper joint loading (Winby et al., 2009). Additional components include articular cartilage, synovial fluid, and other surrounding musculature. Articular cartilage, the meniscus, and synovial fluid provides lubrication to reduce friction and contact pressure during movement (Hunter and Bierma-Zeinstra, 2019; Loeser et al., 2012).

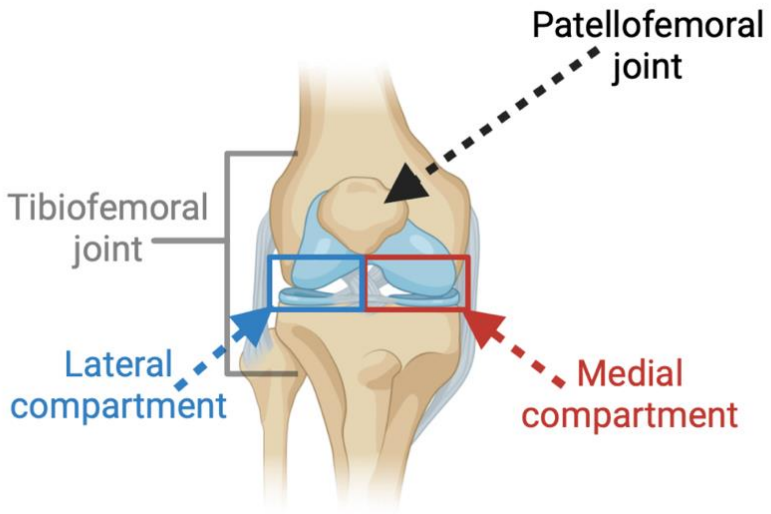

Figure 1.1 The three bones and two articulations that describe the knee. The knee joint includes tibiofemoral and patellofemoral articulations. The tibiofemoral joint includes medial and lateral compartments that are connected at the knee joint center. Created with biorender.com

During the early onset of OA, changes to the joint begin to appear (Loeser et al., 2012). When the joint is injured, an increase in cellular turnover and synovial fluid can occur in attempt to repair damage. Ultimately, OA is an active response to injury (Loeser et al.,

2012) arising from imbalance between repair and destruction of tissues (Hunter and Bierma-Zeinstra, 2019).

Strong risk factors for knee OA include obesity (Messier et al., 2000; Park et al., 2023), prior injury (Richmond et al., 2013), and malalignment (abnormal frontal plane alignment) (Brouwer et al., 2007; Sharma et al., 1998). Perhaps the most prominent risk factor when evaluating structural deterioration of the knee joint is abnormal frontal plane alignment (Felson, 2006; Goldring and Goldring, 2007). Cyclic motions such as walking can further increase the impact of this loading and wear down the respective joint compartment over time. Abnormal frontal plane alignment of the lower limb is typically measured via X-ray using the mechanical axis angle (MAA) (Hunt et al., 2008; A. Specogna et al., 2004; A., Specogna et al., 2007). The MAA is measured as the angle between a line drawn from the center of the hip joint (the femoral head), through the center of the knee joint (between the tibial spines), and a separate line from the center of the knee joint to the center of the ankle joint (top center of the talus) (Figure 1.2) (Marques Luís and Varatojo, 2021). For the purpose of this thesis, a negative MAA indicates frontal plane varus alignment, and a positive MAA indicates frontal plane valgus alignment. The example in Figure 1.2 demonstrates a varus angle of 9.6º (or a MAA of -9.6 º). Furthermore, the weightbearing line (Figure 1.2) is the line from the center of the hip joint to the center of the ankle joint. Cyclic motions such as walking can further increase the impact of this loading and wear down the respective joint compartment over time.

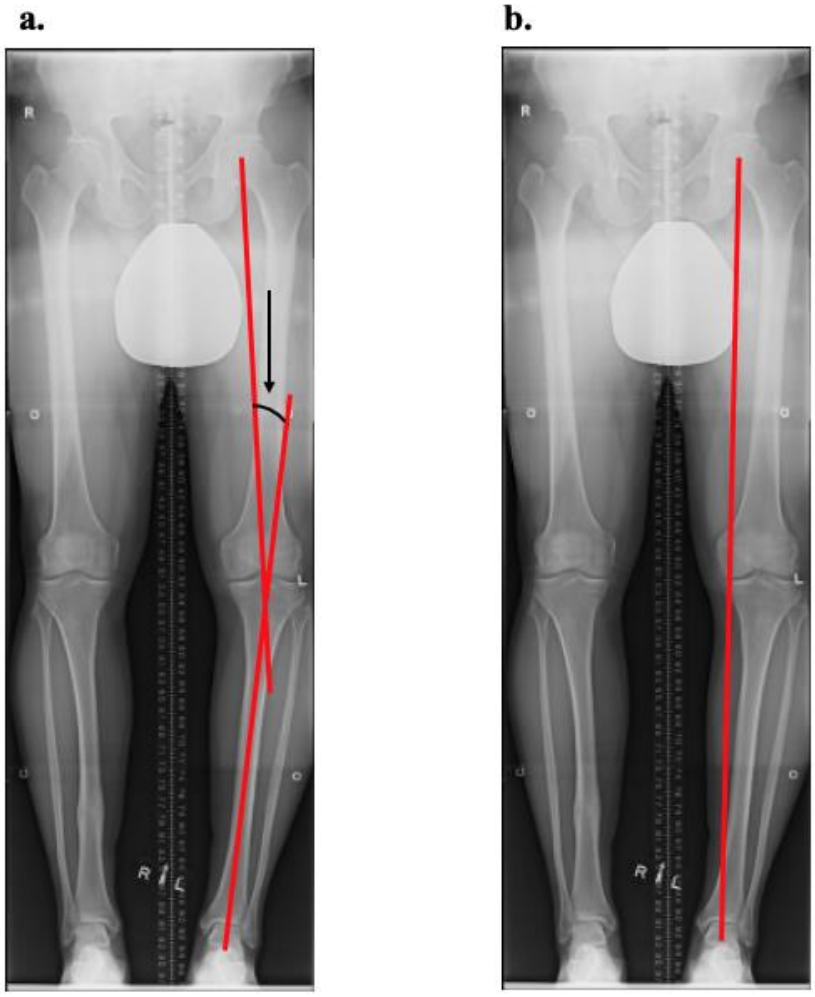

Figure 1.2 a. Antero-posterior hip-to-ankle standing radiograph showing the mechanical axis angle (MAA). The MAA is measured as the angle created by a line drawn from the centre of the femoral head, through the center of the knee joint (between the tibial spines), and a separate line drawn from the centre of the knee joint extending through to the centre of the ankle joint. A negative MAA indicates varus, while a positive MAA indicates valgus, alignment of the lower limb. The angle observed within this radiograph indicates a varus angle of 9.6º. **b.** The weightbearing line is the line from the center of the hip joint to the center of the ankle joint.

Knee OA causes tremendous burden to individuals and societies that is largely due to its effect of limiting mobility. Common activities that are found to increase pain are climbing stairs, getting up after sitting, and walking for long distances (Altman et al., 1986). Clinical assessments often include an evaluation of pain and limitations in function described by the patient (Felson, 2006; Goldring and Goldring, 2007). Patients with knee OA can also experience knee instability or the feeling of their joint "giving-way," which contributes to impaired quality of life (Felson, 2006; Goldring and Goldring, 2007). Clinical assessments often involve obtaining patient-reported outcome measures. For example, the Knee Injury and Osteoarthritis Outcome score (KOOS) is commonly used as it was designed to evaluate both short term and long term patient pain and function related to knee OA (Roos and Lohmander, 2003). Subsections within the KOOS include pain, other symptoms, function in sport and recreation, function in activities of daily living, and knee related quality of life where scores from each section are scored on a 0 to 100 scale. A larger score indicates less knee pain and greater function and quality of life.

Radiographic assessments are also commonly used in diagnosing and staging knee OA. For example, the Kellgren Lawrence (KL) scale was designed to evaluate arthritis by classifying OA progression into five grades (Kellgren and Lawrence, 1957). When classifying the patient's KL grade, changes seen in the joint (compared to a joint without OA) can include joint space narrowing, thickening of subchondral bone (ie. bone surface proximal the cartilage in relation to the femur), and presence of osteophytes (Loeser et al., 2012). More specifically, grade 0 indicates the absence of X-ray changes related to OA, grade 1 indicates doubtful OA with narrowing of the joint space and possible

osteophytic presence, grade 2 indicates minimal OA with definite osteophytes and possible narrowing of the joint space, grade 3 indicates moderate OA with a moderate amount of osteophytes, definite joint space narrowing with some sclerosis (hardening of body tissue), and possible deformity at the end of the bone, and grade 4 indicates severe OA with severe formation of osteophytes, marked joint space narrowing, severe sclerosis, and definite deformity at the end of the bone (Kellgren and Lawrence, 1957). Radiographic assessments indicating the amount of lower limb malalignment (as evaluated using the MAA) may also contribute the radiographic assessment of knee OA (Brouwer et al., 2007; Miyazaki, 2002).

1.2 Biomechanical Interventions for Patients with Knee OA

1.2.1 Biomechanical Interventions

Although there are no (currently approved) interventions proven to restore degraded cartilage, various interventions are under investigation to manage and potentially delay progression of knee OA. These interventions are designed to target modifiable factors that contribute to OA progression (Marriott and Birmingham, 2023). These risk factors include obesity, physical inactivity, muscular weakness, abnormal frontal plane alignment, altered gait biomechanics, and previous joint injury. Current treatments often target these factors through diet, exercise, and biomechanical interventions (Marriott and Birmingham, 2023). For the purpose of this thesis, exercise and biomechanical interventions will be the focus of discussion.

Exercise and diet are guideline-recommended first-line treatments for knee OA (Marriott and Birmingham, 2023). Exercise interventions commonly include resistance, aerobic,

and neuromuscular (includes both resistance and aerobic components) exercise. Resistance and aerobic exercises are recommended to counteract muscle weakness that is associated with knee OA while improving functional capacity, joint range of motion, and pain (Barrow et al., 2019). Findings from several previous studies suggest resistance and aerobic exercise programs can improve exercise tolerance, promote weight loss, and lessen pain in patients with knee OA (Husted et al., 2022; Magni et al., 2017; Nery et al., 2021; Schulz et al., 2020; Zheng et al., 2019). Neuromuscular exercises are designed to address deficiencies that are associated with altered muscle activation patterns (Ageberg and Roos, 2015; Preece et al., 2021) and can also reduce pain. (Primeau et al., 2020). Importantly, evidence to date suggests one type of exercise is not superior to another type of exercise for improving knee pain and function. For example, when comparing 12-week neuromuscular exercise and quadriceps strengthening programs, no difference was found in measures of knee pain, function, and gait biomechanics between exercise programs (Bennell et al., 2014).

Another group of treatments for knee OA is often termed biomechanical interventions because the treatments focus on improving biomechanical risk factors that are associated with knee OA (Marriott and Birmingham, 2023). These risk factors typically include obesity, muscular weakness, altered muscle activity, and abnormal frontal plane alignment. Common biomechanical interventions include bracing, shoe insoles, gait retraining, and gait aids. (Hall et al., 2022; Hinman et al., 2012). A valgus knee brace is most commonly used to provide an external abduction moment to counter a large external knee adduction moment (EKAM) that occurs during gait in patients with medial dominant knee OA (Briem and Ramsey, 2013). Furthermore, previous studies have

identified short term reductions (0.06 BW) in knee loading (Hall et al., 2022) and decreases (12.3% to 28.4%) in CCIs (Fantini Pagani et al., 2013) as a benefit of wearing a valgus knee brace. Previous studies evaluating lateral wedge insoles (Hinman et al., 2012; Tse et al., 2020) and stable supportive shoes (Starkey et al., 2022) have also identified corrections in abnormal frontal plane alignment (0.48º) (Hinman et al., 2012) and reductions in the EKAM (0.22 Nm/BW*HT% and 0.01 Nm/kg, respectively), which is a parameter associated with knee loading that will be described in more detail in section 1.2.2. (Starkey et al., 2022; Tse et al., 2020).

Gait retraining most commonly focuses on shifting the direction of the ground reaction force during stance to alter the distribution of load across the knee. For example, toe out, trunk lean, and other gait adaptations/patterns have been tested (Bowd et al., 2019; Chang et al., 2007; Reeves and Bowling, 2011). Another gait retraining strategy is to lessen the magnitude of the ground reaction force, as for example by increasing cadence for a given walking speed (i.e., taking more, shorter steps) (Hart et al., 2021). Notably, canes (Kemp et al., 2008), and to a lesser extent walking poles (Bechard et al., 2012), can offer substantial, presumably beneficial, changes to gait biomechanics for individuals with knee OA.

1.2.2 Medial Opening Wedge High Tibial Osteotomy

Medial Opening wedge high tibial osteotomy (MOWHTO) is a surgical procedure intended to correct lower limb varus alignment that contributes to increased loading in the medial compartment of the knee joint (Amendola and Bonasia, 2010; Amendola and Panarella, 2005; Fowler et al., 2012). Proposed goals of MOWHTO are to improve pain

and function and delay progression and the need for total knee arthroplasty. MOWHTO is primarily recommended for patients with medial dominant knee OA and varus alignment who likely experience excessively high loads on the medial compartment of the knee. MOWHTO aims to reduce varus alignment by shifting the weightbearing line laterally to establish a more neutral position (Figure 1.3) (Brouwer et al., 2014; Fowler et al., 2012). By improving the distribution of loads on the knee, MOWHTO has the ultimate goal of relieving pain, improving function, and delaying progression of OA (Birmingham et al., 2009; Brouwer et al., 2014; De Pieri et al., 2023; DeMeo et al., 2010).

MOWHTO is typically performed for younger, active patients with medial dominant knee OA and varus alignment, who have symptoms and structural changes localized primarily to the medial compartment of the tibiofemoral joint. More recent studies have identified a benefit of MOWHTO in patients with a greater range of disease characteristics, ages, and stages of OA (Birmingham et al., 2009; Primeau et al., 2023, 2020). Notably, the appropriate selection of patients is still considered an important factor in the success of MOWHTO (Amendola, 2003), and patients with advanced stages of OA, who are older, are typically referred for a total knee joint replacement rather than MOWHTO (Primeau et al., 2021).

Prior to MOWHTO surgery, the patient's frontal plane alignment is assessed to assist in presurgical planning (Amendola, 2003, 2003; Brown and Amendola, 2012; Fowler et al., 2012). This assessment is accomplished by measuring the MAA from an antero-posterior hip-to-ankle radiograph (Amendola, 2003; Brown and Amendola, 2012). A commonly used correction angle shifts the weightbearing line to approximately 62.5% of the medial-

to-lateral width of the tibial plateau (Dougdale et al., 1992). The exact angle of correction, however, varies depending on the surgeons' goals.

MOWHTO is most commonly performed using a medial opening wedge osteotomy system and internal fixation plate (Fowler et al., 2012; Primeau et al., 2023). The planned angle of correction is calculated preoperatively based on the MAA, as described above. The osteotomy is then secured with a metal plate fixed proximally and distally with cancellous and cortical screws, respectively, and cancellous allograft bone is used to fill osteotomies (Figure 1.3).

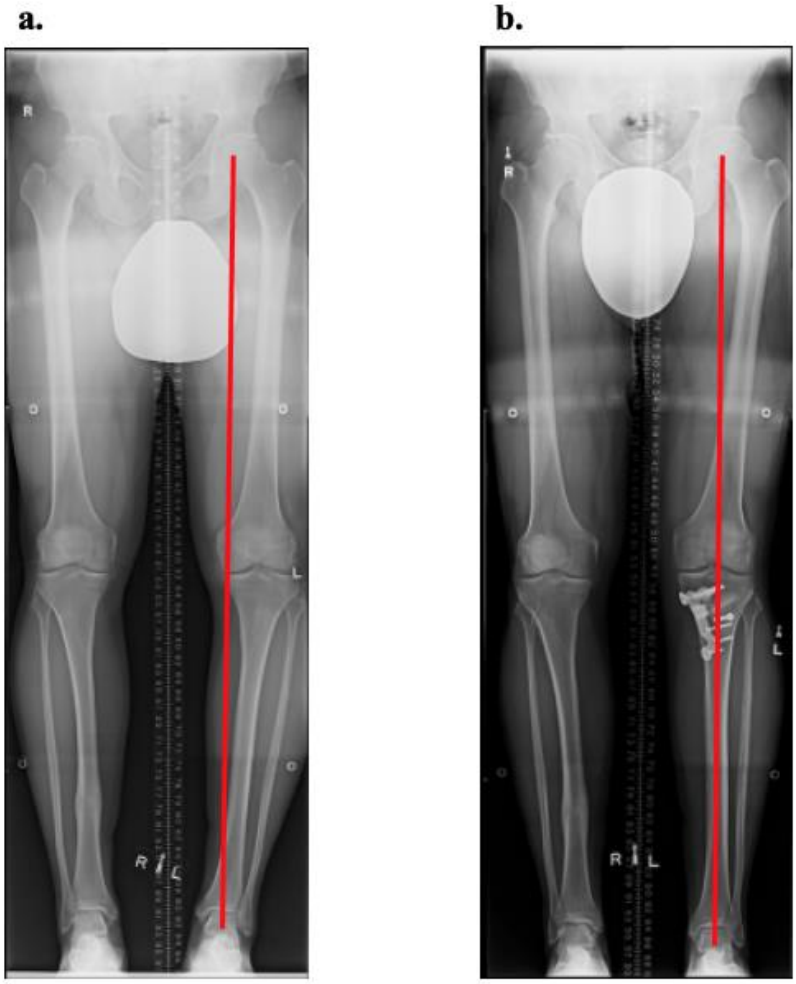

Figure 1.3 Patient radiographs **a.** before and **b.** 12 months after MOWHTO. The red line depicts an estimate of the weight bearing line that displays a shift to neutral after MOWHTO.

Adverse events with MOWHTO can include lateral hinge fractures and hardware failure that may result in loss of correction, insufficient bone healing at the surgical site, and infection (Martin et al., 2014). Such events may also result in prolonged rehabilitation, or in rare cases, additional surgery. Post-operative management typically includes the use of crutches and a hinged knee brace locked in full extension that is to be worn at all times

(Aalderink et al., 2010). With clinical and radiographic evidence of healing of the osteotomy approximately two weeks after the procedure, gradual increase in weightbearing is permitted. Weightbearing is then progressed to full without crutches approximately 12 weeks post-operative (Aalderink et al., 2010). Return to low-impact activity typically occurs after three to four months and at least six months for high impact activity (Aalderink et al., 2010). Patients are monitored throughout the rehabilitation process to ensure they are successfully achieving postoperative milestones.

Both biomechanical and clinical benefits have been reported after MOWHTO. Substantial improvements in gait and patient-reported outcomes have been observed up to five years after MOWHTO (Bhatnagar and Jenkyn, 2010; Birmingham et al., 2017, 2009; De Pieri et al., 2023; Marriott et al., 2015). The effect of MOWHTO on delaying future knee replacement, however, is unknown. Some promising results suggest 95% of patients did not undergo joint replacement within five years after MOWHTO, and 80% did not undergo joint replacement within ten years after MOWHTO (Primeau et al., 2021). Importantly, few studies compare MOWHTO to other surgeries, with no published randomized clinical trials that compare results of MOWHTO to competing nonoperative interventions.

1.3 Biomechanical Assessments of Patients with Knee OA

1.3.1 Kinematics, Kinetics, and Muscle Activity

The pathogenesis of knee OA is complex and associated with aberrant ambulatory mechanics, including the magnitude, distribution, and timing of loads across the tibiofemoral joint (Andriacchi and Mündermann, 2006; Heiden et al., 2009; Hubley-

Kozey et al., 2009; Moyer et al., 2014). Walking produces forces in the knee that are approximately 2-to-3 times body weight (Pandy and Andriacchi, 2010). The total force on the knee includes the summation of dynamic forces, body weight, and muscle forces, with increased muscle co-contraction being the largest contributor (Andriacchi, 1994). Biomechanical assessments for knee OA can include a gait analysis to collect kinematic (joint angle), kinetic (ground reaction force), and electromyography (EMG) (muscle activity) data. These data can provide further insights into factors affecting the patients' knee joint contact forces (KJCFs). Common muscle activity patterns that have been identified in the literature within this population include an increase in muscle activation magnitudes and prolonged activity in the lateral hamstrings and quadriceps muscles (Hubley-Kozey et al., 2009, 2006), and increased (by approximately 2 to 6) lateral muscle co-contraction (Hubley-Kozey et al., 2009) when compared to asymptomatic and healthy controls. The described altered muscle activity may occur as a response to pain, instability, and increased knee loads, all of which contribute to the progression of structural joint damage and symptoms (Hatfield et al., 2021; Heiden et al., 2009; Lewek et al., 2004; Lloyd and Besier, 2003; Winby et al., 2013).

1.3.2 External Knee Adduction Moment

The EKAM is a measure derived from quantitative gait analysis that represents the medial to lateral distribution of load across the knee during walking. The EKAM is computed using kinetic and kinematic data (Figure 1.4) through an inverse dynamics analysis (Robertson et al., 2014). The EKAM has been widely reported as a proxy measure of medial compartment knee joint loading as there is no way to directly obtain this measurement through the intact knee (Bhatnagar and Jenkyn, 2010; Birmingham et

al., 2017; Hunt et al., 2018; Kutzner et al., 2013). The EKAM, however, is only moderately correlated to the medial knee joint contact force (Bhatnagar and Jenkyn, 2010; Miyazaki, 2002; Zhao et al., 2007). Thus, the EKAM does not allow a precise conclusion to be drawn about loads that are transmitted through the medial and lateral compartment of the knee joint (De Pieri et al., 2023).

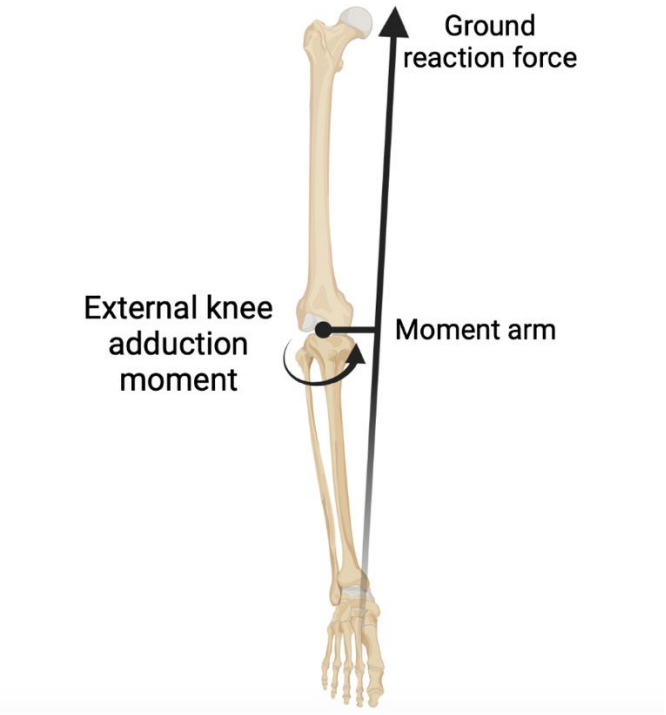

Figure 1.4 External knee adduction moment. The external knee adduction moment assessed with 3D gait analysis is calculated primarily as the product of the ground reaction force and frontal plane moment arm. Created with biorender.com

1.3.3 Musculoskeletal Modelling

1.3.3.1 Model Selection

As it is difficult to evaluate knee joint contact forces *in vivo* in patients with knee OA, musculoskeletal (MSK) modelling provides a means to estimate these loads. MSK models are created with one or more degree(s) of freedom (DOF) corresponding to each joint in the body based on their intended application. DOFs relate to individual segments and planes of motion that each joint can move within. Furthermore, the knee joint can move within six planes of motion including three directions of rotations (flexion/extension, abduction/adduction, and internal/external) and three directions of translations (anterior/posterior, superior/inferior, medial/lateral) (Robertson et al., 2014). To reduce computational complexity, the knee joint is often modeled using one DOF knee models based only on flexion and extension. These models lack internal/external rotation and abduction/adduction, which are important measures when evaluating malalignment during gait. To allow for the computation of frontal plane movement, additions have been made to the one DOF knee models to account for knee internal/external rotation and abduction/adduction (Lerner et al., 2015; Saxby et al., 2016).

1.3.3.2 Patient-Specific Model Modifications

Previous studies have tested the effect of patient-specific modifications made to the generic model scaling that accounts for frontal plane alignment, (Gerus et al., 2013; Lerner et al., 2015; Van Rossom et al., 2019), tibiofemoral contact locations (Lerner et al., 2015; Saliba et al., 2017), bone geometry (Akhundov et al., 2022; Gerus et al., 2013;

Van Rossom et al., 2019), and segment masses (Akhundov et al., 2022) in healthy populations and patients with medial dominant knee OA. These studies have found that, when adjusting for patient-specific frontal plane alignment, the EKAM and medial KJCF significantly increased (up to 2Nm/kg and 1500N, respectively) with an increase in varus alignment in healthy participants (Gerus et al., 2013; Van Rossom et al., 2019). Taking into account patient-specific frontal plane alignment and contact locations has also been found to improve the accuracy of modelled results (in terms of KJCFs) when compared to instrumented knee implant data (differences between 100N and 200N) (Gerus et al., 2013; Lerner et al., 2015). Finally, accounting for patient-specific knee joint geometry and segment masses has also been found to improve model prediction accuracy in terms of comparing external to internal knee flexion/extension moments when evaluating sprinting (RMSE difference of 8.5) and cutting (RMSE difference of 1.4) tasks in healthy participants (Akhundov et al., 2022).

1.3.3.3 Evaluating Modelled Results

Static optimization (SO) and computed muscle control (CMC) have been used previously to predict muscle excitations among healthy athletes and patients with hip OA and knee OA (Brandon et al., 2014; Hoang et al., 2019; Sritharan et al., 2017; Thelen et al., 2003). These optimization methods assume human motion strategies strive for efficiency and are generated by minimizing a cost function that is a weighted sum of muscle activations while subject to constraints of joint motion (Fregly et al., 2012; Winter, 2009). More specifically, SO uses experimental kinematics and kinetics to predict muscle excitations by solving an optimization problem one frame at a time (Delp et al., 2007). CMC takes

SO further by integrating dynamics equations across all time frames to predict a set of muscle excitations that drive the simulation (Delp et al., 2007). Both methods generate muscle excitations using an objective function that is based on experimental kinematics and kinetics, but actual experimental muscle activity is not considered.

Agonist/antagonist co-contraction is a muscle mechanism that occurs to stabilize the knee joint (Lewek et al., 2004). Co-contraction, however, is not physiologically efficient and optimization algorithms cannot accurately model these activation patterns. When evaluating pathological populations such as knee OA, co-contraction indices (CCIs) are increased assumingly due to a lack of stability in the knee joint (Andriacchi, 1994; Lewek et al., 2004). Therefore, optimization algorithms that solely rely on efficient muscle activation strategies do not accurately represent patients with knee OA.

1.3.4 Neuromusculoskeletal Modelling

1.3.4.1 EMG-Driven Neuromusculoskeletal Control Mode

NMSK modelling provides a means for experimentally collected EMG data to drive the computation of muscle forces. One approach to NMSK modelling uses only experimental muscle activations and kinematic data to estimate muscle forces. This method has previously been referred to as EMG-driven NMSK modelling and will be referred to as such throughout this thesis (Ceseracciu and Reggiani, 2015). In more detail, EMG-driven modelling derives neural activations from muscle excitations by modelling the muscle's twitch response (Pizzolato et al., 2015). These activations and muscle-tendon unit (MTU) kinematics are then provided as inputs to a Hill-type model to generate muscle forces. EMG-driven modelling has been used in previous studies when evaluating KJCFs within

healthy participants and assessing total knee replacement in patients with OA (Gerus et al., 2013; Lloyd and Besier, 2003; Saxby et al., 2016). EMG-driven NMSK modelling, however, can be limited as experimentally collected EMG data is subject to measurement error and it is difficult to measure for deep muscles. Additionally this type of modelling neglects additional input data of external (ground reaction force based) joint torques when predicting muscle forces (Sartori et al., 2014). Therefore, when computed muscle forces across the joint are combined to compute internal joint torques, they might not closely match the external (ground reaction force based) joint torques predicted from an inverse dynamic analysis.

1.3.4.2 EMG-Assisted Neuromusculoskeletal Control Mode

Another approach to NMSK modelling uses an objective function to drive the simulation that balances tracking in terms of both muscle activations and joint torques when calculating muscle forces (Sartori et al., 2014). Additionally, this type of model estimates excitation patterns for musculotendon units that were not measured experimentally using a SO approach (Ceseracciu and Reggiani, 2015; Pizzolato et al., 2015). This method has previously been referred to as EMG-assisted NMSK modelling and will be referred to as such throughout this thesis. Although EMG-assisted NMSK modelling demands an increased computational cost when compared to EMG-driven NMSK modelling, this control mode has been used more widely within the knee OA literature to evaluate disease pathology and the effects of interventions to delay disease progression (Hall et al., 2022, 2019; S. Starkey et al., 2022; S. C. Starkey et al., 2022). To our knowledge,

EMG-assisted NMSK modelling has not been used to evaluate patients with medial dominant knee OA before and after HTO.

1.4 Thesis Rationale

Knee OA is a complex disease where aberrant gait biomechanics are thought to contribute substantially to the progression of structural joint damage and symptoms (Felson, 2006; Hunter and Bierma-Zeinstra, 2019). MOWHTO is a limb realignment surgery intended to alter the loads across the knee during ambulation and lessen the KJCF on the more affected medial knee compartment. As it is not possible to measure these loads in the intact knee, different types of musculoskeletal models have been employed to provide an estimates of the changes in KJCFs after interventions. Currently, most models estimate muscle activity based on optimization algorithms. Models that are driven by optimization algorithms alone (i.e., SO and CMC) can be limited as they do not accurately model certain muscle activation patterns such as co-contraction. EMG-driven models incorporate patient-specific muscle activations but are highly sensitive to EMG measurement error. The EMG-assisted NMSK control mode although demands a higher computational cost, overcomes previous modelling limitations and can incorporate muscle co-contraction patterns while also considering kinematics and external torques that are specific to the patient during the simulation (Sartori et al., 2014). Yet, comparisons have not been made between EMG-driven and EMG-assisted control modes to determine which mode is more appropriate to use when evaluating KJCFs in patients with medial dominant knee OA who undergo a variety of interventions intended to improve symptoms and potentially delay disease progression (Hall et al., 2022, 2019; S.

Starkey et al., 2022; S. C. Starkey et al., 2022). Importantly, no previous studies have evaluated the effect of MOWHTO using an EMG-assisted NMSK model.

1.5 Purpose

The purposes of this thesis were to: 1) develop an EMG-informed NMSK modelling framework to predict tibiofemoral medial and lateral compartment KJCF during walking in patients with medial dominant knee OA and varus alignment, and 2) evaluate the effect of MOWHTO on KJCF during walking.

Two research studies were conducted to identify an appropriate modelling framework to effectively evaluate the patient population. A third study was then completed to investigate the effects of MOWHTO. Therefore, the three overall thesis objectives were as follows:

Study 1 (Chapter 2) Objective: to evaluate and compare results from patient specific computational NMSK models using EMG-driven and EMG-assisted NMSK control modes in patients with medial dominant knee OA.

Study 2 (Chapter 3) Objective: To compare results from patient-specific EMG assisted NMSK models with an assumed varus angle of 0 and a patient-specific varus angle in patients with varus alignment and medial dominant knee OA.

Study 3 (Chapter 4) Objective: To investigate: 1) the effect of MOWHTO on medial and lateral tibiofemoral compartment KJCFs during walking using a patient-specific EMG-assisted modelling framework, 2) to investigate changes in the EKAM and CCIs,

and 3) the associations between changes in medial compartment KJCF, EKAM, and CCIs.

1.6 References

Aalderink, K.J., Shaffer, M., Amendola, A., 2010. Rehabilitation Following High Tibial Osteotomy. Clin. Sports Med. 29, 291–301. https://doi.org/10.1016/j.csm.2009.12.005

Ageberg, E., Roos, E.M., 2015. Neuromuscular Exercise as Treatment of Degenerative Knee Disease. Exerc. Sport Sci. Rev. 43, 14–22. https://doi.org/10.1249/JES.0000000000000030

Akhundov, R., Saxby, D.J., Diamond, L.E., Edwards, S., Clausen, P., Dooley, K., Blyton, S., Snodgrass, S.J., 2022. Is subject-specific musculoskeletal modelling worth the extra effort or is generic modelling worth the shortcut? PLoS ONE 17, 1–16. https://doi.org/10.1371/journal.pone.0262936

Altman, R., Asch, E., Bloch, D., Bole, G., Borenstein, D., Brandt, K., Christy, W., Cooke, T.D., Greenwald, R., Hochberg, M., Howell, D., Kaplan, D., Koopman, W., Longley, S., Mankin, H., McShane, D.J., Medsger, T., Meenan, R., Mikkelsen, W., Moskowitz, R., Murphy, W., Rothschild, B., Segal, M., Sokoloff, L., Wolfe, F., 1986. Development of criteria for the classification and reporting of osteoarthritis: Classification of osteoarthritis of the knee. Arthritis Rheum. 29, 1039–1049. https://doi.org/10.1002/art.1780290816

Amendola, A., 2003. Unicompartmental osteoarthritis in the active patient: the role of high tibial osteotomy. Arthrosc. J. Arthrosc. Relat. Surg. 19, 109–116. https://doi.org/10.1016/j.arthro.2003.09.048

Amendola, A., Bonasia, D.E., 2010. Results of high tibial osteotomy: review of the literature. Int. Orthop. 34, 155–160. https://doi.org/10.1007/s00264-009-0889-8

Amendola, A., Panarella, L., 2005. High tibial osteotomy for the treatment of unicompartmental arthritis of the knee. Orthop. Clin. North Am. 36, 497–504. https://doi.org/10.1016/j.ocl.2005.05.009

Andriacchi, T.P., 1994. Dynamics of knee malalignment. Orthop Clin North Am 25, 395–403.

Andriacchi, T.P., Mündermann, A., 2006. The role of ambulatory mechanics in the initiation and progression of knee osteoarthritis. Curr. Opin. Rheumatol. 18, 514–518. https://doi.org/10.1097/01.bor.0000240365.16842.4e

Barrow, D.R., Abbate, L.M., Paquette, M.R., Driban, J.B., Vincent, H.K., Newman, C., Messier, S.P., Ambrose, K.R., Shultz, S.P., 2019. Exercise prescription for weight management in obese adults at risk for osteoarthritis: synthesis from a systematic review. BMC Musculoskelet. Disord. 20, 610. https://doi.org/10.1186/s12891-019-3004-3

Bechard, D.J., Birmingham, T.B., Zecevic, A.A., Jones, I.C., Leitch, K.M., Giffin, J.R., Jenkyn, T.R., 2012. The effect of walking poles on the knee adduction moment in patients with varus gonarthrosis. Osteoarthritis Cartilage 20, 1500–1506. https://doi.org/10.1016/j.joca.2012.08.014

Bennell, K.L., Kyriakides, M., Metcalf, B., Egerton, T., Wrigley, T.V., Hodges, P.W., Hunt, M.A., Roos, E.M., Forbes, A., Ageberg, E., Hinman, R.S., 2014.

Neuromuscular versus quadriceps strengthening exercise in patients with medial knee osteoarthritis and varus malalignment: A randomized controlled trial: Neuromuscular exercise and knee adduction moment. Arthritis Rheumatol. 66, 950–959. https://doi.org/10.1002/art.38317

Bhatnagar, T., Jenkyn, T.R., 2010. Internal kinetic changes in the knee due to high tibial osteotomy are well-correlated with change in external adduction moment: An osteoarthritic knee model. J. Biomech. 43, 2261–2266. https://doi.org/10.1016/j.jbiomech.2010.05.001

Birmingham, T.B., Giffin, J.R., Chesworth, B.M., Bryant, D.M., Litchfield, R.B., Willits, K., Jenkyn, T.R., Fowler, P.J., 2009. Medial opening wedge high tibial osteotomy: A prospective cohort study of gait, radiographic, and patient-reported outcomes. Arthritis Care Res. 61, 648–657. https://doi.org/10.1002/art.24466

Birmingham, T.B., Moyer, R., Leitch, K., Chesworth, B., Bryant, D., Willits, K., Litchfield, R., Fowler, P.J., Giffin, J.R., 2017. Changes in biomechanical risk factors for knee osteoarthritis and their association with 5-year clinically important improvement after limb realignment surgery. Osteoarthritis Cartilage 25, 1999–2006. https://doi.org/10.1016/j.joca.2017.08.017

Bombardier, C., Hawker, G., Mosher, D., 2011. Impact of arthritis in Canada: today and over the next 30 years.

Bowd, J., Biggs, P., Holt, C., Whatling, G., 2019. Does gait retraining have the potential to reduce medial compartmental loading in individuals with knee osteoarthritis

while not adversely affecting the other lower limb joints? A Systematic Review. Arch. Rehabil. Res. Clin. Transl. 1, 100022. https://doi.org/10.1016/j.arrct.2019.100022

Brandon, S.C.E., Miller, R.H., Thelen, D.G., Deluzio, K.J., 2014. Selective lateral muscle activation in moderate medial knee osteoarthritis subjects does not unload medial knee condyle. J. Biomech. 47, 1409–1415. https://doi.org/10.1016/j.jbiomech.2014.01.038

Briem, K., Ramsey, D.K., 2013. The Role of Bracing. Sports Med. Arthrosc. Rev. 21, 11–17. https://doi.org/10.1097/JSA.0b013e31827562b5

Brouwer, G.M., Tol, A.W.V., Bergink, A.P., Belo, J.N., Bernsen, R.M.D., Reijman, M., Pols, H.A.P., Bierma-Zeinstra, S.M.A., 2007. Association between valgus and varus alignment and the development and progression of radiographic osteoarthritis of the knee. Arthritis Rheum. 56, 1204–1211. https://doi.org/10.1002/art.22515

Brouwer, R.W., Huizinga, M.R., Duivenvoorden, T., van Raaij, T.M., Verhagen, A.P., Bierma-Zeinstra, S.M., Verhaar, J.A., 2014. Osteotomy for treating knee osteoarthritis. Cochrane Database Syst. Rev. https://doi.org/10.1002/14651858.CD004019.pub4

Brown, G.A., Amendola, A., 2012. Radiographic evaluation and preoperative planning for high tibial osteotomies. Oper. Tech. Sports Med. 20, 93–102. https://doi.org/10.1053/j.otsm.2012.03.011

Ceseracciu, E., Reggiani, M., 2015. CEINMS user guide documentation 1–58.

Chang, A., Hurwitz, D., Dunlop, D., Song, J., Cahue, S., Hayes, K., Sharma, L., 2007. The relationship between toe-out angle during gait and progression of medial tibiofemoral osteoarthritis. Ann. Rheum. Dis. 66, 1271–1275. https://doi.org/10.1136/ard.2006.062927

Chen, D., Shen, J., Zhao, W., Wang, T., Han, L., Hamilton, J.L., Im, H.J., 2017. Osteoarthritis: Toward a comprehensive understanding of pathological mechanism. Bone Res. 5. https://doi.org/10.1038/boneres.2016.44

Chen, Y., Navratilova, E., Dodick, D.W., Porreca, F., 2020. An emerging role for prolactin in female-selective pain. Trends Neurosci. 43, 635–648. https://doi.org/10.1016/j.tins.2020.06.003

De Pieri, E., Nüesch, C., Pagenstert, G., Viehweger, E., Egloff, C., Mündermann, A., 2023. High tibial osteotomy effectively redistributes compressive knee loads during walking. J. Orthop. Res. 41, 591–600. https://doi.org/10.1002/jor.25403

Delp, S.L., Anderson, F.C., Arnold, A.S., Loan, P., Habib, A., John, C.T., Guendelman, E., Thelen, D.G., 2007. OpenSim: Open-source software to create and analyze dynamic simulations of movement. IEEE Trans. Biomed. Eng. 54, 1940–1950. https://doi.org/10.1109/TBME.2007.901024

DeMeo, P.J., Johnson, E.M., Chiang, P.P., Flamm, A.M., Miller, M.C., 2010. Midterm follow-up of opening-wedge high tibial osteotomy. Am. J. Sports Med. 38, 2077–2084. https://doi.org/10.1177/0363546510371371

Dougdale, T.W., Noyes, F.R., Styer, D., 1992. Preoperative planning for high tibial osteotomy. The effect of lateral tibiofemoral separation and tibiofemoral length. Clin. Orthop. 1992, 248–268.

Fantini Pagani, C.H., Willwacher, S., Kleis, B., Brüggemann, G.-P., 2013. Influence of a valgus knee brace on muscle activation and co-contraction in patients with medial knee osteoarthritis. J. Electromyogr. Kinesiol. 23, 490–500. https://doi.org/10.1016/j.jelekin.2012.10.007

Felson, D.T., 2006. Osteoarthritis of the knee. N. Engl. J. Med.

Fowler, P.J., Tan, J.L., Brown, G.A., 2012. Medial opening wedge high tibial osteotomy: How I do it. Oper. Tech. Sports Med. 20, 87–92. https://doi.org/10.1053/j.otsm.2012.03.010

Fregly, B.J., Besier, T.F., Lloyd, D.G., Delp, S.L., Banks, S.A., Pandy, M.G., D'Lima, D.D., 2012. Grand challenge competition to predict in vivo knee loads: Grand challenge competition. J. Orthop. Res. 30, 503–513. https://doi.org/10.1002/jor.22023

Gerus, P., Sartori, M., Besier, T.F., Fregly, B.J., Delp, S.L., Banks, S.A., Pandy, M.G., D'Lima, D.D., Lloyd, D.G., 2013a. Subject-specific knee joint geometry improves predictions of medial tibiofemoral contact forces. J. Biomech. 46, 2778–2786. https://doi.org/10.1016/j.jbiomech.2013.09.005

Global, regional, and national incidence, prevalence, and years lived with disability for 310 diseases and injuries, 1990–2015: a systematic analysis for the Global Burden

of Disease Study 2015, 2016. . The Lancet 388, 1545–1602. https://doi.org/10.1016/S0140-6736(16)31678-6

Goldring, M.B., Goldring, S.R., 2007. Osteoarthritis. J. Cell. Physiol. 213, 626–634. https://doi.org/10.1002/jcp.21258

Hall, M., Diamond, L.E., Lenton, G.K., Pizzolato, C., Saxby, D.J., 2019. Immediate effects of valgus knee bracing on tibiofemoral contact forces and knee muscle forces. Gait Posture 68, 55–62. https://doi.org/10.1016/j.gaitpost.2018.11.009

Hall, M., Starkey, S., Hinman, R.S., Diamond, L.E., Lenton, G.K., Knox, G., Pizzolato, C., Saxby, D.J., 2022. Effect of a valgus brace on medial tibiofemoral joint contact force in knee osteoarthritis with varus malalignment: A within-participant cross-over randomised study with an uncontrolled observational longitudinal follow-up. PLoS ONE 17, 1–18. https://doi.org/10.1371/journal.pone.0257171

Hart, H.F., Birmingham, T.B., Primeau, C.A., Pinto, R., Leitch, K., Giffin, J.R., 2021. Associations between cadence and knee loading in patients with knee osteoarthritis. Arthritis Care Res. 73, 1667–1671. https://doi.org/10.1002/acr.24400

Hatfield, G.L., Costello, K.E., Astephen Wilson, J.L., Stanish, W.D., Hubley-Kozey, C.L., 2021. Baseline gait muscle activation patterns differ for osteoarthritis patients who undergo total knee arthroplasty five to eight years later from those who do not. Arthritis Care Res. 73, 549–558. https://doi.org/10.1002/acr.24143

Heiden, T.L., Lloyd, D.G., Ackland, T.R., 2009. Knee joint kinematics, kinetics and muscle co-contraction in knee osteoarthritis patient gait. Clin. Biomech. 24, 833–841. https://doi.org/10.1016/j.clinbiomech.2009.08.005

Hinman, R.S., Bowles, K.A., Metcalf, B.B., Wrigley, T.V., Bennell, K.L., 2012. Lateral wedge insoles for medial knee osteoarthritis: Effects on lower limb frontal plane biomechanics. Clin. Biomech. 27, 27–33. https://doi.org/10.1016/j.clinbiomech.2011.07.010

Hoang, H.X., Diamond, L.E., Lloyd, D.G., Pizzolato, C., 2019. A calibrated EMG-informed neuromusculoskeletal model can appropriately account for muscle co-contraction in the estimation of hip joint contact forces in people with hip osteoarthritis. J. Biomech. 83, 134–142. https://doi.org/10.1016/j.jbiomech.2018.11.042

Hubley-Kozey, C.L., Deluzio, K.J., Landry, S.C., McNutt, J.S., Stanish, W.D., 2006. Neuromuscular alterations during walking in persons with moderate knee osteoarthritis. J. Electromyogr. Kinesiol. 16, 365–378. https://doi.org/10.1016/j.jelekin.2005.07.014

Hubley-Kozey, C.L., Hill, N.A., Rutherford, D.J., Dunbar, M.J., Stanish, W.D., 2009. Co-activation differences in lower limb muscles between asymptomatic controls and those with varying degrees of knee osteoarthritis during walking. Clin. Biomech. 24, 407–414. https://doi.org/10.1016/j.clinbiomech.2009.02.005

Hunt, M. A., Birmingham, T. B., Jenkyn, T. R., Giffin, J. R., & Jones, I. C. (2008). Measures of frontal plane lower limb alignment obtained from static radiographs and dynamic gait analysis. *Gait & Posture*, *27*(4), 635–640. https://doi.org/10.1016/j.gaitpost.2007.08.011

Hunt, M.A., Charlton, J.M., Krowchuk, N.M., Tse, C.T.F., Hatfield, G.L., 2018. Clinical and biomechanical changes following a 4-month toe-out gait modification program for people with medial knee osteoarthritis: a randomized controlled trial. Osteoarthritis Cartilage 26, 903–911. https://doi.org/10.1016/j.joca.2018.04.010

Hunter, D.J., Bierma-Zeinstra, S., 2019. Osteoarthritis. The Lancet 393, 1745–1759. https://doi.org/10.1016/S0140-6736(19)30417-9

Husted, R.S., Troelsen, A., Husted, H., Grønfeldt, B.M., Thorborg, K., Kallemose, T., Rathleff, M.S., Bandholm, T., 2022. Knee-extensor strength, symptoms, and need for surgery after two, four, or six exercise sessions/week using a home-based one-exercise program: a randomized dose–response trial of knee-extensor resistance exercise in patients eligible for knee replacement (the QUADX-1 trial). Osteoarthritis Cartilage 30, 973–986. https://doi.org/10.1016/j.joca.2022.04.001

Kellgren, J.H., Lawrence, J.S., 1957. Radiological assessment of osteo-arthrosis. Ann. Rheum. Dis. 494–502. https://doi.org/10.2307/3578513

Kemp, G., Crossley, K.M., Wrigley, T.V., Metcalf, B.R., Hinman, R.S., 2008. Reducing joint loading in medial knee osteoarthritis: Shoes and canes. Arthritis Rheum. 59, 609–614. https://doi.org/10.1002/art.23578

Kutzner, I., Heinlein, B., Graichen, F., Bender, A., Rohlmann, A., Halder, A., Beier, A., & Bergmann, G. (2010). Loading of the knee joint during activities of daily living measured in vivo in five subjects. *Journal of Biomechanics*, *43*(11), 2164–2173. https://doi.org/10.1016/j.jbiomech.2010.03.046

Kutzner, I., Trepczynski, A., Heller, M.O., Bergmann, G., 2013. Knee adduction moment and medial contact force-facts about their correlation during gait. PLoS ONE 8, 8–15. https://doi.org/10.1371/journal.pone.0081036

Lerner, Z.F., DeMers, M.S., Delp, S.L., Browning, R.C., 2015. How tibiofemoral alignment and contact locations affect predictions of medial and lateral tibiofemoral contact forces. J. Biomech. 48, 644–650. https://doi.org/10.1016/j.jbiomech.2014.12.049

Lewek, M.D., Rudolph, K.S., Snyder-Mackler, L., 2004. Control of frontal plane knee laxity during gait in patients with medial compartment knee osteoarthritis. Osteoarthritis Cartilage 12, 745–751. https://doi.org/10.1016/j.joca.2004.05.005

Lloyd, D.G., Besier, T.F., 2003. An EMG-driven musculoskeletal model to estimate muscle forces and knee joint moments in vivo. J. Biomech. 36, 765–776. https://doi.org/10.1016/S0021-9290(03)00010-1

Loeser, R.F., Goldring, S.R., Scanzello, C.R., Goldring, M.B., 2012. Osteoarthritis: A disease of the joint as an organ. Arthritis Rheum. 64, 1697–1707. https://doi.org/10.1002/art.34453

Loudon, J.K., 2016. Biomechanics and pathomechanics of the patellofemoral joint. Int. J. Sports Phys. Ther. 11, 820–830.

Magni, N.E., McNair, P.J., Rice, D.A., 2017. The effects of resistance training on muscle strength, joint pain, and hand function in individuals with hand osteoarthritis: a systematic review and meta-analysis. Arthritis Res. Ther. 19, 131. https://doi.org/10.1186/s13075-017-1348-3

Marques Luís, N., Varatojo, R., 2021. Radiological assessment of lower limb alignment. EFORT Open Rev. 6, 487–494. https://doi.org/10.1302/2058-5241.6.210015

Marriott, K., Birmingham, T.B., Kean, C.O., Hui, C., Jenkyn, T.R., Giffin, J.R., 2015. Five-year changes in gait biomechanics after concomitant high tibial osteotomy and ACL reconstruction in patients with medial knee osteoarthritis. Am. J. Sports Med. 43, 2277–2285. https://doi.org/10.1177/0363546515591995

Marriott, K.A., Birmingham, T.B., 2023. Fundamentals of osteoarthritis. Rehabilitation: Exercise, diet, biomechanics, and physical therapist-delivered interventions. Osteoarthritis Cartilage S1063458423008518. https://doi.org/10.1016/j.joca.2023.06.011

Martin, R., Birmingham, T.B., Willits, K., Litchfield, R., LeBel, M.-E., Giffin, J.R., 2014. Adverse event rates and classifications in medial opening wedge high tibial osteotomy. Am. J. Sports Med. 42, 1118–1126. https://doi.org/10.1177/0363546514525929

Messier, S.P., Loeser, R.F., Mitchell, M.N., Valle, G., Morgan, T.P., Rejeski, W.J., Ettinger, W.H., 2000. Exercise and weight loss in obese older adults with knee osteoarthritis: A Preliminary Study. J. Am. Geriatr. Soc. 48, 1062–1072. https://doi.org/10.1111/j.1532-5415.2000.tb04781.x

Miyazaki, T., 2002. Dynamic load at baseline can predict radiographic disease progression in medial compartment knee osteoarthritis. Ann. Rheum. Dis. 61, 617–622. https://doi.org/10.1136/ard.61.7.617

Moyer, R.F., Ratneswaran, A., Beier, F., Birmingham, T.B., 2014. Osteoarthritis year in review 2014: mechanics – basic and clinical studies in osteoarthritis. Osteoarthritis Cartilage 22, 1989–2002. https://doi.org/10.1016/j.joca.2014.06.034

Nery, M., Natour, J., Jennings, F., Fernandes, A.D.R.C., Souza, M.C., Jones, A., 2021. Effects of a progressive resistance exercise program in patients with hand osteoarthritis: A randomized, controlled trial with a blinded assessor. Clin. Rehabil. 35, 1757–1767. https://doi.org/10.1177/02692155211030622

Pandy, M.G., Andriacchi, T.P., 2010. Muscle and joint function in human locomotion. Annu. Rev. Biomed. Eng. 12, 401–433. https://doi.org/10.1146/annurev-bioeng-070909-105259

Park, D., Park, Y.-M., Ko, S.-H., Hyun, K.-S., Choi, Y.-H., Min, D.-U., Han, K., Koh, H.-S., 2023. Association of general and central obesity, and their changes with risk of knee osteoarthritis: a nationwide population-based cohort study. Sci. Rep. 13, 3796. https://doi.org/10.1038/s41598-023-30727-4

Pizzolato, C., Lloyd, D.G., Sartori, M., Ceseracciu, E., Besier, T.F., Fregly, B.J., Reggiani, M., 2015. CEINMS: A toolbox to investigate the influence of different neural control solutions on the prediction of muscle excitation and joint moments during dynamic motor tasks. J. Biomech. 48, 3929–3936. https://doi.org/10.1016/j.jbiomech.2015.09.021

Preece, S.J., Brookes, N., Williams, A.E., Jones, R.K., Starbuck, C., Jones, A., Walsh, N.E., 2021. A new integrated behavioural intervention for knee osteoarthritis: development and pilot study. BMC Musculoskelet. Disord. 22, 1–14. https://doi.org/10.1186/s12891-021-04389-0

Primeau, C.A., Birmingham, T.B., Appleton, C.T., Leitch, K.M., Fowler, P.J., Marsh, J.D., Giffin, J.R., 2023. Responders to medial opening wedge high tibial osteotomy for knee osteoarthritis. J. Rheumatol. 50, 809–816. https://doi.org/10.3899/jrheum.220956

Primeau, C.A., Birmingham, T.B., Leitch, K.M., Willits, K.R., Litchfield, R.B., Fowler, P.J., Marsh, J.D., Chesworth, B.M., Dixon, S.N., Bryant, D.M., Giffin, J.R., 2021. Total knee replacement after high tibial osteotomy: time-to-event analysis and predictors. Can. Med. Assoc. J. 193, E158–E166. https://doi.org/10.1503/cmaj.200934

Primeau, C.A., Birmingham, T.B., Moyer, R.F., O'Neil, K.A., Werstine, M.S., Alcock, G.K., Giffin, J.R., 2020. Trajectories of perceived exertion and pain over a 12-week neuromuscular exercise program in patients with knee osteoarthritis. Osteoarthritis Cartilage 28, 1427–1431. https://doi.org/10.1016/j.joca.2020.07.011

Reeves, N., Bowling, F., 2011. Conservative biomechanical strategies for knee osteoarthritis 7, 113–122. http://dx.doi.org.proxy1.lib.uwo.ca/10.1038/nrrheum.2010.212

Richmond, S.A., Fukuchi, R.K., Ezzat, A., Schneider, K., Schneider, G., Emery, C.A., 2013. Are joint injury, sport activity, physical activity, obesity, or occupational activities predictors for osteoarthritis? A Systematic Review. J. Orthop. Sports Phys. Ther. 43, 515-B19. https://doi.org/10.2519/jospt.2013.4796

Robertson, D.G.E., Caldwell, G.E., Hamill, J., Kamen, G., Whittlesey, Saunders.N., 2014. Methods in Biomechanics. Human Kinetics, Champaign, IL.

Roos, E.M., Lohmander, L.S., 2003. The knee injury and osteoarthritis outcome score (KOOS): from joint injury to osteoarthritis. Health Qual. Life Outcomes.

Saliba, C.M., Brandon, S.C.E., Deluzio, K.J., 2017. Sensitivity of medial and lateral knee contact force predictions to frontal plane alignment and contact locations. J. Biomech. 57, 125–130. https://doi.org/10.1016/j.jbiomech.2017.03.005

Sartori, M., Farina, D., Lloyd, D.G., 2014. Hybrid neuromusculoskeletal modeling to best track joint moments using a balance between muscle excitations derived from electromyograms and optimization. J. Biomech. 47, 3613–3621. https://doi.org/10.1016/j.jbiomech.2014.10.009

Saxby, D.J., Modenese, L., Bryant, A.L., Gerus, P., Killen, B., Fortin, K., Wrigley, T.V., Bennell, K.L., Cicuttini, F.M., Lloyd, D.G., 2016. Tibiofemoral contact forces

during walking, running and sidestepping. Gait Posture 49, 78–85. https://doi.org/10.1016/j.gaitpost.2016.06.014

Schulz, J.M., Birmingham, T.B., Atkinson, H.F., Woehrle, E., Primeau, C.A., Lukacs, M.J., Al-Khazraji, B.K., Khan, M.C.M., Zomar, B.O., Petrella, R.J., Beier, F., Appleton, C.T., Shoemaker, J.K., Bryant, D.M., 2020. Are we missing the target? Are we aiming too low? What are the aerobic exercise prescriptions and their effects on markers of cardiovascular health and systemic inflammation in patients with knee osteoarthritis? A systematic review and meta-analysis. Br. J. Sports Med. 54, 771–775. https://doi.org/10.1136/bjsports-2018-100231

Sharma, L., Hurwitz, D.E., Thonar, E.J.-M.A., Sum, J.A., Lenz, M.E., Dunlop, D.D., Schnitzer, T.J., Kirwan-Mellis, G., Andriacchi, T.P., 1998. Knee adduction moment, serum hyaluronan level, and disease severity in medial tibiofemoral osteoarthritis. Arthritis Rheum. 41, 1233–1240. https://doi.org/10.1002/1529-0131(199807)41:7<1233::AID-ART14>3.0.CO;2-L

Specogna, A., Birmingham, T., DaSilva, J., Milner, J., Kerr, J., Hunt, M., Jones, I., Jenkyn, T., Fowler, P., & Giffin, J. (2004). Reliability of Lower Limb Frontal Plane Alignment Measurements Using Plain Radiographs and Digitized Images. *The Journal of Knee Surgery*, *17*(04), 203–210. https://doi.org/10.1055/s-0030-1248222

Specogna, A., Birmingham, T. B., Hunt, M. A., Jones, I. C., Jenkyn, T. R., Fowler, P. J., & Giffin, J. R. (2007). Radiographic Measures of Knee Alignment in Patients with varus Gonarthrosis: Effect of Weightbearing Status and Associations with

Dynamic Joint Load. *The American Journal of Sports Medicine*, *35*(1), 65–70. https://doi.org/10.1177/0363546506293024

Sritharan, P., Lin, Y.C., Richardson, S.E., Crossley, K.M., Birmingham, T.B., Pandy, M.G., 2017. Musculoskeletal loading in the symptomatic and asymptomatic knees of middle-aged osteoarthritis patients. J. Orthop. Res. 35, 321–330. https://doi.org/10.1002/jor.23264

Starkey, S., Hinman, R., Paterson, K., Saxby, D., Knox, G., Hall, M., 2022. Tibiofemoral contact force differences between flat flexible and stable supportive walking shoes in people with varus-malaligned medial knee osteoarthritis: A randomized cross-over study. PLoS ONE 17, 1–20. https://doi.org/10.1371/journal.pone.0269331

Starkey, S.C., Diamond, L.E., Hinman, R.S., Saxby, D.J., Knox, G., Hall, M., 2022. Muscle forces during weight-bearing exercises in medial knee osteoarthritis and varus malalignment: A cross-sectional study. Med. Sci. Sports Exerc. 54, 1448–1458. https://doi.org/10.1249/MSS.0000000000002943

Thelen, D.G., Anderson, F.C., Delp, S.L., 2003. Generating dynamic simulations of movement using computed muscle control. J. Biomech. 36, 321–328. https://doi.org/10.1016/S0021-9290(02)00432-3

Thomas, M.J., Neogi, T., 2020. Flare-ups of osteoarthritis: what do they mean in the short-term and the long-term? Osteoarthritis Cartilage 28, 870–873. https://doi.org/10.1016/j.joca.2020.01.005

Tse, C.T.F., Ryan, M.B., Hunt, M.A., 2020. Influence of foot posture on immediate biomechanical responses during walking to variable-stiffness supported lateral wedge insole designs. Gait Posture 81, 21–26. https://doi.org/10.1016/j.gaitpost.2020.06.026

Van Rossom, S., Wesseling, M., Smith, C.R., Thelen, D.G., Vanwanseele, B., Dieter, V.A., Jonkers, I., 2019. The influence of knee joint geometry and alignment on the tibiofemoral load distribution: A computational study. Knee 26, 813–823. https://doi.org/10.1016/j.knee.2019.06.002

Vos, T. et al., 2016. Global, regional, and national incidence, prevalence, and years lived with disability for 310 diseases and injuries, 1990–2015: a systematic analysis for the Global Burden of Disease Study 2015. The Lancet 388, 1545–1602. https://doi.org/10.1016/S0140-6736(16)31678-6

Winby, C.R., Gerus, P., Kirk, T.B., Lloyd, D.G., 2013. Correlation between EMG-based co-activation measures and medial and lateral compartment loads of the knee during gait. Clin. Biomech. 28, 1014–1019. https://doi.org/10.1016/j.clinbiomech.2013.09.006

Winby, C.R., Lloyd, D.G., Besier, T.F., Kirk, T.B., 2009. Muscle and external load contribution to knee joint contact loads during normal gait. J. Biomech. 42, 2294–2300. https://doi.org/10.1016/j.jbiomech.2009.06.019

Winter, D.A., 2009. Biomechanics and Motor Control of Human Movement. John Wiley & Sons, Inc., Hoboken, New Jersey. https://doi.org/10.1002/9780470549148

Zhao, D., Banks, S.A., Mitchell, K.H., D'Lima, D.D., Colwell, C.W., Fregly, B.J., 2007. Correlation between the knee adduction torque and medial contact force for a variety of gait patterns. J. Orthop. Res. 25, 789–797. https://doi.org/10.1002/jor.20379

Zheng, G., Qiu, P., Xia, R., Lin, H., Ye, B., Tao, J., Chen, L., 2019. Effect of aerobic exercise on inflammatory markers in healthy middle-aged and older adults: A systematic review and meta-analysis of randomized controlled trials. Front. Aging Neurosci. 11, 98. https://doi.org/10.3389/fnagi.2019.00098

Chapter 2

2 Evaluation of EMG-Assisted and EMG-Driven Control Modes in Patients with Medial Compartment Knee Osteoarthritis

2.1 Summary

Knee osteoarthritis (OA) is associated with increased knee joint contact forces (KJCFs) that cannot be directly measured in the intact knee. Patient-specific neuromusculoskeletal (NMSK) models estimate these loads using EMG-driven and -assisted control modes. There is limited research comparing both control modes for models of patients with medial dominant knee OA. The purpose of this study was to evaluate a patient-specific NMSK modelling framework using two NMSK control modes in patients with medial dominant knee OA.

Gait data were measured from 27 patients with medial dominant knee OA. An OpenSim model was scaled to patient-specific anthropometrics, including frontal plane knee alignment. Inverse kinematics and dynamics analyses were performed. Computed kinematics, external torques, and experimental muscle activations were inputted into the Calibrated Electromyography Informed Neuromusculoskeletal Modelling Toolbox (CEINMS). Muscle forces and joint contact forces were estimated using both control modes.

The EMG-assisted control mode yielded a lower (p=0.001) knee flexion/extension torque error (2.7 ±2.1Nm) than the EMG-driven control mode (12.6 ±3.9Nm). The largest difference in the KJCFs occurred in the second peak of the medial compartment, where the EMG-assisted control mode calculated a greater first peak in the lateral compartment joint contact forces (2.3 ± 1.1BW) than the EMG-driven control mode (2.1 ± 0.9BW).

Therefore, it is evident that NMSK model-based estimates of knee joint contact forces in patients with medial dominant knee OA are sensitive to the selected control mode.

2.2 Introduction

Knee osteoarthritis (OA) has a complex pathogenesis that is associated with increased joint contact forces across the tibiofemoral joint (Andriacchi and Mündermann, 2006). Although there are currently no proven disease modifying interventions, rehabilitative and surgical interventions aim to improve symptoms and function (Madry, 2022; Marriott and Birmingham, 2023). These interventions also aim to reduce the medial knee joint contact forces (KJCFs) that are related to progression of medial dominant knee OA (Andriacchi, 1994; Lewek et al., 2004). To assess the effects of these interventions on the medial compartment KJCFs, the knee adduction moment is commonly used as a proxy measure because of its moderate correlation with medial KJCFs (Holder et al., 2023; Kutzner et al., 2013; Miyazaki et al., 2002; Walter et al., 2010; Zhao et al., 2007). The knee adduction moment is computed using propagated ground reaction forces and lower extremity kinematics. Internal KJCFs, however, are computed based on the vector sum of propagated ground reaction forces, lower extremity kinematics, and muscle contributions of knee-spanning muscles.

KJCFs cannot be directly measured within the intact knee; however, patient-specific computational models offer a means to estimate these loads (Gerus et al., 2013; Pizzolato et al., 2015; Saxby et al., 2016). This includes patient-specific neuromusculoskeletal (NMSK) computational models, which can estimate muscle forces (and therefore KJCFs) based on an EMG-driven or EMG-assisted control mode (Ceseracciu and Reggiani, 2015). The EMG-*driven* NMSK control mode drives the simulation based on

experimental EMG activations and kinematic data. This control mode is beneficial if experimental kinetic data was not experimentally collected. Yet as a result, the EMG-driven NMSK control mode might predict internal joint torques that do not closely match the external joint torques predicted from an inverse dynamic analysis. The hybrid EMG-*assisted* NMSK control, on the other hand, is driven by an objective function that balances tracking in terms of both muscle activations and external joint torques when calculating muscle forces (Sartori et al., 2014). Although this control mode requires a higher computational cost and additional experimentally collected kinetic data, this hybrid model can also estimate excitation patterns using a static optimization approach for musculotendon units (MTUs) that were not measured experimentally (Ceseracciu and Reggiani, 2015; Pizzolato et al., 2015).

EMG-driven and EMG-assisted NMSK control modes have been employed within the literature to estimate relative muscle and external load contributions to KJCFs within healthy populations (Gerus et al., 2013; Saxby et al., 2016). Previous literature, however, has not examined which NMSK control mode is the most accurate for predicting KJCFs in patients with medial dominant knee OA. As with the EMG-driven mode, the EMG-assisted mode provides the ability to incorporate abnormal muscle patterns into its prediction. This hybrid EMG-assisted NMSK control mode, however, is assumed to be more appropriate for studies of pathological populations, such as those involving patients with medial dominant knee OA. This is because collecting the high-quality EMG data that EMG-driven models require is difficult for these populations due to specific risk factors such as obesity. Therefore, muscle force estimates are likely subject to greater measurement error and solely relying on these data to compute muscle forces can be

problematic (Gerus et al., 2013; Sartori et al., 2014). Since the EMG-assisted mode also allows muscle forces to deviate from measured EMG data to match the external knee flexion/extension torques derived from an inverse dynamics analysis, it is more robust. A direct comparison of the results obtained using both control modes, however, has not been reported for patients with medial dominant knee OA.

The purpose of this study was to evaluate a patient-specific NMSK computational modelling framework using EMG-driven and EMG-assisted NMSK control modes to study patients with medial dominant knee OA. It was hypothesized that the KJCFs estimated using EMG-driven and EMG-assisted NMSK control modes would differ because of differing muscle force estimates. Furthermore, we anticipated that KJCFs estimated using the EMG-assisted NMSK control mode would be more comparable to the literature collecting data from instrumented knee implants, as this control mode emphasises achieving greater consistency between external and internal joint torques.

2.3 Methodology

2.3.1 Participants

Twenty-seven patients (Table 2.1) with medial dominant knee OA who were undergoing rehabilitative and surgical interventions at the Fowler Kennedy Sport Medicine were recruited as a subgroup of patients from those already participating in a larger study (Primeau et al., 2020). Recruitment occurred after approval from the Research Ethics Board for Health Sciences Research Involving Human Subjects of the University of Western Ontario was obtained. Standing radiographs were taken by a radiology technician following standard procedures. Consistent rotation of the lower limb was achieved by having the patient maintain a forward knee position with the patella centered

on the femoral condyles (Hunt et al., 2008; A. Specogna et al., 2004; A., Specogna et al., 2007). Patients who had neutral to varus alignment and greater joint space narrowing in the medial tibiofemoral compartment were included. Patients were excluded if they had valgus alignment, joint replacement or high tibial osteotomy on either limb, multi-ligamentous instability, inflammatory or infectious arthritis of the knee, neurologic conditions affecting gait, or possible pregnancy.

Table 2.1 Patient Demographics and Clinical Characteristics

		Values (Mean ± SD)*
Patient Demographics	Age (years)	53 (± 5)
	Sex (male/female, # of patients)	(20/9)
	BMI (kg/m^2)***	29.8 (± 4.2)
	MAA**	-6.5 (± 1.8)
Clinical Characteristics	KL Scale Grade (N)****	1(4); 2(13); 3(12); 4(0)

*Values are the mean varus angle ± SD unless otherwise stated.

**MAA = mechanical axis angle. Negative values indicate varus.

*** BMI = body mass index.

****Kellgren & Lawrence (KL) scale grade of osteoarthritis severity.

2.3.2 Gait Data Collection

Lower extremity gait biomechanics were measured at the Wolf Orthopedic Biomechanics Laboratory at Western University and followed the overall framework detailed in Figure 2.1. During data collection, participants walked barefoot on level ground at their self-selected pace while EMG, kinematic, and kinetic data from the affected limb were collected. A minimum of 3 trials and a maximum of 5 trials were recorded. The kinematic data were collected using a 10-camera motion capture system (Motion Analysis Corporation, Santa Rosa, CA, USA) and a full-body passive reflective modified Helen Hayes marker set, sampled at 60Hz (Moyer et al., 2013). Kinetic data were collected using a floor-embedded force plate (AMTI, Watertown, MA, USA) and sampled at 600Hz. Surface EMG was collected across 8 channels to capture knee spanning muscle activations at 600Hz using Ag surface electrode pairs arranged in a bipolar configuration spaced 10 mm apart (Trigno, Delsys, Natick, MA). This system has an input impedance of 10 Giga Ohms, a common mode rejection ratio of 80dB at 60Hz (exceeding recommended minimum specifications) (De Luca, 1997), and a bandwidth of 20-450Hz. While EMG sampling rates >1000 Hz are usually recommended, comparisons of results computed using our musculoskeletal modelling framework with EMG data collected at 1200Hz and reanalyzed with EMG downsampled to 600 Hz demonstrated differences that were less than 1 N in the estimated KJCFs (based on four participants). Electrodes were placed over the muscle bellies of eight knee spanning muscles the rectus femoris (RF), vastus medialis (VM), vastus lateralis (VL), medial hamstring (MH), lateral hamstring (LH), medial gastrocnemius (MG), lateral gastrocnemius (LG), and

tibialis anterior (TA) on the limb that was being studied (Deluca, 1997). To provide a consistent standard for normalization of measured EMG data, maximum voluntary isometric contractions (MVICs), collected after gait trials, were used. Participants completed four exercises to elicit their MVIC for each muscle group (Rueterbories et al., 2010). For all muscle groups, participants were asked to sit in a chair with their knee flexed to approximately 90°. For the quadriceps muscle group (RF, VL, and VM), manual resistance was applied to the middle portion of the tibia as the participant was asked to kick their leg out and resist the force. For the hamstring muscle group (MH and LH) manual resistance was applied from the opposite direction and participants were asked to pull their leg in to resist the force. For the gastrocnemii, participants were asked to plantarflex their foot and resist a manual force applied to the bottom of the foot. Finally for the TA, participants were asked to dorsiflex their foot to resist a manual force applied to the top of the foot. MVIC Exercises were held for a minimum of 3 seconds and verbal encouragement was given.

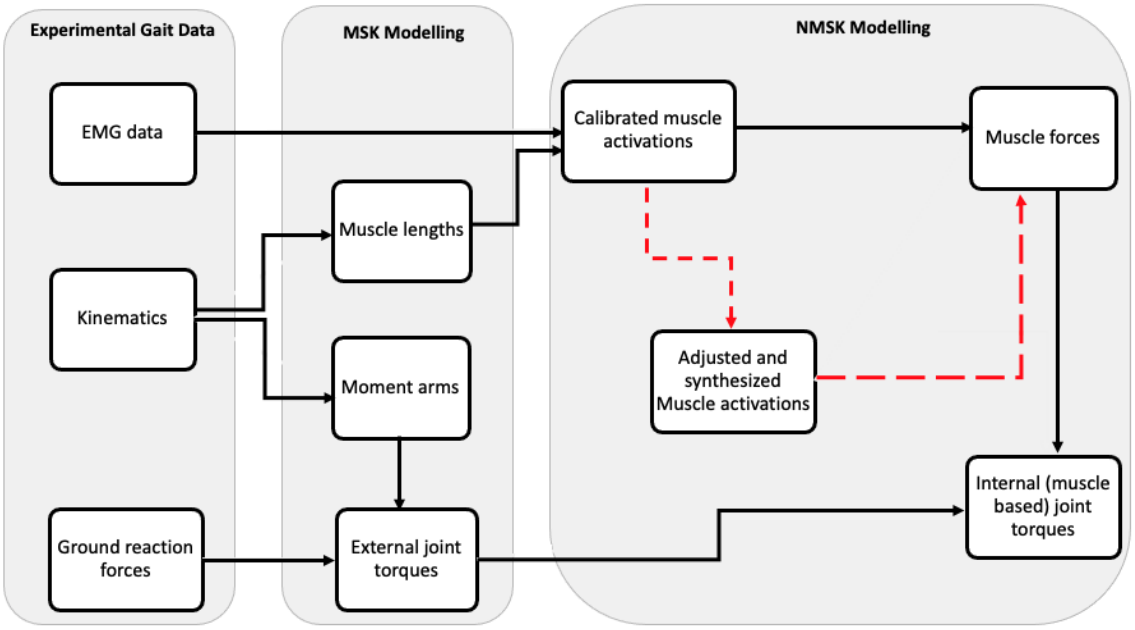

Figure 2.1 Overall framework to estimate joint contact forces. This includes gait data collection, data processing, musculoskeletal modelling in OpenSim, and neuromusculoskeletal modelling in CEINMS. The EMG-driven mode pathway is identified by a solid line. Deviations of the EMG-assisted mode follow the pathway identified by a dashed line.

2.4 Data Processing

Gait data were processed within MATLAB (The MathWorks, Inc. Natick MA) using the Motion Data Elaboration Toolbox for Musculoskeletal Applications (MOtoNMS) toolbox (Mantoan et al., 2015). The kinematic and kinetic data for all static and gait trials were lowpass filtered using a zero-lag 2nd order Butterworth filter with a cut-off frequency of 6Hz (Mantoan et al., 2015). The knee and ankle joint centers were obtained by taking the midpoint between the respective medial and lateral knee and ankle markers during the static trial. The position of the hip joint center was determined by a sphere fit of the

center of the knee relative to the pelvis during a leg swing trial using a custom MATLAB script.

To calculate linear envelopes representing muscle activation, EMG data were highpass filtered (20Hz lower cut-off), full wave rectified, and then lowpass filtered using a zero-lag 2nd order Butterworth filter with a 6Hz cut-off frequency (De Luca et al., 2010). Subsequently, all linear envelopes were amplitude-normalized to the maximum value of all recorded linear envelopes (considering MVIC and gait trials) for each muscle (Lloyd and Besier, 2003). All kinematic, kinetic, and EMG data from each trial were then truncated to include only the stance phase of gait (force plate heel strike to toe off) (Rueterbories et al., 2010), with a margin of 0.33 seconds added to the beginning and end of each trial. Electromyography data was visually screened at this stage of processing by a single investigator to ensure they fell within requirements outlined in the literature for neuromusculoskeletal modelling (Akhundov et al., 2019).

2.4.1 Musculoskeletal Modelling

2.4.1.1 Modifications to Base Model

Gait biomechanics were calculated using OpenSim v4.1 (Delp et al., 2007) using a generic musculoskeletal computational model (gait 2392) that was developed for a previous study of running dynamics (Hamner et al., 2010). The one degree of freedom (DOF) knee model was modified to allow the computation of three-dimensional knee torques and tibiofemoral contact forces (Saxby et al., 2016). Modifications occurred by adding an internal/external rotational DOF to the knee (15º and 5º, respectively), as described by Saxby et al. (2016). Additionally, knee abduction/adduction DOFs were added to allow net frontal plane joint torques and muscle tendon moment arms to be

calculated with respect to the medial and lateral compartments of the knee (Figure 2.2). Although the angle at the knee abduction/adduction DOF can be adjusted when scaling the model, they remained locked during motion analyses, in keeping with previous studies (Saxby et al., 2016). The first contact point, referred to as the medial contact point, was located on the medial femoral condyle to aid in calculation of medial compartment KJCFs. The second contact point, referred to as the lateral contact point, was located on the lateral portion of the tibial plateau to aid in the calculation of lateral compartment KJCFs. The location of each contact point on the tibial plateau of the generic model was adjusted to match the distance of the patient-specific medial and lateral femoral contact points from the joint center. These locations were obtained as the distance from the most prominent point of the femoral condyles to the knee joint center in each patient's radiograph (average medial compartment distance from the joint center = 23.9 ± 4.7mm, average lateral compartment distance from the joint center = 23.7 ± 6.5mm, average overall intercondylar distance = 47.6 ±8.7mm).

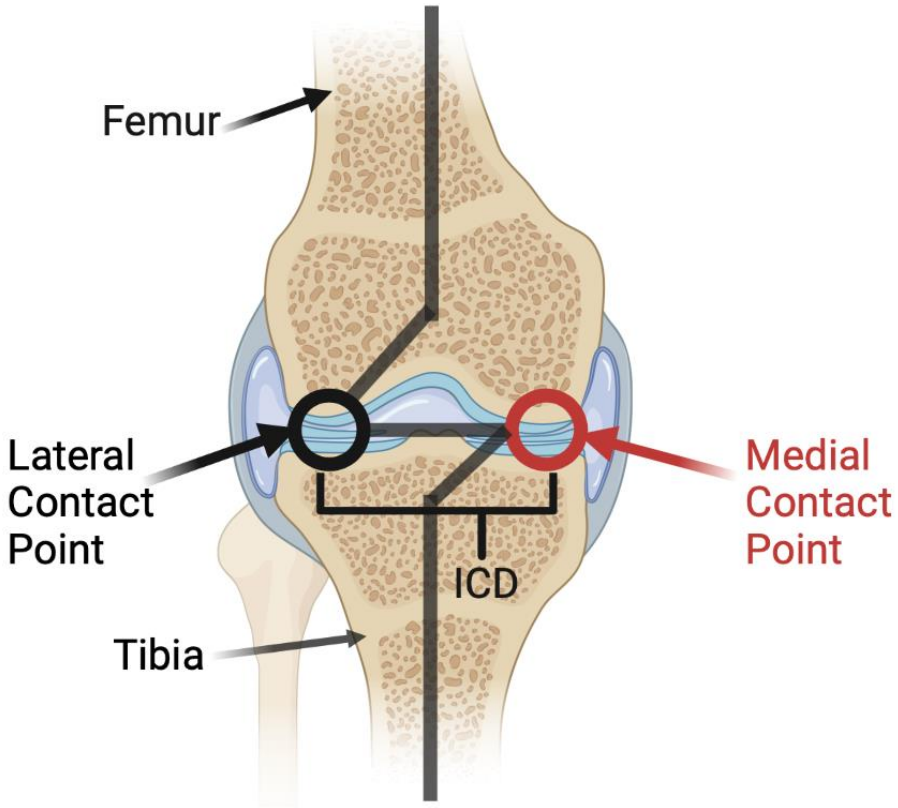

Figure 2.2 Adaptation of the Saxby et al. (2016) tibiofemoral mechanism. Two contact points are modelled as hinges. The two contact points allow joint forces and kinematics to be calculated about the medial (red circle) and lateral (black circle) compartment of the tibiofemoral joint. The two contact points are separated by the participant's patient-specific ICD (black bracket) obtained via hip to ankle radiograph. The segment corresponding to the medial contact point outlined in red was also modified to predict the participant's frontal plane alignment angle during scaling (Bowd et al., 2023). Created with biorender.com.

2.4.1.2 Model Scaling

The medial contact point was permitted to match the static pose data, thus accounting for the patient-specific frontal plane mechanical axis angle (MAA). This step was performed to account for the large knee varus angle within the inclusion criteria for this current study (Bowd et al., 2023). This step was also taken under the assumption that the deformity was primarily affecting the tibia segment (Bowd et al., 2023). Each model was then linearly scaled with the torso, pelvis, and foot segments scaled to the participant's height, and the thigh and shank segments linearly scaled to match the participant's marker positions in the static trial. After the model was scaled, the medial contact point was locked to the model-predicted MAA (mean of $7.6^{o} \pm 2.7^{o}$ varus).

2.4.2 Motion Analysis

Gait kinematic and kinetic data were provided as inputs to each scaled model to perform inverse kinematics (all markers were given a weight of 10) and dynamics analyses, and an analysis of the muscle-tendon unit kinematics (Saxby et al., 2016). Following previously described OpenSim best practices (Hicks et al., 2015), marker errors were reviewed, and 2 participants were excluded as they had either a total square marker error over 2cm (average total square error for remaining patients = 0.5 ±0.7cm) or a maximum marker error RMS over 4cm (average maximum marker error RMS for remaining patients = 1.5 ±0.8cm).

2.4.3 Neuromusculoskeletal Modelling

The OpenSim-computed kinematic and sagittal plane inverse dynamics results, along with corresponding experimentally collected EMG activations were then provided as inputs to the Calibrated Electromyography Informed Neuromusculoskeletal Modelling

Toolbox (CEINMS) for simulations using both the EMG-driven and the EMG-assisted neuromusculoskeletal (NMSK) control modes (Pizzolato et al., 2015). Eight lower extremity EMG linear envelopes were mapped to 11 MTU excitations in the model for both control modes (Lloyd and Besier, 2003). The vastus intermedius was derived from the average of the vastus medialis and vastus lateralis waveforms, the medial hamstring waveform was assumed for both the semimembranosus and semitendinosus excitations, and the lateral hamstring waveform was assumed for both the biceps femoris short and long head excitations (Sartori et al., 2014). When a muscle crosses multiple joints, its activation level depends not just on the torque-demands of the knee, but also the torque demands and forces crossing the complementary joint. To account for this (for the EMG-assisted mode only), the remaining lower extremity muscle activations that corresponded to 32 MTUs, were synthesized to improve the prediction of muscle forces that also span the hip and ankle joints. These additional MTUs were not included with the EMG-driven mode. Using the technique described by Gerus et al. (2013), activation dynamics and muscular model parameters were functionally calibrated to minimize a cost function that used sagittal plane joint torques. Models were calibrated using input data from a single trial (the first gait trial) for each participant and weighting coefficients were adjusted based on the error between model inputs to outputs.

The subject-specific NMS models were then executed in CEINMS using both the EMG-driven and the EMG-assisted NMSK control modes for the remaining (2-4) gait trials that were not used during calibration. For the EMG-driven mode, the 11 experimentally-collected activations and the kinematic data were used to drive the computation of muscle forces by deriving neural excitations from the activations to model the muscle's twitch

response (Ceseracciu and Reggiani, 2015; Pizzolato et al., 2015). The MTU kinematics and muscle activations were then used as an input for a Hill-type muscle activation model (Pizzolato et al., 2015).

The EMG-assisted mode was driven by all 43 MUTS and was driven using an objective function (Equation 2.1) that included three components (Sartori et al., 2014).

$$F_{obj} = \sum_{d}^{DOFs} \alpha \, (\overline{M_d} - M_d)^2 + \sum_{j}^{MTUsynth} \beta \; e_j^2 + \sum_{k}^{MTUadj} \gamma \; (\overline{e_k} - e_k)^2 + \beta e_k^2 \quad (2.1)$$

Each component provided the ability to adjust its weighting (or importance) during minimization using α, β, and γ coefficients. The α coefficient scaled the importance of minimization of squared differences between OpenSim computed external joint torques and CEINMS computed internal joint torques ($\sum_{d}^{DOFs} \alpha \, (\overline{M_d} - M_d)^2$). The β coefficient scaled the importance of minimization of the sum of absolute differences between adjusted and experimentally collected activations ($\sum_{j}^{MTUsynth} \beta \; e_j^2$). The γ coefficient scaled the importance of the minimization of the sum of squared activations for all 32 predicted MTUs ($\sum_{k}^{MTUadj} \gamma \; (\overline{e_k} - e_k)^2 + \beta e_k^2$) (Ceseracciu and Reggiani, 2015; Sartori et al., 2014). Within our study, the α coefficient was held constant (α = 1), following CEINMS guidelines (Ceseracciu and Reggiani, 2015). The β and γ coefficients were both set to 1.5, based on an analysis that manually varied coefficient values greater than 1 to find the lowest values of the weighted sum across n = 5 participants; a method that was previously described by others (Sartori et al., 2014). CEINMS-computed outputs for each NMSK control mode included adjusted muscle activations and sagittal plane

torques, and predicted muscle forces. Data were cropped to the stance phase only (removing the 0.33s before/after data margin previously included).

2.4.4 Joint Contact Force Analysis

CEINMS-computed muscle forces and net knee spanning muscle torques (n=11 MTUs for the EMG-driven mode and *n*=13 MTUs for the EMG-assisted mode) from the subject-specific NMSK models were then provided as inputs to an established algorithm for computing medial (F^{MC}) and lateral (F^{LC}) KJCFs (Winby et al., 2009). These internal contact forces were calculating using equations 2.2 and 2.3:

$$F^{MC} = \frac{M_{MTU}^{LC} - M_{EXT}^{LC}}{d_{IC}} \quad \text{and} \quad F^{LC} = \frac{M_{MTU}^{MC} - M_{EXT}^{MC}}{d_{IC}} \tag{2.2}$$

where

$$M_{MTU}^{LC} = \sum_{i=1}^{n} F_{MTU}(i) r_{MTU}^{LC}(i) \quad \text{and} \quad M_{MTU}^{MC} = \sum_{i=1}^{n} F_{MTU}(i) r_{MTU}^{MC}(i) \tag{2.3}$$

Where *F* represents the contact force, M_{MTU}^{LC} represents the abduction/adduction moment arms of the *i*th MTU about the lateral contact point and M_{MTU}^{MC}, the medial, and d_{IC} represents the intercondylar distance. M_{EXT}^{LC}represents the external abduction/adduction moments around the lateral contact point and M_{EXT}^{MC}, the medial (Lloyd and Buchanan, 2001, 1996). F_{MTU} represents the muscle force and r_{MTU}^{LC} and r_{MTU}^{MC} represents the moment arms (lateral compartment and medial compartment, respectively) for the eleven (11) MTUs that were included to account for the knee spanning muscles.

The overall knee contact force was calculated by adding the medial and lateral compartment contact forces for each participant. Resulting knee joint contact forces

(KJCFs) were then time normalized to 100 points across the stance phase and amplitude normalized to the participant's body weight (BW). This was repeated for data obtained using both the EMG-driven and the EMG-assisted NMSK control modes. The first and second peaks of the overall and medial compartment KJCFs were then recorded by extracting the highest value in the first and second half of the stance phase, respectively. For the lateral compartment KJCF, the first peak was extracted as the highest value from the first 20% of the stance phase and the second peak was extracted as the highest value between 50 to 90% of the cycle. These portions of the stance phase were extracted based on a previous study examining the effects of a surgical intervention on patients with knee OA that identified statistically significant differences in lateral compartment KJCFs within these ranges of the stance phase (De Pieri et al., 2023).

2.5 Data Analysis

The knee flexion/extension torques computed by both OpenSim (external knee flexion/extension torques) and CEINMS (internal knee flexion/extension torques) using both the EMG-driven and EMG-assisted NMSK control modes were time-normalized to 100 points across the stance phase of gait. Coefficient of determination (R^2) and root mean square error (RMSE) were then calculated for internal knee flexion/extension torques computed with each NMSK control mode (EMG-assisted and EMG-driven NMSK control modes) versus the external knee flexion/extension torques, for a measure of the model's flexion torque prediction accuracy. Differences in RMSE and R^2 for the knee flexion/extension torques and first and second peak KJCFs between control modes were tested using paired samples *t*-tests. The threshold for statistical significance was set to 0.05.

2.6 Results

2.6.1 Knee Flexion/Extension Torque Model Prediction Accuracy

There was a statistically significant improvement in model flexion torque prediction accuracy (p = 0.001) when using the EMG-assisted (RMS error of 2.7 ±2.1Nm) versus the EMG-driven (RMS error of 12.6 ±3.9Nm) NMSK control mode (Figure 2.3). Additionally, there was a statistically significant decrease (p = 0.001) in the correlations between external and internal knee flexion/extension torques using the EMG-driven NMSK control mode (R^2=0.6 ±0.2) when compared to the EMG-assisted NMSK control mode (R^2=0.9 ±0.1).

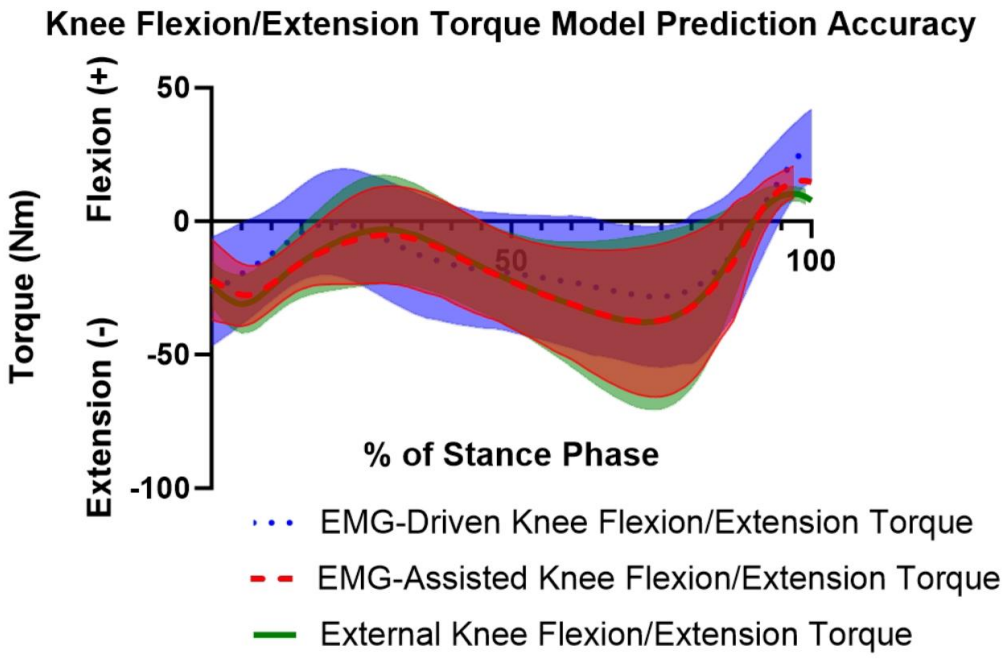

Figure 2.3 Ensemble mean (±SD) waveforms for knee flexion/extension torques computed by EMG-driven and EMG-assisted NMSK control modes and external knee

flexion/extension torques computed by OpenSim with torque (Nm) on the vertical axis and % of stance phase on the horizontal axis.

2.6.2 Knee Joint Contact Forces

Ensemble average KJCF waveforms for the EMG-driven and EMG-assisted NMSK control modes are presented in Figure 2.4 and comparisons are presented in Table 2.2. There were no statistically significant differences between KJCFs computed by both control modes. The largest difference occurred in the second peak of the medial compartment KJCF where EMG-assisted control mode calculated a greater first peak in the lateral compartment joint contact forces (2.3 ± 1.1BW) than the EMG-driven control mode (2.1 ± 0.9BW).

a.

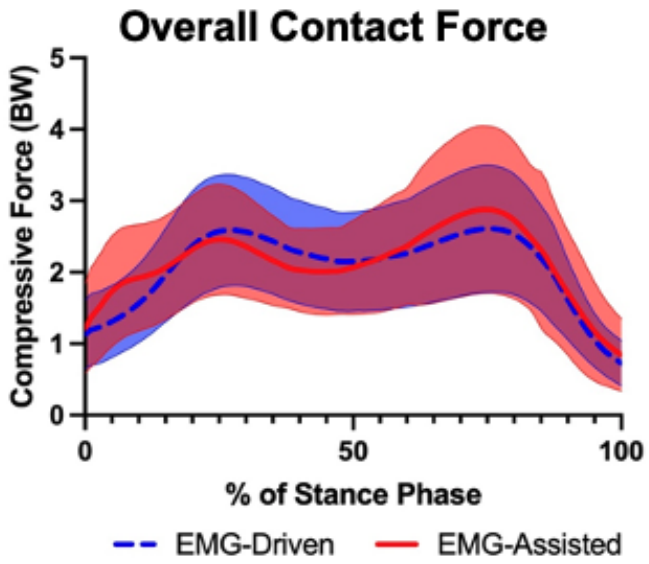
Overall Contact Force
Compressive Force (BW)
5
4
3
2
1
0
0
50
100
% of Stance Phase
EMG-Driven
EMG-Assisted

b.

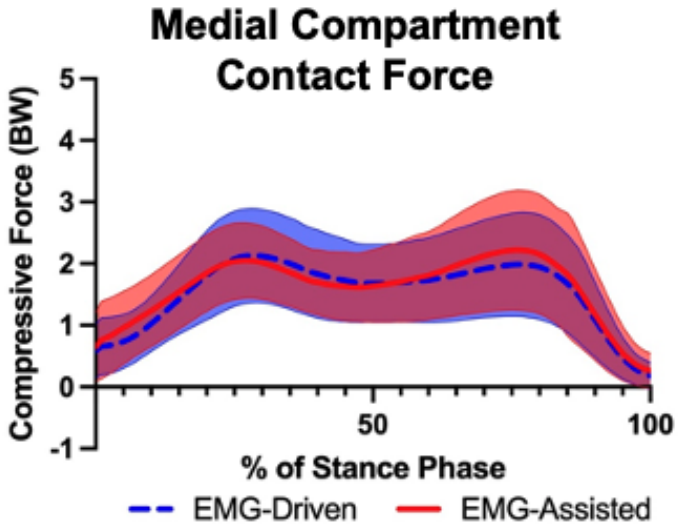
Medial Compartment Contact Force
Compressive Force (BW)
5
4
3
2
1
0
-1
50
100
% of Stance Phase
EMG-Driven
EMG-Assisted

c.

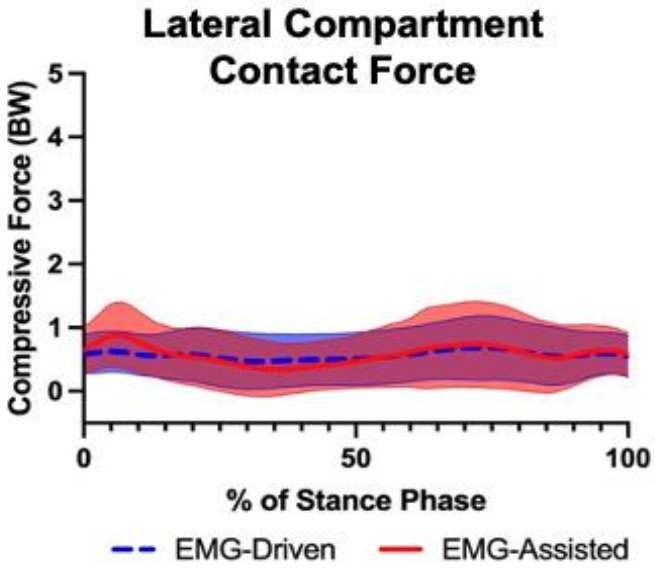

Figure 2.4 Ensemble mean (±SD) waveforms for a. Overall contact force, b. Medial compartment contact force, and c. Lateral compartment contact force computed by EMG-driven and EMG-assisted NMSK control modes with contact force (BW) on the y-axis and % of stance phase on the x-axis.

Table 2.2 Descriptive Statistics and Dependent Samples *t*-Test Results for Total, Medial, and Lateral Compartment Contact Forces for EMG-Driven and EMG-Assisted NMSK Control Modes

		EMG-Driven (BW) (±SD)	EMG-Assisted (BW) (±SD)	*p*-value
Overall Contact Force	First Peak	2.7 (± 0.8)	2.6 (± 0.8)	0.53
	Second Peak	2.7 (± 0.9)	2.9 (± 1.2)	0.55
Medial Compartment Contact Force	First Peak	2.2 (± 0.8)	2.1 (± 0.7)	0.26
	Second Peak	2.1 (± 0.9)	2.3 (± 1.1)	0.06
Lateral Compartment Contact Force	First Peak	0.8 (± 0.4)	0.9 (± 0.5)	0.08
	Second Peak	0.9 (± 0.5)	1.0 (± 0.6)	0.35

Values are presented as mean (±SD) and mean [95%CI], *p*-value.

2.7 Discussion

This study evaluated results from patient-specific computational NMSK models using two simulated NMSK control modes in patients with medial dominant knee OA. When first evaluating consistency in external versus internal knee flexion/extension torques as a

measure of model prediction accuracy, the EMG-assisted NMSK control mode had a statistically significant lower RMSE and higher R^2 than the EMG-driven NMSK control mode. Based on a previous study (Sartori et al., 2014) and the respective emphases of the different NMSK control mode algorithms, this finding was expected. The EMG-driven mode does not incorporate external knee flexion/extension torques in its calculation and predicts internal knee flexion/extension torques and muscle forces based on experimentally collected EMG (11 MTUs) and kinematic data (Ceseracciu and Reggiani, 2015). In addition, it appears a phase shift occurred within the EMG-driven NMSK control mode's knee flexion torques compared to the external and EMG-assisted NMSK knee flexion torques. It is possible that this phase shift occurred as the EMG-driven NMSK mode solely relies on muscle activations to predict muscle forces. Furthermore, this control mode may have been more sensitive to an increased muscle activation that occurs to stabilize the leg in the early stance phase to prepare for impact with the ground. The EMG-assisted mode, however, seeks to minimize errors between external and internal torques, computed muscle activations (11MTUs), and synthesized muscle activations (32 MTUs) (Ceseracciu and Reggiani, 2015). Therefore, it is understandable why this NMSK control mode would predict a closer comparison to the external knee flexion/extension torques.

When comparing the error between external and internal knee flexion/extension torques computed using the EMG-driven control mode to that previously described by others, our RMSE values of 12.6 ±3.9Nm were comparable to the range of 10-13Nm that has been cited previously when using a similar model of gait of patients with knee OA (Gerus et al., 2013b). When comparing our EMG-assisted modelling results to a previous study

using a similar model, our RMSE values of 2.7 ±2.1Nm were larger than what has been previously reported (knee flexion/extension torques of >0.1Nm) in hip OA and healthy populations (Hoang et al., 2019; Pizzolato et al., 2015). Differences between these previous studies and our current study are potentially related to differences in data collection procedures and modelling frameworks. Furthermore, both of those studies collected experimental EMG signals from 16 muscles of the same limb whereas our current study collected from only 8 muscles and synthesized values for the remainders. Both previous studies also included a more detailed marker set and utilized a different generic model in OpenSim (gait2392). Combined, these factors may have strengthened the consistency of internal to external knee flexion/extension torques of the previous studies (Hoang et al., 2019; Pizzolato et al., 2015). Still, when assessing the coefficient of determination (R^2) results, our EMG-assisted results were comparable to previous literature and indicate a strong correlation and therefore a high amount of consistency between external knee flexion/extension torques and internal knee flexion/extension torques (Hoang et al., 2019; Sartori et al., 2014).

Between the two control modes, there were no statistically significant differences within the overall knee and medial and lateral compartment KJCFs. Larger differences were expected between the predicted KJCFs from each control mode due to their differing method of predicting muscle forces. As mentioned previously, the EMG-driven control mode only relies on experimentally-collected activations and kinematics to predict muscle forces. The KJCF equations for both NMSK control modes; however, considered external knee flexion/extension torques to calculate KJCFs. Therefore, although

differences occurred within the muscle force predictions, it appears that these differences were not significant in the KJCF predictions.

Our EMG-driven (first peak=2.7 ± 0.8BW, second peak=2.7 ± 0.9BW) and EMG-assisted (first peak=2.6 ± 0.8BW, second peak=2.9 ± 1.2BW) NMSK control modes' computed overall KJCFs were within the approximate range (1.8BW to 3.5BW for the first peak and 1.9BW to 4.8BW for the second peak) previously identified in patients with hip and knee OA, that also used EMG-driven and -assisted NMSK control modes (Hall et al., 2019; Hoang et al., 2019). When comparing medial compartment KJCFs, our EMG-driven (first peak=2.2 ± 0.8BW), second peak=2.1 ± 0.9BW) and EMG-assisted (first peak=2.1 ± 0.7BW, second peak=2.3 ± 1.1BW) NMSK mode's results were once again within the approximate range for the first peaks (1.6 to 2.7BW) and slightly over the range for the second peaks (0.9 to 1.9BW) described in previous studies (Hall et al., 2019; Hoang et al., 2019; S. Starkey et al., 2022, 2022). Finally, when comparing our lateral compartment results, both our EMG-driven (first peak=0.8 ± 0.4BW, second peak=0.9 ± 0.5BW) and EMG-assisted (first peak=0.9 ± 0.5BW, second peak=1.0 ± 0.6BW) NMSK mode's results were still lower than the peak value of 1.2BW that was reported in previous studies evaluating patients with knee OA (Hall et al., 2019).

This study has limitations. Our EMG-driven NMSK control mode results are compared to studies that included experimentally-collected EMG data for a greater number of muscles. Regardless of this potential shortcoming, our EMG-assisted NMSK control mode's results were comparable to the previous literature and did not appear to be impacted. Additionally, we were unable to directly compare our knee joint contact forces with instrumented implant data. Our conclusions, however, are directly compared to

previous literature reporting knee joint contact forces that were verified by instrumented knee implant data within the same population (Hall et al., 2019; S. Starkey et al., 2022; S. C. Starkey et al., 2022).

2.8 Conclusion

The EMG-assisted NMSK control mode provided greater model prediction accuracy when comparing external to internal knee flexion/extension torques than the EMG-driven control mode and comparable KJCF predictions when compared to other literature reporting instrumented knee implant data and models of patients with OA. Our results support the use of an EMG-assisted NMSK control mode over an EMG-driven NMSK control mode when evaluating KJCFs in patients with medial dominant knee OA.

2.9 References

Akhundov, R., Saxby, D.J., Edwards, S., Snodgrass, S., Clausen, P., Diamond, L.E., 2019. Development of a deep neural network for automated electromyographic pattern classification. J. Exp. Biol. 222, 1–5. https://doi.org/10.1242/jeb.198101

Andriacchi, T.P., 1994. Dynamics of knee malalignment. Orthop Clin North Am 25, 395–403.

Andriacchi, T.P., Mündermann, A., 2006. The role of ambulatory mechanics in the initiation and progression of knee osteoarthritis. Curr. Opin. Rheumatol. 18, 514–518. https://doi.org/10.1097/01.bor.0000240365.16842.4e

Bowd, J., Van Rossom, S., Williams, D., Elson, D., Wilson, C., Whatling, G., Holt, C., Jonkers, I., 2023. Using musculoskeletal modelling to estimate knee joint loading pre and post high tibial osteotomy. Clin. Biomech. 101, 105855. https://doi.org/10.1016/j.clinbiomech.2022.105855

Ceseracciu, E., Reggiani, M., 2015. CEINMS User Guide Documentation 1–58.

De Luca, C. J. (1977). The use of surface electromyography in biomechanics. *Journal of Applied Biomechanics*, *13*(2), 135–163. https://doi.org/10.1123/jab.13.2.135

De Luca, C.J., Donald Gilmore, L., Kuznetsov, M., Roy, S.H., 2010. Filtering the surface EMG signal: Movement artifact and baseline noise contamination. J. Biomech. 43, 1573–1579. https://doi.org/10.1016/j.jbiomech.2010.01.027

De Pieri, E., Nüesch, C., Pagenstert, G., Viehweger, E., Egloff, C., Mündermann, A., 2023. High tibial osteotomy effectively redistributes compressive knee loads during walking. J. Orthop. Res. 41, 591–600. https://doi.org/10.1002/jor.25403

Delp, S.L., Anderson, F.C., Arnold, A.S., Loan, P., Habib, A., John, C.T., Guendelman, E., Thelen, D.G., 2007. OpenSim: Open-source software to create and analyze dynamic simulations of movement. IEEE Trans. Biomed. Eng. 54, 1940–1950. https://doi.org/10.1109/TBME.2007.901024

Gerus, P., Sartori, M., Besier, T.F., Fregly, B.J., Delp, S.L., Banks, S.A., Pandy, M.G., D'Lima, D.D., Lloyd, D.G., 2013. Subject-specific knee joint geometry improves predictions of medial tibiofemoral contact forces. J. Biomech. 46, 2778–2786. https://doi.org/10.1016/j.jbiomech.2013.09.005

Hall, M., Diamond, L.E., Lenton, G.K., Pizzolato, C., Saxby, D.J., 2019. Immediate effects of valgus knee bracing on tibiofemoral contact forces and knee muscle forces. Gait Posture 68, 55–62. https://doi.org/10.1016/j.gaitpost.2018.11.009

Hamner, S.R., Seth, A., Delp, S.L., 2010. Muscle contributions to propulsion and support during running. J. Biomech. 43, 2709–2716. https://doi.org/10.1016/j.jbiomech.2010.06.025

Hicks, J.L., Uchida, T.K., Seth, A., Rajagopal, A., Delp, S.L., 2015. Is my model good enough? Best practices for verification and validation of musculoskeletal models and simulations of movement. J. Biomech. Eng. 137, 1–24. https://doi.org/10.1115/1.4029304

Hoang, H.X., Diamond, L.E., Lloyd, D.G., Pizzolato, C., 2019. A calibrated EMG-informed neuromusculoskeletal model can appropriately account for muscle co-contraction in the estimation of hip joint contact forces in people with hip osteoarthritis. J. Biomech. 83, 134–142. https://doi.org/10.1016/j.jbiomech.2018.11.042

Holder, J., Van Drongelen, S., Uhlrich, S.D., Herrmann, E., Meurer, A., Stief, F., 2023. Peak knee joint moments accurately predict medial and lateral knee contact forces in patients with valgus malalignment. Sci. Rep. 13, 2870. https://doi.org/10.1038/s41598-023-30058-4

Hunt, M. A., Birmingham, T. B., Jenkyn, T. R., Giffin, J. R., & Jones, I. C. (2008). Measures of frontal plane lower limb alignment obtained from static radiographs and dynamic gait analysis. *Gait & Posture*, *27*(4), 635–640. https://doi.org/10.1016/j.gaitpost.2007.08.011

Kutzner, I., Trepczynski, A., Heller, M.O., Bergmann, G., 2013. Knee adduction moment and medial contact force-facts about their correlation during gait. PLoS ONE 8, 8–15. https://doi.org/10.1371/journal.pone.0081036

Lewek, M.D., Rudolph, K.S., Snyder-Mackler, L., 2004. Control of frontal plane knee laxity during gait in patients with medial compartment knee osteoarthritis. Osteoarthritis Cartilage 12, 745–751. https://doi.org/10.1016/j.joca.2004.05.005

Lloyd, D.G., Besier, T.F., 2003. An EMG-driven musculoskeletal model to estimate muscle forces and knee joint moments in vivo. J. Biomech. 36, 765–776. https://doi.org/10.1016/S0021-9290(03)00010-1

Lloyd, D.G., Buchanan, T.S., 2001. Strategies of muscular support of varus and valgus isometric loads at the human knee. J. Biomech. 34, 1257–1267. https://doi.org/10.1016/S0021-9290(01)00095-1

Lloyd, D.G., Buchanan, T.S., 1996. A model of load sharing between muscles and soft tissues at the human knee during static Tasks. J. Biomech. Eng. 118, 367–376. https://doi.org/10.1115/1.2796019

Madry, H., 2022. Surgical therapy in osteoarthritis. Osteoarthritis Cartilage 30, 1019–1034. https://doi.org/10.1016/j.joca.2022.01.012

Mantoan, A., Pizzolato, C., Sartori, M., Sawacha, Z., Cobelli, C., Reggiani, M., 2015. MOtoNMS: A MATLAB toolbox to process motion data for neuromusculoskeletal modeling and simulation. Source Code Biol. Med. 10, 1–14. https://doi.org/10.1186/s13029-015-0044-4

Marriott, K.A., Birmingham, T.B., 2023. Fundamentals of osteoarthritis. Rehabilitation: Exercise, diet, biomechanics, and physical therapist-delivered interventions. Osteoarthritis Cartilage S1063458423008518. https://doi.org/10.1016/j.joca.2023.06.011

Miyazaki, T., Wada, M., Kawahara, H., Sato, M., Baba, H., Shimada, S., 2002. Dynamic load at baseline can predict radiographic disease progression in medial

compartment knee osteoarthritis. Ann. Rheum. Dis. 61, 617–622. https://doi.org/10.1136/ard.61.7.617

Moyer, R.F., Birmingham, T.B., Dombroski, C.E., Walsh, R.F., Leitch, K.M., Jenkyn, T.R., Giffin, J.R., 2013. Combined Effects of a Valgus Knee Brace and Lateral Wedge Foot Orthotic on the External Knee Adduction Moment in Patients With Varus Gonarthrosis. Arch. Phys. Med. Rehabil. 94, 103–112. https://doi.org/10.1016/j.apmr.2012.09.004

Pizzolato, C., Lloyd, D.G., Sartori, M., Ceseracciu, E., Besier, T.F., Fregly, B.J., Reggiani, M., 2015. CEINMS: A toolbox to investigate the influence of different neural control solutions on the prediction of muscle excitation and joint moments during dynamic motor tasks. J. Biomech. 48, 3929–3936. https://doi.org/10.1016/j.jbiomech.2015.09.021

Primeau, C.A., Birmingham, T.B., Moyer, R.F., O'Neil, K.A., Werstine, M.S., Alcock, G.K., Giffin, J.R., 2020. Trajectories of perceived exertion and pain over a 12-week neuromuscular exercise program in patients with knee osteoarthritis. Osteoarthritis Cartilage 28, 1427–1431. https://doi.org/10.1016/j.joca.2020.07.011

Rueterbories, J., Spaich, E.G., Larsen, B., Andersen, O.K., 2010. Methods for gait event detection and analysis in ambulatory systems. Med. Eng. Phys. 32, 545–552. https://doi.org/10.1016/j.medengphy.2010.03.007

Sartori, M., Farina, D., Lloyd, D.G., 2014. Hybrid neuromusculoskeletal modeling to best track joint moments using a balance between muscle excitations derived from

electromyograms and optimization. J. Biomech. 47, 3613–3621. https://doi.org/10.1016/j.jbiomech.2014.10.009

Saxby, D.J., Modenese, L., Bryant, A.L., Gerus, P., Killen, B., Fortin, K., Wrigley, T.V., Bennell, K.L., Cicuttini, F.M., Lloyd, D.G., 2016. Tibiofemoral contact forces during walking, running and sidestepping. Gait Posture 49, 78–85. https://doi.org/10.1016/j.gaitpost.2016.06.014

Specogna, A., Birmingham, T., DaSilva, J., Milner, J., Kerr, J., Hunt, M., Jones, I., Jenkyn, T., Fowler, P., & Giffin, J. (2004). Reliability of Lower Limb Frontal Plane Alignment Measurements Using Plain Radiographs and Digitized Images. *The Journal of Knee Surgery*, *17*(04), 203–210. https://doi.org/10.1055/s-0030-1248222

Specogna, A., Birmingham, T. B., Hunt, M. A., Jones, I. C., Jenkyn, T. R., Fowler, P. J., & Giffin, J. R. (2007). Radiographic Measures of Knee Alignment in Patients with varus Gonarthrosis: Effect of Weightbearing Status and Associations with Dynamic Joint Load. *The American Journal of Sports Medicine*, *35*(1), 65–70. https://doi.org/10.1177/0363546506293024

Starkey, S., Hinman, R., Paterson, K., Saxby, D., Knox, G., Hall, M., 2022. Tibiofemoral contact force differences between flat flexible and stable supportive walking shoes in people with varus-malaligned medial knee osteoarthritis: A randomized cross-over study. PLoS ONE 17, 1–20. https://doi.org/10.1371/journal.pone.0269331

Starkey, S.C., Diamond, L.E., Hinman, R.S., Saxby, D.J., Knox, G., Hall, M., 2022. Muscle forces during weight-bearing exercises in medial knee osteoarthritis and varus malalignment: A cross-sectional study. Med. Sci. Sports Exerc. 54, 1448–1458. https://doi.org/10.1249/MSS.0000000000002943

Walter, J.P., D'Lima, D.D., Colwell, C.W., Fregly, B.J., 2010. Decreased knee adduction moment does not guarantee decreased medial contact force during gait. J. Orthop. Res. 28, 1348–1354. https://doi.org/10.1002/jor.21142

Winby, C.R., Lloyd, D.G., Besier, T.F., Kirk, T.B., 2009. Muscle and external load contribution to knee joint contact loads during normal gait. J. Biomech. 42, 2294–2300. https://doi.org/10.1016/j.jbiomech.2009.06.019

Zhao, D., Banks, S.A., Mitchell, K.H., D'Lima, D.D., Colwell, C.W., Fregly, B.J., 2007. Correlation between the knee adduction torque and medial contact force for a variety of gait patterns. J. Orthop. Res. 25, 789–797. https://doi.org/10.1002/jor.20379

Chapter 3

3 The Effect of Adjusting Frontal Plane Knee Alignment When Scaling Patient-Specific Neuromusculoskeletal Models in Patients with Knee Osteoarthritis

3.1 Summary

After determining which NMSK control mode was more appropriate to use when evaluating patients with medial dominant knee osteoarthritis (OA), the next step in developing the EMG-informed NMSK modelling framework within this thesis was to explore the effect of adjusting patient-specific frontal plane alignment of the models. Abnormal frontal plane alignment is associated with increased medial tibiofemoral compartment loading during ambulation in patients with knee OA. Patient-specific neuromusculoskeletal (NMSK) computational models provide an estimate of these loads as they cannot be easily measured. There is limited literature exploring the effect of adjusting frontal plane alignment to improve patient specificity of EMG-assisted NMSK models. The purpose of this study was to compare knee flexion/extension joint torques and knee joint contact forces (KJCFs) computed using a patient-specific EMG-assisted NMSK model with an assumed neutral frontal plane alignment and a patient-specific frontal plane alignment in patients with varus alignment and medial dominant knee OA. Gait data were collected from 27 patients with medial dominant knee OA. A generic musculoskeletal model with a neutral frontal plane alignment was scaled for each patient in OpenSim. A second patient-specific varus (PSV) model was created where patient-specific frontal plane alignment was predicted for during scaling. Gait kinematic and kinetic data were provided as inputs to inverse kinematics and inverse dynamics analyses. OpenSim-computed results, along with corresponding experimental muscle activations,

were provided as inputs to the Calibrated Electromyography Informed Neuromusculoskeletal Modelling Toolbox (CEINMS) for both models.

A statistically significant difference in static pose hip abduction angle was found, with the neutral model's being significantly lower (by 2.8°) than the PSV model's. Model computed knee flexion/extension torques and knee joint contact forces (KJCFs) were not statistically significantly different. An observable increase of 0.1 BW in the overall KJCFs and 0.1BW in the medial compartment the lateral compartment JKCFs occurred for the PSV model.

As there were no statistically significant differences in the predicted KJCFs between models, it appears that potential changes in KJCFs do not occur after adjusting this parameter. Future literature evaluating the sensitivity of patient-specific model parameters might identify parameters that contribute to a larger difference.

3.2 Introduction

There is a strong association between abnormal frontal plane alignment and OA progression, which has been observed to increase loading in the medial compartment of the knee joint (Miyazaki, 2002; Sharma et al., 1998; Van Rossom et al., 2019). Patient-specific neuromusculoskeletal (NMSK) computational models offer a means to estimate these loads as they cannot easily be measured in the intact knee (Gerus et al., 2013; Pizzolato et al., 2015; Saxby et al., 2016). Previous studies have indicated that musculoskeletal models with generic knee joint characteristics overestimate modeled KJCFs (up to 1500N) when compared with KJCFs measured directly using load-sensing implants (Fregly et al., 2012; Gerus et al., 2013; Lerner et al., 2015). Increasing the patient-specificity of NMSK models has been found to improve KJCF prediction

accuracy in the first peak of the medial and lateral compartment KJCFs by 51% and 30%, respectively (Gerus et al., 2013; Lerner et al., 2015). Thus, when using NMSK models to estimate medial and lateral compartment knee KJCFs, tailoring the models to the participants is important for obtaining sufficient accuracy (Lerner et al., 2015; Saliba et al., 2017; Saxby et al., 2016).

Previous studies accounting for patient-specific frontal plane alignment in patients with knee OA while walking have been conducted only on models undergoing static optimization or EMG-driven modelling approaches. EMG-driven models use experimentally-collected EMG activations and the kinematic data in their computations of muscle forces (Ceseracciu and Reggiani, 2015). EMG-assisted models, however, simulate muscle forces using an objective function that balances tracking in terms of both muscle activations and joint torques (Sartori et al., 2014). Additionally, this model estimates excitation patterns for musculotendon units that were not measured experimentally (Ceseracciu and Reggiani, 2015; Pizzolato et al., 2015). To our knowledge, there is no current study exploring the effect of adjusting frontal plane alignment in EMG-assisted NMSK models to improve patient specificity for patients with medial dominant knee OA and varus alignment. The purpose of this study was to compare patient-specific EMG-assisted NMS models incorporating actual versus assumed neutral (0^o) frontal plane alignment in patients with varus alignment and medial dominant knee OA. It was hypothesized that model-based joint contact force distributions would be different when using a neutral frontal plane alignment versus the true patient-specific frontal plane alignment.

3.3 Methodology

3.3.1 Participants

Twenty-seven patients meeting the clinical criteria for knee OA (Table 3.1) were recruited from the Fowler Kennedy Sport Medicine Clinic (Birmingham et al., 2017; Primeau et al., 2020). Standing radiographs were taken by a radiology technician following standard procedures. Consistent rotation of the lower limb was achieved by having the patient maintain a forward knee position with the patella centered on the femoral condyles (Hunt et al., 2008; A. Specogna et al., 2004; A., Specogna et al., 2007). Eligible patients had greater joint space narrowing in the medial tibiofemoral compartment than the lateral compartment and varus alignment. They also were currently undergoing rehabilitative and surgical interventions. Patients were excluded if they had valgus alignment, joint replacement or high tibial osteotomy on either limb, multi-ligamentous instability, inflammatory or infectious arthritis of the knee, neurologic conditions affecting gait, or possible pregnancy. This study was approved by the Western University Research Ethics Board for Health Sciences Research Involving Human Subjects.

Table 3.1 Patient Demographics and Clinical Characteristics

		Values (Mean ± SD)*
Patient Demographics	Age (years)	53 (± 5)
	Sex (male/female, N of patients)	(20/9)
	BMI (kg/m^2)**	29.8 (± 4.2)
	MAA***	-6.5 (± 1.8)
Clinical Characteristics	KL Scale Grade (N)****	1(4); 2(13); 3(13); 4(0)

*Values are the mean MAA varus angle ± SD unless otherwise stated.

**BMI = body mass index.

***MAA = mechanical axis angle. Negative values indicate varus.

****Kellgren & Lawrence (KL) scale grade of osteoarthritis severity.

3.3.2 Gait Data Collection

Data collection occurred at the Wolf Orthopaedic Biomechanics Laboratory at Western University where lower extremity gait biomechanics were measured. These data then followed the overall framework detailed in Figure 3.1. During the gait analysis, participants walked barefoot across the laboratory at their self-selected pace.

Electromyography (EMG), kinematic, and kinetic data from the affected limb were collected for a minimum of 3 trials and a maximum of 5 trials. Kinematic data were collected using a 10-camera motion capture system (Motion Analysis Corporation, Santa Rosa, CA, USA). A full-body passive reflective modified Helen Hayes marker set was applied to each patient and kinematic data were sampled at 60Hz (Moyer et al., 2013). Kinetic ground reaction force data were collected using a floor-embedded force plate (AMTI, Watertown, MA, USA) and sampled at 600Hz.

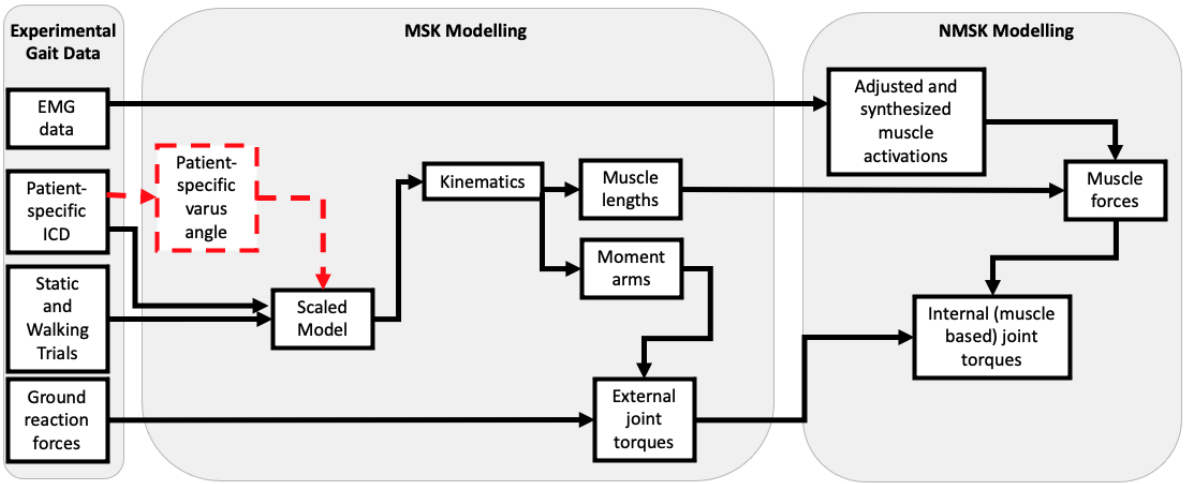

Figure 3.1 Overall framework to estimate joint contact forces. This includes gait data collection, data processing, musculoskeletal modelling in OpenSim, and neuromusculoskeletal modelling in CEINMS. The neutral model follows the pathway identified with a solid line (——). Differences in the PSV model pathway are identified in with a dashed line (– –).

Surface EMG was collected across 8 channels to capture knee spanning muscle activations at 600Hz using Ag surface electrode pairs arranged in a bipolar configuration spaced 10 mm apart (Trigno, Delsys, Natick, MA). Additionally, EMG data were collected using a system that had an input impedance of 10 Giga Ohms and a common

mode rejection ratio of 80 dB at 60Hz, so to not exceed recommended minimum specifications (De Luca, 1997), and a bandwidth of 20 - 450Hz. Electrodes were placed on the affected study limb over the muscle bellies of the rectus femoris (RF), vastus medialis (VM), vastus lateralis (VL), medial hamstring (MH), lateral hamstring (LH), medial gastrocnemius (MG), lateral gastrocnemius (LG), and tibialis anterior (TA). Although ground reaction force and EMG data are typically sampled at a rate >1000Hz, these data were sampled at 600Hz as previous results with EMG data collected at 1200Hz demonstrated differences of less than 1 N in the medial, lateral, and overall compartment contact forces across four participants, and minimal differences in commonly reported EMG parameters. Additionally, a comparison of EMG parameters commonly used to evaluate patients with medial dominant knee OA confirmed similar findings when data are sampled at 1200Hz or 600Hz (Cava et al., 2023).

After gait, participants then performed maximum voluntary isometric contractions (MVICs) to provide a consistent standard for normalization of measured EMG data. Participants completed four exercises to elicit their MVIC for each muscle group of the affected study limb (Rueterbories et al., 2010). For all muscle groups, participants were asked to sit in a chair with their affected knee flexed approximately 90º. For the first MVIC exercise, manual resistance was applied to the middle portion of the tibia as the participant was asked to kick their leg out and resist the force by contracting their quadriceps muscle group (RF, VL, and VM). For the second MVIC exercise, manual resistance was applied from the opposite direction and participants were asked to pull their leg in to resist the force by contracting their hamstring muscle group (MH and LH). For the third MVIC exercise, participants were asked to plantarflex their foot and resist a

manual force applied to the bottom of the foot by contracting the gastrocnemius. Finally for the fourth MVIC exercise, participants were asked to dorsiflex their foot by contracting their TA to resist a manual force applied to the top of the foot. MVIC exercises were held for a minimum of 3 seconds and verbal encouragement was given.

3.4 Data Processing

Gait data were processed using the MATLAB Motion Data Elaboration Toolbox for Musculoskeletal Applications (MOtoNMS) toolbox (Mantoan et al., 2015) within MATLAB (The MathWorks, Inc. Natick MA). Kinematic and kinetic data for all static and gait trials were lowpass filtered with a zero-lag 2nd order Butterworth filter (6Hz cut-off) (Mantoan et al., 2015). EMG linear envelopes were calculated using a highpass filter (20Hz cut-off), full wave rectification, and a lowpass filter using a zero-lag 2nd order Butterworth filter (6Hz cut-off) to represent muscle activations (De Luca et al., 2010). All linear envelopes were then amplitude-normalized to the maximum value of all recorded linear envelopes (considering MVIC and gait trials) for each muscle (Lloyd and Besier, 2003). The position of the hip joint center was determined using a custom MATLAB script by applying a sphere fit of the center of the knee relative to the pelvis during a leg swing trial. The knee and ankle joint centers were obtained by taking the midpoint between the respective medial and lateral knee and ankle markers during the static trial. All kinematic, kinetic, and EMG data from each trial were then cropped to include only the stance phase of gait (force plate heel strike to toe off) (Rueterbories et al., 2010). A margin of 0.33 seconds was added to the beginning and end of each trial to allow a buffer of data for the NMSK optimization algorithm to properly calibrate. Additionally, electromyography data were visually screened by a single investigator to ensure they

were of adequate quality compared to that which has been outlined in the literature for neuromusculoskeletal modelling (Akhundov et al., 2019).

3.4.1 Musculoskeletal Modelling

A generic musculoskeletal (MSK) computational model, based on a previous study of running dynamics (Hamner et al., 2010), was used to calculate gait biomechanics in OpenSim v4.1 (Delp et al., 2007). As described in Saxby et al., 2016, the generic one degree of freedom (DOF) model (gait2392) was modified by adding internal/external rotation as an extra DOF. Abduction/adduction rotations were also added to allow the calculation of net joint torques and muscle moment arms with respect to the medial and lateral compartment of the knee. This DOF was enabled during scaling but locked during the gait simulations to prevent non-physiological condylar liftoff (Saxby et al., 2016). This knee mechanism is detailed in Figure 3.2 and was accomplished by adding two contact points on the tibial plateau. The first contact point, referred to as the medial point, was attached to the medial femoral condyle to aid in calculating the medial compartment KJCF. The second contact point, referred to as the lateral point, was attached to the lateral femoral condyle to aid in calculating the lateral compartment KJCF. The distance between the two contact points (intercondylar distance) was also adjusted to match the distance between the medial and lateral femoral condyle contact points from the joint center on the tibial plateau obtained via the participant's radiograph. The average medial compartment distance from the joint center was 23.9 ± 4.7mm, the average lateral compartment distance from the joint center was 23.7 ± 6.5mm, and the average total intercondylar distance (ICD) was = 47.6 ± 8.7mm.

Two models were created for each participant. The first model, referred to as the “neutral model”, underwent a typical scaling procedure where each model was linearly scaled with the torso, pelvis, and foot segments scaled to the participant’s height. The thigh and shank segments were linearly scaled to match the participants’ marker data acquired from the static trial and had the varus angle constrained to 0° (Figure 3.3). The second model, patient-specific varus (PSV), was permitted to vary the knee varus angle by a means of the medial contact point to match the static pose data during scaling, to account for the patient-specific frontal plane alignment (Figure 3.3). This model was given freedom to predict patient-specific frontal plane alignment rather than scaling to a prescribed the x-ray measured value to better match the remaining marker data from the patient’s static pose. Each patient’s PSV model was then linearly scaled in the same manner as the neutral model. After the model was scaled, the medial contact point was locked to the model predicted MAA. Experimental gait kinematic and kinetic data were provided as inputs to each model to perform inverse kinematics and dynamics analyses (Delp et al., 2007). Two participants were excluded from the analysis as they exceeded recommended marker errors resulting in an analysis with 27 patients (Hicks et al., 2015).

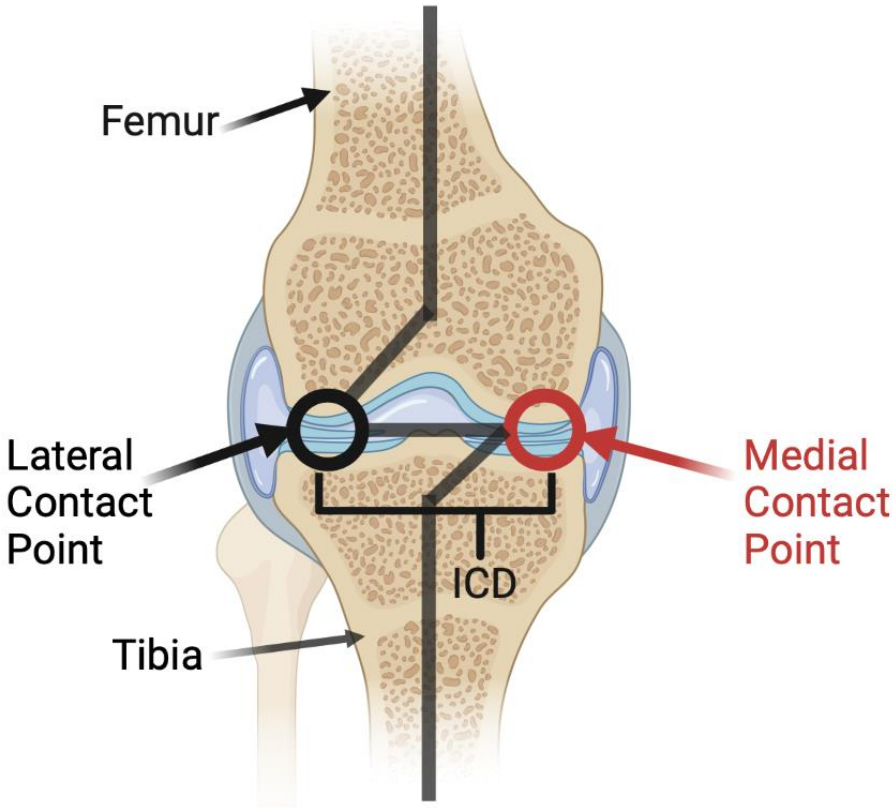

Figure 3.2 Adaptation of the Saxby et al. (2016) tibiofemoral mechanism. Two contact points are modelled as hinges. The two contact points allow joint forces and kinematics to be calculated about the medial (red circle) and lateral (black circle) compartment of the tibiofemoral joint. The two contact points are separated by the participant's patient-specific ICD (black bracket) obtained via hip to ankle radiograph. The segment corresponding to the medial contact point outlined in red was also modified to predict the participant's frontal plane alignment angle during scaling (Bowd et al., 2023). Created with biorender.com.

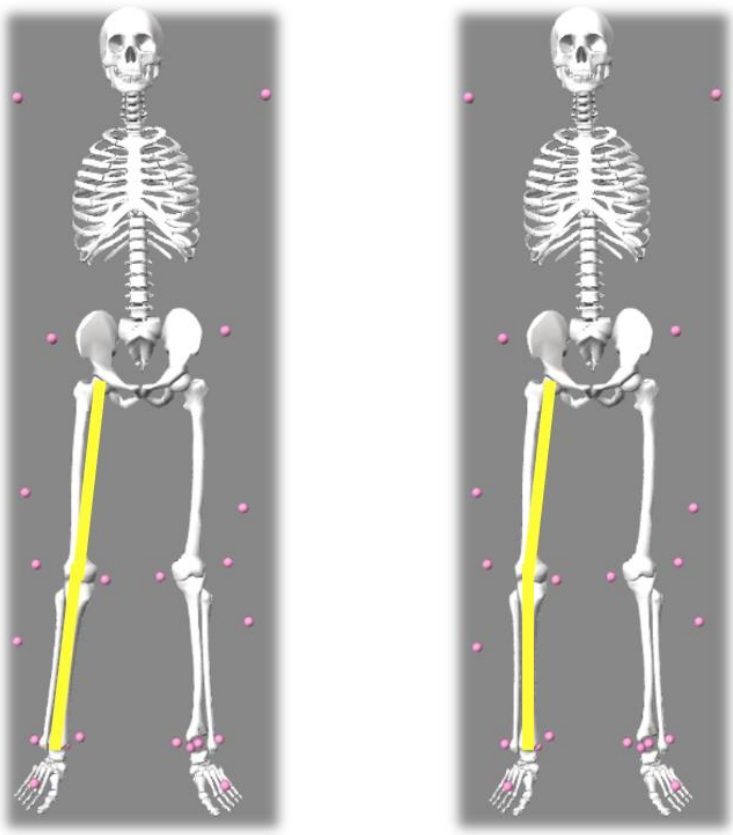

Figure 3.3 Differences between scaled a. Neutral and b. PSV models. The MAA for both models is indicated by the angle between the yellow lines. The Neutral model was scaled to represent a MAA of 0º varus and the PSV patient model was scaled to represent a MAA of 6.4º varus.

3.4.2 Neuromusculoskeletal Modelling

The OpenSim-computed kinematic and inverse dynamics results, along with corresponding experimental muscle activation linear envelopes, were provided as inputs to the Calibrated Electromyography Informed Neuromusculoskeletal Modelling Toolbox (CEINMS) using the EMG-assisted NMSK control mode for both models (Pizzolato et al., 2015). Eight lower extremity EMG linear envelopes were mapped to 11 muscle-

tendon unit excitations (Lloyd and Besier, 2003). The vastus intermedius was derived from the average waveform between the vastus medialis and vastus lateralis and the medial hamstring waveform drove both the semimembranosus and semitendinosus excitations. The lateral hamstring waveform drove the biceps femoris long and short head excitations. When a muscle crosses multiple joints, its activation level depends not just on the torque-demands of the knee, but also the torque demands and forces crossing the complementary joint. To account for this (for the EMG-assisted mode only), the remaining 32 muscle-tendon units (MTUs) that corresponded to the study limb were synthesized to improve the prediction of muscle forces that also span the hip and ankle joints. Activation dynamics and muscular model parameters were functionally calibrated to minimize joint torque prediction errors for sagittal plane torques (Gerus et al., 2013). Models were calibrated by adjusting error coefficients between model inputs to outputs from the first gait trial.

Both the neutral and the PSV NMSK models were executed in CEINMS using the EMG-assisted NMSK control mode for the remaining two to four gait trials that were not used during calibration. The EMG-assisted mode was driven by an objective function using Equation 3.1 that included three components (Sartori et al., 2014).

$$F_{obj} = \sum_{d}^{DOFs} \alpha \, (\overline{M_d} - M_d)^2 + \sum_{j}^{MTUsynth} \beta \; e_j^2 + \sum_{k}^{MTUadj} \gamma \; (\overline{e_k} - e_k)^2 + \beta e_k^2 \quad (2.1)$$

Each component provided the ability to adjust its weighting (or importance) during minimization using α, β, and γ coefficients. The α coefficient scaled the importance of minimization of squared differences between OpenSim computed external joint torques and CEINMS computed internal joint torques ($\sum_{d}^{DOFs} \alpha \, (\overline{M_d} - M_d)^2$). The β coefficient

scaled the importance of minimization of the sum of absolute differences between adjusted and experimentally collected activations ($\sum_j^{MTUsynth} \beta\ e_j^2$). The γ coefficient scaled the importance of the minimization of the sum of squared activations for all 32 predicted MTUs ($\sum_k^{MTUadj} \gamma\ (\overline{e_k} - e_k)^2 + \beta e_k^2$) (Ceseracciu and Reggiani, 2015; Sartori et al., 2014). Within our study, the α coefficient was held constant (α = 1), following CEINMS guidelines (Ceseracciu and Reggiani, 2015). The β and γ coefficients were both set to 1.5, based on an analysis that manually varied coefficient values greater than 1 to find the lowest values of the weighted sum across n = 5 participants; a method that was previously described by others (Sartori et al., 2014). CEINMS-computed outputs for each NMSK model included adjusted muscle activations and sagittal plane torques, and predicted muscle forces that were cropped to include the stance phase only.

3.4.3 Joint Contact Force Analysis

CEINMS-computed muscle forces and internal (knee spanning muscle) torques (13 MTUs) from each model were provided as inputs to previously established equations 3.2 and 3.3 to calculate internal contact forces acting across the medial (F^{MC}) and lateral (F^{LC}) compartment of the knee (Winby et al., 2009).

$$F^{MC} = \frac{M_{MTU}^{LC} - M_{EXT}^{LC}}{d_{IC}} \quad \text{and} \quad F^{LC} = \frac{M_{MTU}^{MC} - M_{EXT}^{MC}}{d_{IC}} \tag{3.2}$$

where

$$M_{MTU}^{LC} = \sum_{i-1}^{13} F_{MTU}\,(i) r_{MTU}^{LC}(i) \quad \text{and} \quad M_{MTU}^{MC} = \sum_{i-1}^{13} F_{MTU}\,(i) r_{MTU}^{MC}(i) \tag{3.3}$$

Where F represents the contact force, M_{MTU}^{LC} represents the abduction/adduction moment arms of the ith MTU about the lateral contact point and M_{MTU}^{MC}, the medial, and d_{IC} represents the intercondylar distance. M_{EXT}^{LC}represents the external abduction/adduction moments around the lateral contact point and M_{EXT}^{MC}, the medial (Lloyd and Buchanan, 2001, 1996). F_{MTU} represents the muscle force and r_{MTU}^{LC} and r_{MTU}^{MC} represents the moment arms (lateral compartment and medial compartment, respectively) for the eleven (11) MTUs that were included to account for the knee spanning muscles. Overall knee compartment contact force was calculated by adding the medial contact force to lateral contact force for each participant. Resulting knee joint contact forces (KJCFs) from each model were time normalized to 100 points of the stance phase and amplitude normalized to the participant's body weight (BW). This step was repeated using data produced from both the neutral and PSV models. The first and second peaks of the overall and medial compartment KJCFs were extracted as the highest value in the first and second half of the stance phase, respectively. The first and second peak of the lateral compartment KJCF was extracted as the highest value from the first 20% of stance and the last 50-90% of stance, respectively (De Pieri et al., 2023).

3.5 Data Analysis

External (OpenSim-computed) and internal (CEINMS-computed) knee flexion/extension torques were time-normalized to 100 points. Bland-Altman plots were then generated to compare the model-predicted varus angle to the X-ray measured varus angles and the root mean squared error (RMSE) difference in external and internal knee flexion/extension torques computed for both the neutral and PSV model. The coefficient of determination (R^2) for each model was determined between model-predicted varus angle and X-ray

measured varus angles and knee flexion/extension torque RMSE and X-ray measured varus angles for the PSV model. The R^2 and RMSE were also calculated for each model between external and internal knee flexion/extension torques for the neutral and PSV model as a measure of the model's prediction accuracy. Differences in scaled model poses and RMSE and R^2 for the knee flexion/extension torques, and first and second peak KJCFs computed with the neutral and PSV models were detected using a paired samples *t*-test. The statistical significance was set to 0.05.

3.6 Results

3.6.1 Patient-Specific Varus Prediction

The PSV model predicted an average frontal plane alignment of 7.6 ± 2.7^{o} varus compared to the X-ray measured MAA of $6.5^{o} \pm 2.0^{o}$ varus. A Bland-Altman plot comparing model-predicted frontal plane alignment to X-ray measured MAA is displayed in Figure 3.4. Limits of agreement were within a -2.5^{o} to 3.5^{o} range and the mean bias was just under 1^{o} indicating good agreement of the model-predicted varus. The R^2 value between model-predicted varus angle and X-ray measured varus angle was moderate (0.57).

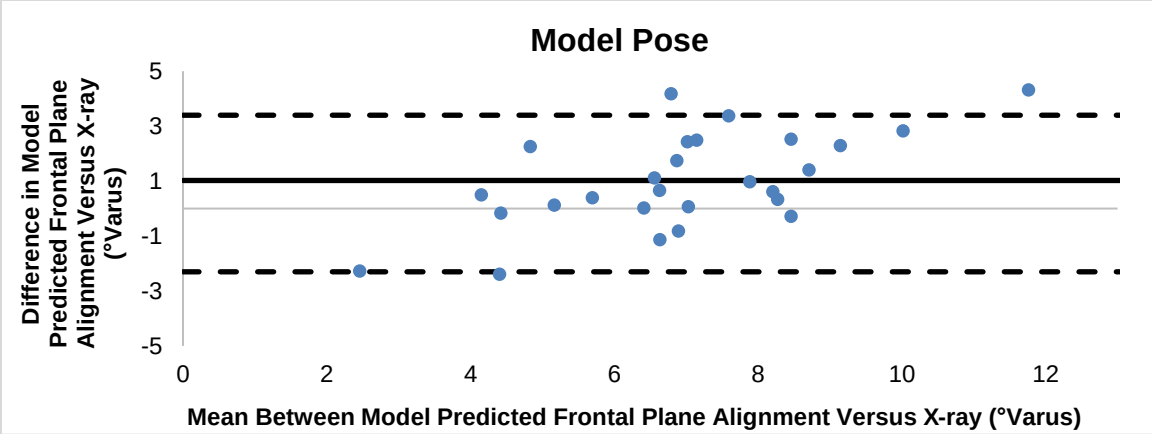

Figure 3.4 Bland-Altman plot for model-predicted frontal plane alignment vs. X-ray measured MAA with the mean between each comparison on the x-axis and the difference between each comparison on the y-axis during the stance phase of gait. Limits of agreement (dashed lines) and mean bias (central line) are displayed with individual participant data points represented by dot (•) symbols.

3.6.2 Scaled Model Pose

Comparisons between the scaled pose for the neutral model compared to the PSV model are presented in Table 3.2. There was a statistically significant increase (p = 0.001) in hip abduction when using the PSV model (5.2º ± 2.9 º) compared to the neutral (2.3 º ± 2.8 º). Additionally, although not statistically significant, the highest mean decrease occurred in the subtalar inversion angle when using the PSV model (-0.3 º ± 8.8 º) compared to the neutral model (3.2 º ± 12.1º).

Table 3.2 Descriptive Statistics and Dependent Samples *t*-Test Results for Average Scaled Model Pose for the PSV Model Compared to the Neutral Model.

	Mean Difference Between PSV Model and Neutral Model (º) [95% CI]	*p*-value
Hip Flexion	0.1 [-0.1 to 0.3]	0.4
Hip Abduction	2.8 [2.4 to 3.3)]	**0.001**
Hip Internal Rotation	-0.2 [-2.9 to 2.5]	0.9
Knee Flexion/Extension	0.03 [-0.4 to 0.4]	0.9
Ankle Dorsiflexion	-1.1 [-2.6 to 0.3]	0.1
Subtalar Inversion	-3.6 [-7.7 to 0.6]	0.1

Values are presented as mean (±SD) and mean [95%CI], *p*-value, and statistically significant results are bolded.

3.6.3 Knee Flexion/Extension Torques

There were no statistically significant differences when comparing the RMSE between external to internal knee flexion/extension torques for both neutral (2.7 ± 1.6Nm) and PSV (2.7 ± 2.1Nm) models. Additionally, there was no statistically significant

differences in the correlation (R^2) between external and internal knee flexion/extension torques for both neutral (0.9 ± 0.1) and PSV (0.9 ± 0.1) models. The Bland-Altman plot displayed in Figure 3.5 demonstrated limits of agreement within a –1.6 to 1.6Nm range and with a mean bias of 0 indicating good agreement between both models. The R^2 value between knee flexion/extension torque RMSE for the PSV model and X-ray measured varus angle was very small (0.01).

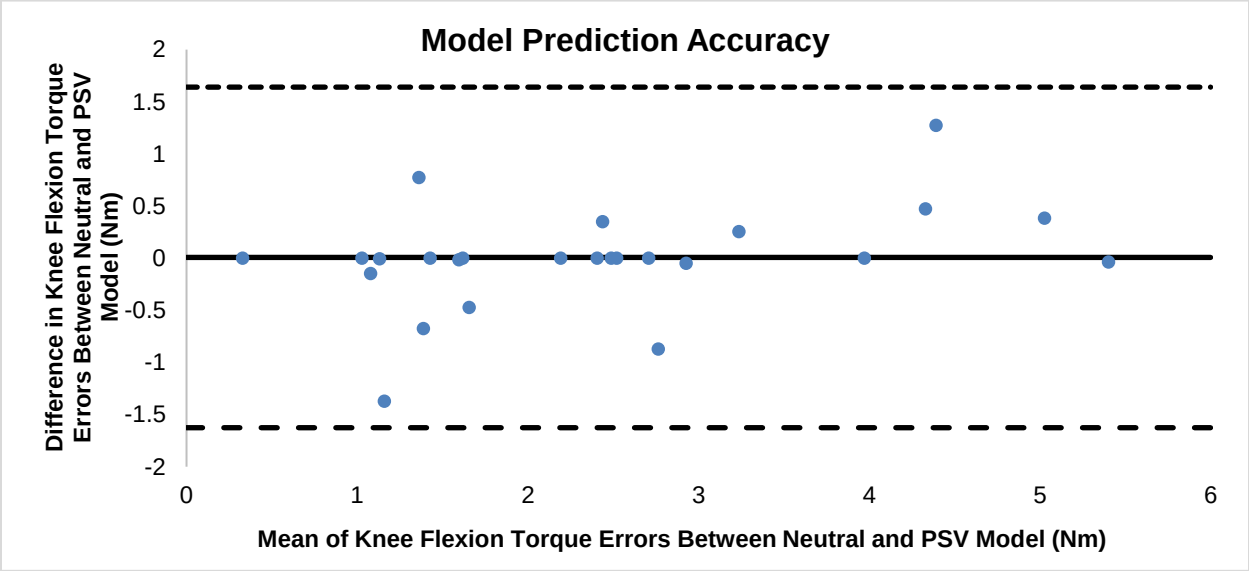

Figure 3.5 Bland-Altman plot for Neutral and PSV model prediction accuracy with the mean between each model on the x-axis and the difference between each model on the y-axis during the stance phase of gait. Limits of agreement (dashed lines) and mean bias (central line) are displayed with individual participant data points represented by dot (•) symbols.

3.6.4 Knee Joint Contact Forces

Ensemble average KJCF waveforms (medial, lateral and overall) for the neutral and PSV model are presented in Figure 3.6. When comparing the neutral model to the PSV model,

there were no statistically significant differences among any of the KJCFs (Table 3.3). The largest mean difference was observed in the second peak of the lateral KJCF where the neutral model's forces (0.8 ± 0.6BW) were lower than the PSV model (1.0 ± 0.6BW). The PSV model consistently produced larger KJCFs in the overall, medial, and lateral compartment when compared to the neutral model.

a.

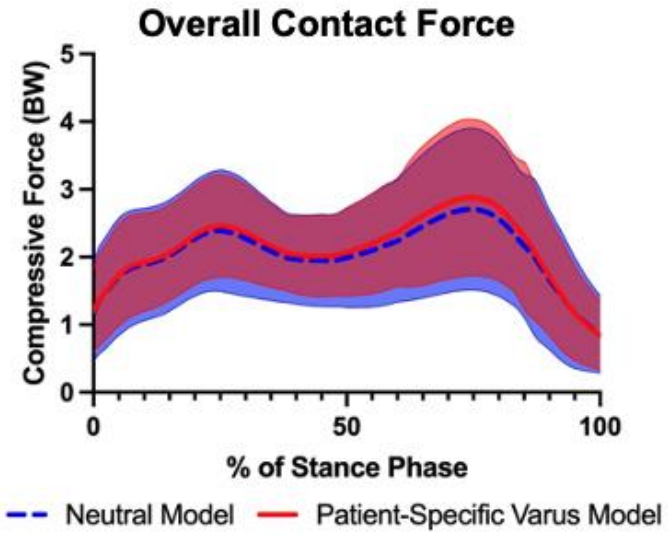
Overall Contact Force
Compressive Force (BW)
5
4
3
2
1
0
0
50
100
% of Stance Phase
Neutral Model
Patient-Specific Varus Model

b.

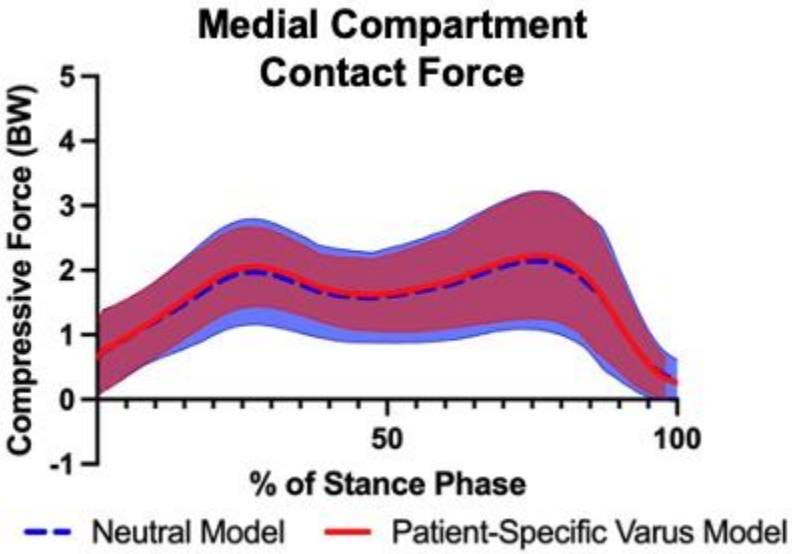
Medial Compartment
Contact Force
Compressive Force (BW)
5
4
3
2
1
0
-1
50
100
% of Stance Phase
Neutral Model
Patient-Specific Varus Model

c.

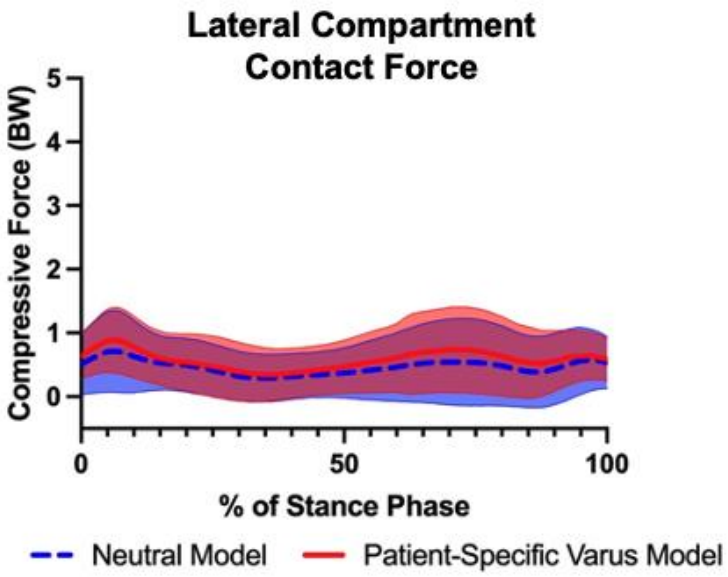

Figure 3.6 Ensemble mean (±SD) waveforms for a. Overall contact force, b. Medial compartment contact force, and c. Lateral compartment contact force computed by the Neutral (dashed line ▬ ▪) and PSV (solid line ▬) models with contact force (BW) on the y-axis and % of stance phase on the x-axis.

Table 3.3 Descriptive Statistics and Dependent Samples *t*-Test Results Overall, Medial, and Lateral Compartment Contact Force for Neutral and PSV Models

		Neutral model (BW) (±SD)	PSV Model (BW) (±SD)	Mean Difference (BW) [95% CI]	*p*-value
Overall Contact Force	First Peak	2.6 (± 0.9)	2.6 (± 0.8)	0.1 [-0.4 to 0.7]	0.93
	Second Peak	2.8 (± 1.3)	2.9 (±1.2)	0.1 [-0.5 to 0.7]	0.77
Medial Compartment Contact Force	First Peak	2.1 (±0.8)	2.1 (± 0.7)	0.1 [-0.1 to 0.2]	0.50
	Second Peak	2.2 (±1.2)	2.3 (± 1.1)	0.1 [-0.2 to 0.2]	0.65
Lateral Compartment Contact Force	First Peak	0.8 (± 0.5)	0.9 (± 0.5)	0.1 [-0.1 to 0.3]	0.26

	Second Peak	0.8 (± 0.6)	1.0 (± 0.6)	0.1 [-0.01to 0.3]	0.24

Values are presented as mean (±SD) and mean [95%CI], *p*-value.

3.7 Discussion

This study evaluated results obtained from two EMG-assisted NMSK models for patients with varus alignment and medial dominant knee OA that underwent typical scaling with an assumed neutral (0º) frontal plane alignment and a model that was adjusted to account for patient-specific frontal plane alignment (PSV model). When first evaluating the patient-specific model's ability to predict the MAA, an increase of 1.1º varus was observed in the PSV model's frontal plane alignment prediction when compared to the X-ray MAA. Additionally, as shown using Bland-Altman plots, the mean bias was close to 0° but the limits of agreement ranged from 3.3º varus to 2.3º valgus indicating large error in the modelled predictions at the individual level not reflected at the level of the overall population. Regardless, a moderate correlation (0.57) was still observed between model-predicted varus angles and X-ray measured varus angles.

There was a statistically significant decrease of 2.8º in hip abduction with the neutral model. Although statistical significance was not reached within the subtalar joint, this DOF is where the largest difference between scaled model poses occurred where an increase of 3.6º inversion was observed with the neutral model. As increased knee varus can be identified through medial deviation of the foot in relation to the femur, the decreased ankle inversion and increased hip abduction that occurred within the PSV

scaled model poses provides better representation of the malalignment that is present within this population.

When evaluating the neutral and PSV model's prediction accuracy based on the knee flexion/extension torques, there were no statistically significant differences, with similar RMSE (2.7 ± 1.6Nm and 2.7 ± 2.1Nm, respectively) and R^2 values (0.9 ± 0.1 and 0.9 ± 0.1, respectively) obtained from both models. A previous study evaluating patient-specific knee joint geometry in knee OA has also identified no difference in model prediction accuracy when testing patient-specific model features with an EMG-driven NMSK modelling framework while walking (Gerus et al., 2013). Our results, therefore, suggest both models consistently reproduced internal knee flexion/extension torques that match external knee flexion/extension torque NMSK model inputs. Furthermore, a very small correlation (0.01) was identified between knee flexion/extension torque RMSE and X-ray measured varus angle indicating a lack of relation between torque errors and degree of varus angle.

When evaluating KJCFs, there were no statistically significant differences between the neutral and PSV models in the overall knee and medial and lateral compartment KJCFs. Average increases, however, were observed in the first (mean differences of 0.1BW) and second (mean differences of 0.1BW) peak KJCFs for the PSV model when compared to the neutral model. A previous study that explored the effect of adding patient-specific knee joint bone geometry, segment masses, and joint centers using an EMG-assisted NMSK modelling framework evaluated sprinting and cutting tasks in a healthy population (Akhundov et al., 2022). This paper identified an increase in computed muscle forces with the patient-specific models. Another study indicated that generic modeled

predictions increase KJCFs when compared to patient-specific models (Gerus et al., 2013). Although this is contrary to our current results, the KJCFs in the previous paper were predicted using an EMG-driven NMSK model within a healthy population (Gerus et al., 2013). As we only tested one patient-specific parameter, it is possible that future research focusing on adjusting patient-specific knee joint bone geometries and segment masses to further improve predictions might lead to significant differences between modelled outputs.

Limitations within this current study include a two-contact point representation to evaluate medial and lateral compartment contact locations. Although a more detailed contact model used in a finite element model may improve the model predicted KJCFs, this method has been widely used and validated based on instrumented implant data within the literature (Gerus et al., 2013; Saxby et al., 2016; Winby et al., 2009). Additionally, patient-specific frontal plane alignments were estimated by using a simple marker set compared to X-ray measures of MAA. It is possible a more complex marker set would have predicted frontal plane alignment closer to the measured MAA. Yet, mean differences of less than 1º within our current study are within the previously identified range of ±0.9º relating to the minimal detectible difference (Specogna et al., 2004).

3.8 Conclusion

As increased frontal plane varus alignment is commonly observed in patients with medial dominant knee OA, this paper examined the effect of adjusting for frontal plane alignment in NMSK models with a neutral (0º) versus patient-specific knee varus angle. Statistically significant differences were observed in the initial scaled model poses between the neutral model and the PSV model. As there were no statistically significant

differences in the predicted KJCFs, it appears that potential changes to the computed muscle forces are not reflected by adjusting this parameter alone. Thus, contrary to our hypothesis, there was no effect on modelled KJCFs when accounting for patient-specific frontal plane alignment.

3.9 References

Akhundov, R., Saxby, D.J., Diamond, L.E., Edwards, S., Clausen, P., Dooley, K., Blyton, S., Snodgrass, S.J., 2022. Is subject-specific musculoskeletal modelling worth the extra effort or is generic modelling worth the shortcut? PLoS ONE 17, 1–16. https://doi.org/10.1371/journal.pone.0262936

Akhundov, R., Saxby, D.J., Edwards, S., Snodgrass, S., Clausen, P., Diamond, L.E., 2019. Development of a deep neural network for automated electromyographic pattern classification. J. Exp. Biol. 222, 1–5. https://doi.org/10.1242/jeb.198101

Birmingham, T.B., Moyer, R., Leitch, K., Chesworth, B., Bryant, D., Willits, K., Litchfield, R., Fowler, P.J., Giffin, J.R., 2017. Changes in biomechanical risk factors for knee osteoarthritis and their association with 5-year clinically important improvement after limb realignment surgery. Osteoarthritis Cartilage 25, 1999–2006. https://doi.org/10.1016/j.joca.2017.08.017

Bowd, J., Van Rossom, S., Williams, D., Elson, D., Wilson, C., Whatling, G., Holt, C., Jonkers, I., 2023. Using musculoskeletal modelling to estimate knee joint loading pre and post high tibial osteotomy. Clin. Biomech. 101, 105855. https://doi.org/10.1016/j.clinbiomech.2022.105855

Cava, D., Birmingham, T., Willing, R., 2023. The effect of reducing sampling rate on electromyography parameters during gait in patients with knee osteoarthritis. Osteoarthritis Cartilage 31, S136–S137. https://doi.org/10.1016/j.joca.2023.01.094

Ceseracciu, E., Reggiani, M., 2015. CEINMS User Guide Documentation 1–58.

De Luca, C.J., Donald Gilmore, L., Kuznetsov, M., Roy, S.H., 2010. Filtering the surface EMG signal: Movement artifact and baseline noise contamination. J. Biomech. 43, 1573–1579. https://doi.org/10.1016/j.jbiomech.2010.01.027

De Pieri, E., Nüesch, C., Pagenstert, G., Viehweger, E., Egloff, C., Mündermann, A., 2023. High tibial osteotomy effectively redistributes compressive knee loads during walking. J. Orthop. Res. 41, 591–600. https://doi.org/10.1002/jor.25403

Delp, S.L., Anderson, F.C., Arnold, A.S., Loan, P., Habib, A., John, C.T., Guendelman, E., Thelen, D.G., 2007. OpenSim: Open-source software to create and analyze dynamic simulations of movement. IEEE Trans. Biomed. Eng. 54, 1940–1950. https://doi.org/10.1109/TBME.2007.901024

Fregly, B.J., Besier, T.F., Lloyd, D.G., Delp, S.L., Banks, S.A., Pandy, M.G., D'Lima, D.D., 2012. Grand challenge competition to predict in vivo knee loads: Grand challenge competition. J. Orthop. Res. 30, 503–513. https://doi.org/10.1002/jor.22023

Gerus, P., Sartori, M., Besier, T.F., Fregly, B.J., Delp, S.L., Banks, S.A., Pandy, M.G., D'Lima, D.D., Lloyd, D.G., 2013. Subject-specific knee joint geometry improves predictions of medial tibiofemoral contact forces. J. Biomech. 46, 2778–2786. https://doi.org/10.1016/j.jbiomech.2013.09.005

Hamner, S.R., Seth, A., Delp, S.L., 2010. Muscle contributions to propulsion and support during running. J. Biomech. 43, 2709–2716. https://doi.org/10.1016/j.jbiomech.2010.06.025

Hicks, J.L., Uchida, T.K., Seth, A., Rajagopal, A., Delp, S.L., 2015. Is my model good enough? Best practices for verification and validation of musculoskeletal models and simulations of movement. J. Biomech. Eng. 137, 1–24. https://doi.org/10.1115/1.4029304

Lerner, Z.F., DeMers, M.S., Delp, S.L., Browning, R.C., 2015. How tibiofemoral alignment and contact locations affect predictions of medial and lateral tibiofemoral contact forces. J. Biomech. 48, 644–650. https://doi.org/10.1016/j.jbiomech.2014.12.049

Lloyd, D.G., Besier, T.F., 2003. An EMG-driven musculoskeletal model to estimate muscle forces and knee joint moments in vivo. J. Biomech. 36, 765–776. https://doi.org/10.1016/S0021-9290(03)00010-1

Lloyd, D.G., Buchanan, T.S., 2001. Strategies of muscular support of varus and valgus isometric loads at the human knee. J. Biomech. 34, 1257–1267. https://doi.org/10.1016/S0021-9290(01)00095-1

Lloyd, D.G., Buchanan, T.S., 1996. A model of load sharing between muscles and soft tissues at the human knee during static tasks. J. Biomech. Eng. 118, 367–376. https://doi.org/10.1115/1.2796019

Mantoan, A., Pizzolato, C., Sartori, M., Sawacha, Z., Cobelli, C., Reggiani, M., 2015. MOtoNMS: A MATLAB toolbox to process motion data for neuromusculoskeletal modeling and simulation. Source Code Biol. Med. 10, 1–14. https://doi.org/10.1186/s13029-015-0044-4

Miyazaki, T., 2002. Dynamic load at baseline can predict radiographic disease progression in medial compartment knee osteoarthritis. Ann. Rheum. Dis. 61, 617–622. https://doi.org/10.1136/ard.61.7.617

Moyer, R.F., Birmingham, T.B., Dombroski, C.E., Walsh, R.F., Leitch, K.M., Jenkyn, T.R., Giffin, J.R., 2013. Combined effects of a valgus knee brace and lateral wedge foot orthotic on the external knee adduction moment in patients with Varus gonarthrosis. Arch. Phys. Med. Rehabil. 94, 103–112. https://doi.org/10.1016/j.apmr.2012.09.004

Pizzolato, C., Lloyd, D.G., Sartori, M., Ceseracciu, E., Besier, T.F., Fregly, B.J., Reggiani, M., 2015. CEINMS: A toolbox to investigate the influence of different neural control solutions on the prediction of muscle excitation and joint moments during dynamic motor tasks. J. Biomech. 48, 3929–3936. https://doi.org/10.1016/j.jbiomech.2015.09.021

Primeau, C.A., Birmingham, T.B., Moyer, R.F., O'Neil, K.A., Werstine, M.S., Alcock, G.K., Giffin, J.R., 2020. Trajectories of perceived exertion and pain over a 12-week neuromuscular exercise program in patients with knee osteoarthritis. Osteoarthritis Cartilage 28, 1427–1431. https://doi.org/10.1016/j.joca.2020.07.011

Rueterbories, J., Spaich, E.G., Larsen, B., Andersen, O.K., 2010. Methods for gait event detection and analysis in ambulatory systems. Med. Eng. Phys. 32, 545–552. https://doi.org/10.1016/j.medengphy.2010.03.007

Saliba, C.M., Brandon, S.C.E., Deluzio, K.J., 2017. Sensitivity of medial and lateral knee contact force predictions to frontal plane alignment and contact locations. J. Biomech. 57, 125–130. https://doi.org/10.1016/j.jbiomech.2017.03.005

Sartori, M., Farina, D., Lloyd, D.G., 2014. Hybrid neuromusculoskeletal modeling to best track joint moments using a balance between muscle excitations derived from electromyograms and optimization. J. Biomech. 47, 3613–3621. https://doi.org/10.1016/j.jbiomech.2014.10.009

Saxby, D.J., Modenese, L., Bryant, A.L., Gerus, P., Killen, B., Fortin, K., Wrigley, T.V., Bennell, K.L., Cicuttini, F.M., Lloyd, D.G., 2016. Tibiofemoral contact forces during walking, running and sidestepping. Gait Posture 49, 78–85. https://doi.org/10.1016/j.gaitpost.2016.06.014

Sharma, L., Hurwitz, D.E., Thonar, E.J.-M.A., Sum, J.A., Lenz, M.E., Dunlop, D.D., Schnitzer, T.J., Kirwan-Mellis, G., Andriacchi, T.P., 1998. Knee adduction moment, serum hyaluronan level, and disease severity in medial tibiofemoral osteoarthritis. Arthritis Rheum. 41, 1233–1240. https://doi.org/10.1002/1529-0131(199807)41:7<1233::AID-ART14>3.0.CO;2-L

Specogna, A., Birmingham, T., DaSilva, J., Milner, J., Kerr, J., Hunt, M., Jones, I., Jenkyn, T., Fowler, P., Giffin, J., 2004. Reliability of lower limb frontal plane

alignment measurements using plain radiographs and digitized images. J. Knee Surg. 17, 203–210. https://doi.org/10.1055/s-0030-1248222

Van Rossom, S., Wesseling, M., Smith, C.R., Thelen, D.G., Vanwanseele, B., Dieter, V.A., Jonkers, I., 2019. The influence of knee joint geometry and alignment on the tibiofemoral load distribution: A computational study. Knee 26, 813–823. https://doi.org/10.1016/j.knee.2019.06.002

Winby, C.R., Lloyd, D.G., Besier, T.F., Kirk, T.B., 2009. Muscle and external load contribution to knee joint contact loads during normal gait. J. Biomech. 42, 2294–2300. https://doi.org/10.1016/j.jbiomech.2009.06.019

Chapter 4

4 The Effect of High Tibial Osteotomy on Knee Joint Contact Force During Walking in Patients with Knee Osteoarthritis and Varus Alignment

4.1 Summary

Background: Once an evaluation of important parameters that might affect our modelling framework was obtained, the developed framework was then used to evaluate changes in knee joint contact forces after medial opening wedge high tibial osteotomy (MOWHTO). Clinical rationales for MOWHTO are to reduce pain and improve function. A biomechanical rationale for MOWHTO is to decrease the force on the medial compartment of the knee during ambulation. Although muscle activity contributes substantially to knee joint contact forces (KJCF), electromyography (EMG)-assisted neuromusculoskeletal (NMSK) models have not been used to investigate the biomechanical effects of MOWHTO.

Purposes: To investigate: 1) the effect of MOWHTO on medial and lateral tibiofemoral compartment KJCFs during walking, using a patient-specific EMG-assisted modelling framework, 2) changes in the external knee adduction moment (EKAM), and muscle co-contraction indices (CCIs), and 3) the association between changes in medial compartment KJCF and changes in the EKAM and CCIs.

Study Design: Laboratory-based biomechanical study; Case series.

Methods: Twenty-seven patients (53 ±5 years) with varus malalignment (mechanical axis angle -6.5º ±2.0º) and medial dominant knee OA underwent three-dimensional gait analysis with surface EMG before and after MOWHTO. An EMG-assisted NMSK model

with patient-specific features of alignment and muscle activity was used to calculate KJCF in the medial and lateral compartments.

Results: After MOWHTO (17 ±7 months), there were moderate reductions (standardized response mean, SRM>0.60) in the first peak (-0.5BW [95%CI -0.9 to -0.2]) and second peak (-0.7BW [95%CI (-1.2 to -0.3]) medial compartment KJCFs. There were small-to-moderate increases (SRM >0.10) in the first peak (0.2BW [95%CI -0.1 to 0.5]) and second peak (0.2BW [95%CI (-0.2 to 0.6]) lateral compartment KJCFs. There were larger reductions (SRM>0.90) in the first peak (-1.0%BW*Ht [95%CI -0.6 to -1.3]) and second peak (-0.9%BW*Ht [95%CI -0.6 to -1.3]) EKAM. There were also decreased muscle CCIs (SRM>0.20). For example, CCI for the vastus lateralis-lateral gastrocnemius muscle pair was -12.3 [95%CI -20.0 to -4.6]. Overall, these changes suggest substantial decreases in knee medial compartment load during walking. Correlations between changes in medial compartment KJFC and changes in EKAM and muscle CCI were low-to-moderate (r<0.5), demonstrating these biomechanical parameters quantify different aspects of gait that may provide different information for planning and evaluating MOWHTO.

Conclusion: When considering patient-specific features of alignment and muscle activity, a substantial reduction in medial compartment load was observed after MOWHTO.

Clinical Relevance: These findings support the biomechanical rationale for MOWHTO and the potential importance of EMG-assisted modelling to provide more reasonable estimates of KJCFs given the major role of muscle contraction to overall force on the knee.

Key Terms: EMG-assisted modelling; high tibial osteotomy; gait biomechanics

4.2 Introduction

Osteoarthritis (OA) commonly affects the knee and is a leading cause of pain and disability worldwide (Hunter and Bierma-Zeinstra, 2019; Vos et al., 2016). The pathogenesis of knee OA is complex and associated with aberrant ambulatory mechanics, including the magnitude, distribution, and timing of loads across the tibiofemoral joint (Andriacchi and Mündermann, 2006; Heiden et al., 2009; Hubley-Kozey et al., 2009; Moyer et al., 2014). Walking produces forces in the knee that are approximately 2-to-3 times body weight (Pandy and Andriacchi, 2010). The overall force on the knee includes the summation of dynamic forces, body weight and muscle forces, with muscle co-contraction being the largest contributor (Andriacchi, 1994). Importantly, the mechanics of walking tend to move the limb towards varus alignment, creating an external knee adduction moment (EKAM) and a greater portion of load on the medial relative to the lateral tibiofemoral compartment (Andriacchi, 1994). Knee OA most commonly affects the medial tibiofemoral compartment because of the greater proportion of load it accepts during ambulation (Andriacchi, 1994). In the presence of varus alignment of the lower limb, the disproportionately greater load on the medial compartment is exacerbated; accordingly, varus alignment is a strong risk factor for the development and progression of knee OA causing structural damage, symptoms, and functional declines (Andriacchi and Mündermann, 2006; Sharma, 2001).

Medial opening wedge high tibial osteotomy (MOWHTO) is a limb realignment surgery for patients with varus alignment of the lower limb and medial dominant knee OA (Brouwer et al., 2014; Lorbergs et al., 2019). Proposed clinical and biomechanical goals

of MOWHTO are to improve pain and function and delay progression and the need for total knee arthroplasty Although less commonly performed than arthroscopy and arthroplasty, MOWHTO is an important treatment option for younger, active patients with medial dominant knee OA (Amendola and Panarella, 2005). MOWHTO corrects varus frontal plane alignment with the aim of shifting load away from the medial tibiofemoral compartment and establishing more equal distribution of knee joint contact forces (KJCF) across the tibiofemoral joint. Previous gait biomechanical studies have reported large, sustained decreases in the EKAM during walking in patients after undergoing MOWHTO (Birmingham et al., 2009, 2007; De Pieri et al., 2023; DeMeo et al., 2010; Leitch et al., 2015; Marriott et al., 2015). Fewer studies have modeled the change in actual knee loads after MOWHTO using various musculoskeletal and contact modelling approaches (Bowd et al., 2023; De Pieri et al., 2023; Whatling et al., 2020). Given the major role of muscle contraction to overall force on the knee, EMG-assisted neuromusculoskeletal (NMSK) models may provide more reasonable estimations of patient-specific KJCFs before and after MOWHTO (Gerus et al., 2013; Pizzolato et al., 2015; Saxby et al., 2016). However, we are unaware of previous studies using EMG-assisted models to investigate changes after MOWHTO. This is a particularly important gap in knowledge as patients with knee OA may walk with altered muscle activity including agonist/antagonist muscle co-contraction (Heiden et al., 2009; Hubley-Kozey et al., 2009; Ramsey et al., 2007) who may benefit from MOWHTO (Briem et al., 2007; Ramsey et al., 2007). Therefore, this paper's objectives were to investigate: 1) the effect of MOWHTO on medial and lateral tibiofemoral compartment KJCFs during walking, using a patient-specific EMG-assisted modelling framework, 2) changes in the external

knee adduction moment (EKAM) and muscle co-contraction indices (CCIs), and 3) the associations between changes in medial compartment KJCF and changes in EKAM and CCIs.

4.3 Methodology

4.3.1 Participants

Patients meeting the clinical criteria for knee OA were recruited from the Fowler Kennedy Sport Medicine Clinic, London Ontario Canada. Patients were included if they had varus alignment of the lower limb (mechanical axis angle (MAA) less than 0) and greater joint space narrowing in the medial tibiofemoral compartment than the lateral compartment. Patients were excluded if they had valgus alignment, joint replacement or HTO on either limb, multi-ligamentous instability, inflammatory or infectious arthritis of the knee, neurologic conditions affecting gait, or possible pregnancy. Study participants were evaluated preoperatively and 12-to-24 months after MOWHTO using three-dimensional gait analysis, full-limb standing radiographs (to measure the MAA) (Specogna et al., 2004), and the Knee Injury and Osteoarthritis Outcomes Score (KOOS) (Roos and Lohmander, 2003). The primary outcome measure was the change in medial compartment KJCF during walking. Sample size was based on ability to detect a moderate-to-large effect size (eg, standardized response mean (SRM) >0.70), previously reported for change in modeled knee loads after MOWHTO (De Pieri et al., 2023). Using a two-sided p value of less than 0.05, 20 participants were sufficient to provide 80% power to detect an effect size of at least 0.7 using a dependent samples *t*-test (Dhand and Khatkar, 2014). To accommodate for potential loss to follow-up and or unusable data, we recruited a total of 29 patients. This study was approved by the Western University

Research Ethics Board for Health Sciences Research Involving Human Subjects. All patients provided written informed consent.

4.3.2 Intervention

MOWHTO was performed using an operative technique similar to that previously described in detail (Fowler et al., 2012; Primeau et al., 2023). An opening wedge osteotomy system and internal fixation plate was used (Figure 4.1). The planned angle of correction was calculated preoperatively with the aim of moving the weightbearing line (hip center to ankle center) laterally, typically to a maximum position of 62.5% of the medial-to-lateral width of the tibia (ie. creating <3 degrees of valgus alignment) according to the method described by Dugdale et al. (Dougdale et al., 1992). The exact angle of the correction was at the surgeon's discretion.

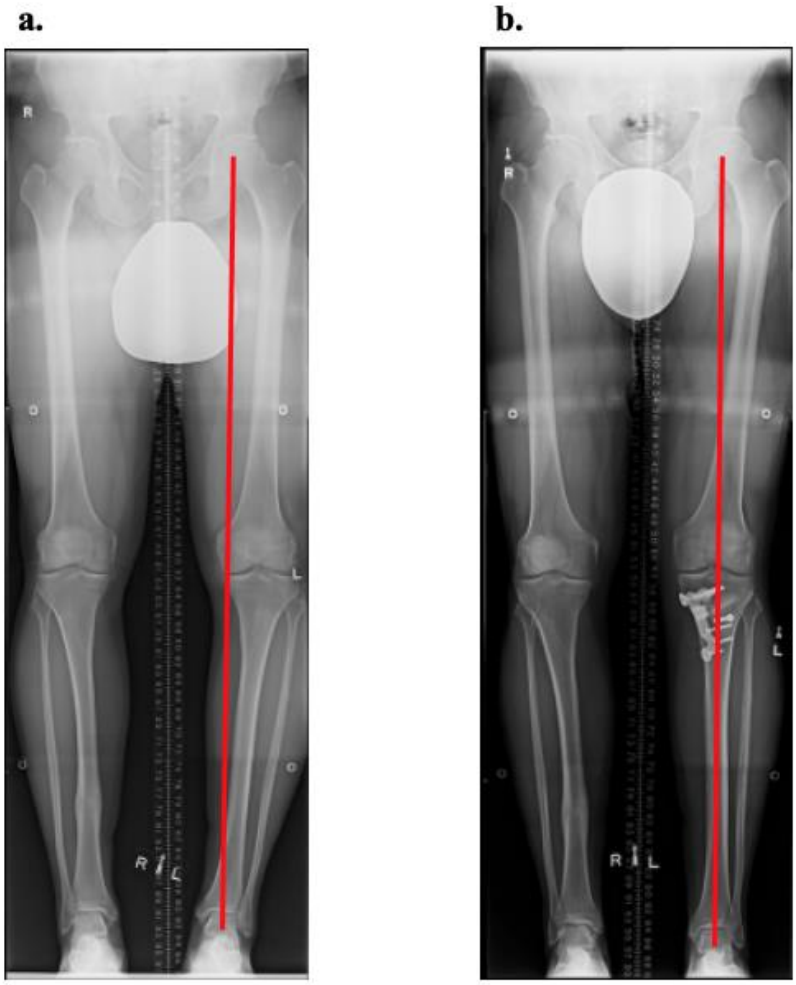

Figure 4.1 Patient radiographs before a. and 12 months after b. MOWHTO. The red line depicts an estimate of the weight bearing line that displays a shift to neutral after MOWHTO.

The osteotomy was secured with a metal plate fixed proximally and distally with cancellous and cortical screws, respectively, and cancellous allograft bone was used to fill osteotomies. All surgeries and examinations were performed by one surgeon (J.R.G.). Postoperative management included the use of a hinged knee brace and crutches. With clinical and radiographic evidence of healing of the osteotomy, gradual increase in weightbearing was permitted. Weightbearing then progressed to full without crutches

approximately 12 weeks postoperative. Patients received a standardized postoperative rehabilitation protocol including exercise progressions and milestones that were reviewed with the patient on postoperative day 1 and 2, and during 6- and 12- week follow-up visits.

4.3.3 Gait Assessment

Patients walked barefoot on level ground at their self-selected pace while EMG, kinematic, and kinetic data were collected for a minimum of 3 trials and a maximum of 5 trials. Kinematic data were collected at 60Hz using a 10-camera motion capture system (Motion Analysis Corporation, Santa Rosa, CA, USA) and a full-body 22 passive reflective modified Helen Hayes marker set (Moyer et al., 2013). Prior to the walking trials, a static trial was completed using four additional markers placed over the medial knee joint line and medial malleolus. These additional markers were removed prior to gait testing. Kinetic data were collected using a floor-mounted force plate (AMTI, Watertown, MA, USA) and sampled at 600Hz. Surface EMG was collected across 8 channels to capture knee spanning muscle activations at 600Hz using Ag surface electrode pairs arranged in a bipolar configuration spaced 10 mm apart (Trigno, Delsys, Natick, MA). Comparison of EMG parameters commonly used to evaluate patients with medial dominant knee OA confirmed similar findings when data are sampled at 1200Hz or 600Hz (Cava et al., 2023). Additionally, pilot EMG data collected from four of the present patients demonstrated differences of less than 1 N in the medial, lateral, and overall KJCFs when EMG data were sampled at 1200 versus 600Hz. The EMG system had an input impedance of 10 Giga Ohms and a common mode rejection ratio of 80 dB at 60Hz (exceeding recommended minimum specifications; De Luca, 1997), and a

bandwidth of 20-450Hz. Electrodes were placed on the affected limb over the muscle bellies of the rectus femoris (RF), vastus medialis (VM), vastus lateralis (VL), medial hamstring (MH), lateral hamstring (LH), medial gastrocnemius (MG), lateral gastrocnemius (LG), and tibialis anterior (TA). Maximum voluntary isometric contractions (MVICs) were collected after gait trials. Patients completed four MVICs for each muscle group (Rueterbories et al., 2010). For all muscle groups, patients were asked to sit in a chair with their knee flexed approximately 90^{o}. For the quadriceps muscle group (RF, VL, and VM), manual resistance was applied in a posterior direction to the distal portion of the anterior tibia as the patient was asked to kick their leg out and resist the force. For the hamstring muscle group (MH and LH) manual resistance was applied in an anterior direction to the distal calf as the patient was asked to pull their leg in and resist the force. For the TA, patients were asked to pull their foot up (dorsiflex) and resist a manual force applied to the top of the foot. For the gastrocnemius, patients were asked to push their foot down (plantar flex) to resist a manual force applied to the bottom of the foot. MVICs were held for a minimum of 3 seconds and verbal encouragement was given.

4.3.3.1 *Gait Data Processing*

Gait data for each patient at each timepoint were processed within MATLAB (The MathWorks, Inc. Natick MA) using the Motion Data Elaboration Toolbox for Musculoskeletal Applications (MOtoNMS) (Mantoan et al., 2015). The kinematic and kinetic data for all static and walking trials were lowpass filtered using a zero-lag 2nd order Butterworth filter with a cut-off frequency of 6Hz (Mantoan et al., 2015). The position of the hip joint center was determined by a sphere fit of the center of the knee

relative to the pelvis during a leg swing trial using a custom MATLAB script. The knee and ankle joint centers were obtained by taking the midpoint between the respective medial and lateral knee and ankle markers during the static trial.

To calculate linear envelopes representing muscle activation before and after MOWHTO, EMG data were 115ighpass filtered (20Hz cut-off), full wave rectified, and lowpass filtered using a zero-lag 2nd order Butterworth filter (6Hz cut-off) (De Luca et al., 2010). Subsequently, all linear envelopes were amplitude-normalized to the maximum value of all recorded linear envelopes (considering MVIC and walking trials) for each muscle (Lloyd and Besier, 2003). All kinematic, kinetic, and EMG data from each trial were then cropped to include only the stance phase of gait (force plate heel strike to toe off) (Rueterbories et al., 2010), with a margin of 0.33 seconds added to the beginning and end of each trial. Electromyography data were visually screened at this stage of processing by a single investigator to ensure they fell within requirements suggested in the literature for neuromusculoskeletal modelling (Akhundov et al., 2019). Experimental EMG data were time-normalized to 100 points across the stance phase of gait.

4.3.4 Musculoskeletal Modelling

Gait biomechanics for each patient at each timepoint were calculated in OpenSim v4.1 (Delp et al., 2007) using a generic musculoskeletal computational model (Hamner et al., 2010). As described in Saxby et al., 2016, this model with one degree of freedom representing the knee joint (DOF) was modified by adding an internal/external rotation. Knee abduction/adduction rotations were also added as a DOF but were locked during the analysis to prevent non-physiological condylar liftoff (Saxby et al., 2016). This model was further modified by including an additional tibia body to allow computation of three-

dimensional knee torques and tibiofemoral contact forces (Saxby et al., 2016). This was accomplished via to two contact points located on the tibial plateau that allow net joint torques and muscle tendon unit moment arms to be calculated with respect to the medial and lateral compartments of the knee (Figure 4.2).

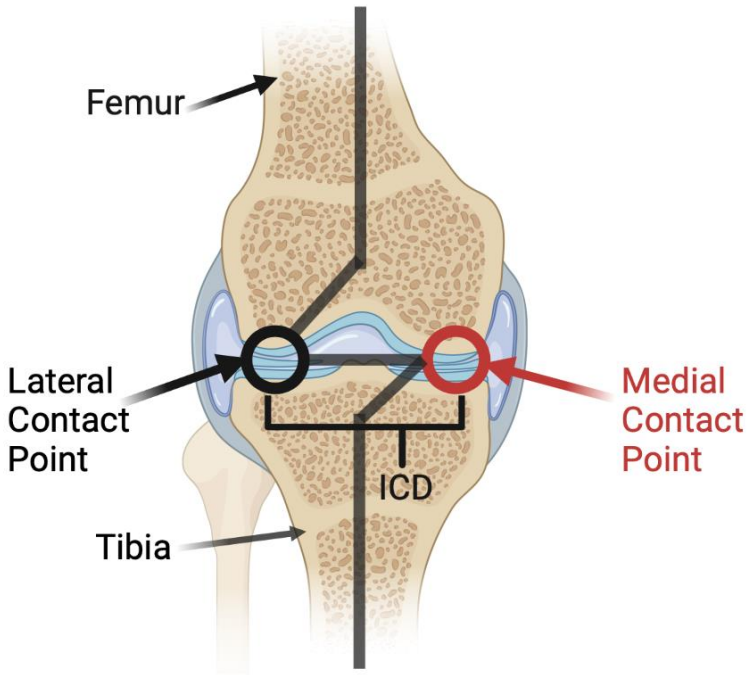

Figure 4.2 Adaptation of the Saxby et al. (2016) tibiofemoral mechanism. Two contact points are modelled as hinges. The two contact points allow joint forces and kinematics to be calculated about the medial (red circle) and lateral (black circle) compartment of the tibiofemoral joint. The two contact points are separated by the participant's patient-specific ICD (black bracket) obtained via hip to ankle radiograph. The segment corresponding to the medial contact point outlined in red was also modified to predict the participant's frontal plane alignment angle during scaling (Bowd et al., 2023). Created with biorender.com.

The distance between medial and lateral contact points was adjusted on the generic OpenSim model for each patient based on the intercondylar distance (ICD) measured via standing radiograph (Figure 4.3). The sample mean ± SD were as follows: medial compartment distance from the joint center was 23.9 ± 4.7mm; lateral compartment distance from the joint center was 23.7 ± 6.5mm; overall ICD was 47.6 ±8.7mm.

a. **b.**

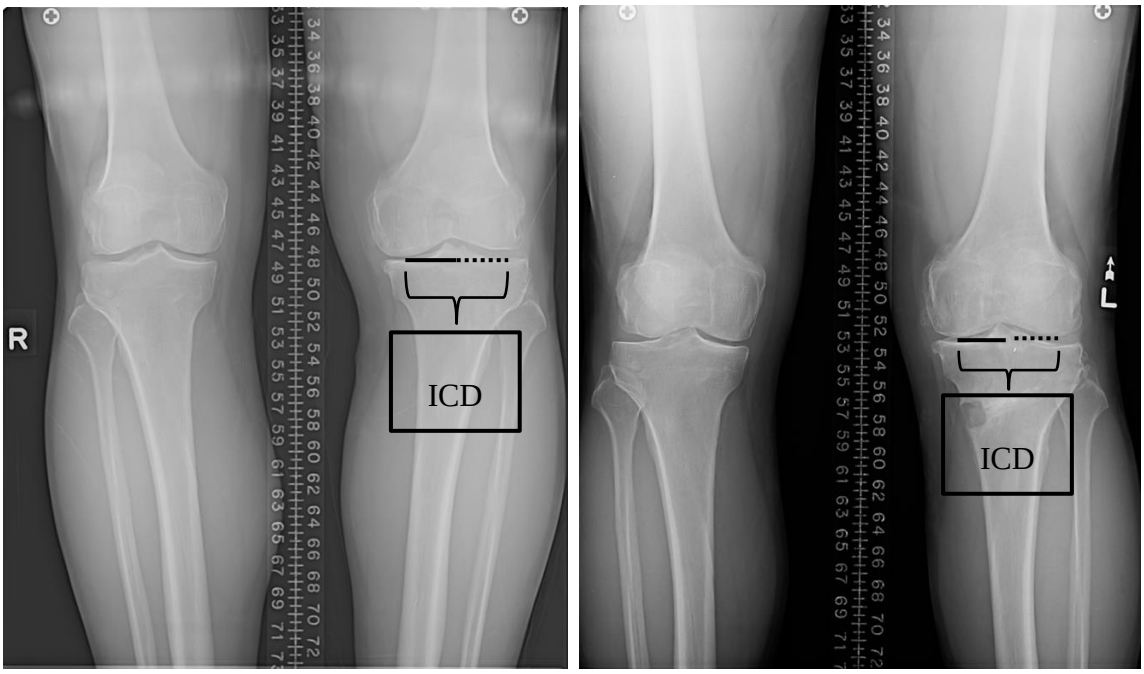

Figure 4.3 Example of patient radiograph. A. before and b. 12 months after MOWHTO where the affected study limb is the left knee. The distance of the medial contact point to the knee joint center was obtained by measuring the distance between the medial femoral contact point and the knee joint center (solid line). The distance of the lateral contact point to the knee joint center was obtained by measuring the distance between the lateral femoral contact point and the knee joint center (dotted line). The total intercondylar

distance was obtained by measuring the distance between the medial and lateral contact points.

During scaling, OpenSim was permitted to match the static pose data to account for patient-specific frontal plane alignment for each patient before and after MOWHTO (Bowd et al., 2023). Each model was then linearly scaled with the torso, pelvis, and foot segments scaled to match the patient's height and the thigh and shank segments that were scaled to match the patient's marker data that was acquired from the static trial. After the model was scaled, the medial knee contact point coordinate representing varus malalignment was locked to the model-predicted gait frontal plane alignment (sample mean ± SD respectively before MOWHTO was 7.6 ±2.7^{o} varus and post MOWHTO surgery was 0.6 ±3.0^{o} varus). Gait kinematic and kinetic data were provided as inputs to each model to perform inverse kinematics analysis and inverse dynamics analyses (Saxby et al., 2016). The EKAM was extracted after completing inverse dynamics analysis.

4.3.5 Neuromusculoskeletal Modelling

The OpenSim-computed kinematic and inverse dynamics results along with corresponding experimental muscle activations for each timepoint were then provided as inputs to the Calibrated Electromyography Informed Neuromusculoskeletal (NMS) Modelling Toolbox (CEINMS) (Pizzolato et al., 2015). Eight lower extremity EMG linear envelopes were mapped to 11 muscle-tendon unit excitations in the model (Lloyd and Besier, 2003) where the vastus intermedius was derived from the average waveform between the vastus medialis and vastus lateralis (Sartori et al., 2014). Additionally, the lateral hamstring EMG waveform drove the semimembranosus and semitendinosus simulations. When a muscle crosses multiple joints, its activation level depends not just

on the torque-demands of the knee, but also the torque demands and forces crossing the complementary joint. To account for this (for the EMG-assisted mode only) the remaining 32 MTUs corresponding to the affected lower extremity were synthesized via static optimization to improve the prediction of muscle forces that also span the hip and ankle joints. Using the technique described by Gerus et al. (2013), activation dynamics and muscular model parameters were functionally calibrated at each time point to minimize a cost function that used sagittal plane joint torques. Models were calibrated using input data from a single trial (the first gait trial) for each participant and weighting coefficients were adjusted based on the error between model inputs to outputs.

The patient-specific NMSK models for each timepoint were then run in CEINMS using the EMG-assisted NMSK control mode for the remaining 2-4 walking trials that were not used during calibration. The EMG-assisted NMSK control mode provided the ability to adjust the weighting (or importance) of minimization of squared differences between OpenSim computed external joint torques and CEINMS computed internal joint torques. This was accomplished using an objective function with three components represented by α, β, and γ coefficients (equation 4.1) (Sartori et al., 2014).

$$F_{obj} = \sum_{d}^{DOFs} \alpha \, (\overline{M_d} - M_d)^2 + \sum_{j}^{MTUsynth} \beta \; e_j^2 + \sum_{k}^{MTUadj} \gamma \; (\overline{e_k} - e_k)^2 + \beta e_k^2 \quad (2.1)$$

Each component provided the ability to adjust its weighting (or importance) during minimization using α, β, and γ coefficients. The α coefficient scaled the importance of minimization of squared differences between OpenSim computed external joint torques and CEINMS computed internal joint torques ($\sum_{d}^{DOFs} \alpha \, (\overline{M_d} - M_d)^2$). The β coefficient scaled the importance of minimization of the sum of absolute differences between

adjusted and experimentally collected activations ($\sum_{j}^{MTUsynth} \beta\ e_j^2$). The γ coefficient scaled the importance of the minimization of the sum of squared activations for all 32 predicted MTUs ($\sum_{k}^{MTUadj} \gamma\ (\overline{e_k} - e_k)^2 + \beta e_k^2$) (Ceseracciu and Reggiani, 2015; Sartori et al., 2014). Within our study, the α coefficient was held constant with a value of 1, and the β and γ coefficients were increased to 1.5 and 1.5 respectively. The a value was determined by following CEINMS guidelines (Ceseracciu and Reggiani, 2015), and the β and γ coefficients were held at 1.5 after completing an analysis that manually varied coefficient values greater than 1 to find the lowest error across 5 patients based on a previously cited method (Sartori et al., 2014). CEINMS-computed outputs for each time point included adjusted and estimated muscle activations and sagittal plane torques, and predicted muscle forces.

4.3.6 Knee Joint Contact Force Analysis

CEINMS-computed muscle forces and net muscle torques (13 MTUs) were provided as inputs to previously established equations 4.1 ad 4.2 to calculate internal compression forces acting across the medial and lateral compartment of the knee for each timepoint (Winby et al., 2009).

$$F^{MC} = \frac{M_{MTU}^{LC} - M_{EXT}^{LC}}{d_{IC}} \quad \text{and} \quad F^{LC} = \frac{M_{MTU}^{MC} - M_{EXT}^{MC}}{d_{IC}} \tag{4.1}$$

where

$$M_{MTU}^{LC} = \sum_{i-1}^{13} F_{MTU}\,(i) r_{MTU}^{LC}(i) \quad \text{and} \quad M_{MTU}^{MC} = \sum_{i-1}^{13} F_{MTU}\,(i) r_{MTU}^{MC}(i) \tag{4.2}$$

Where *F* represents the contact force, M_{MTU}^{LC} represents the abduction/adduction moment arms of the *i*th MTU about the lateral contact point and M_{MTU}^{MC}, the medial, and d_{IC} represents the intercondylar distance. M_{EXT}^{LC}represents the external abduction/adduction moments around the lateral contact point and M_{EXT}^{MC}, the medial (Lloyd and Buchanan, 2001, 1996). F_{MTU} represents the muscle force and r_{MTU}^{LC} and r_{MTU}^{MC} represents the moment arms (lateral compartment and medial compartment, respectively) for the eleven (11) MTUs that were included to account for the knee spanning muscles. Overall knee compartment contact force was calculated by adding the medial contact force to lateral contact force. Resulting KJCFs (N) were then time normalized to 100 points.

4.3.7 Co-Contraction Index Analysis

CCIs were computed using normalized experimental EMG data within quadriceps versus gastrocnemius muscle pairs on the medial and lateral side of the knee (VM-MG, and VL-LG), as well as quadriceps versus hamstring muscle pairs (VM-MH, and VL-LH), using the following equation 4.3 (Zeni et al., 2012).

$$\text{CCI} = \frac{1}{\text{n}} \sum_{i=1}^{n} \left[\frac{lower\ EMG_i}{higher\ EMG_i}\ x\ (lower\ EMG_i + \ higher\ EMG_i) \right] \quad (4.3)$$

Where *lower EMG* represents the instantaneous measure of the linear envelope of the less active muscle and *higher EMG* represents the instantaneous measure of the linear envelope of the more active muscle. For each participant, the sum of data points from initial contact leading up to the first peak of the medial compartment contact force was included in the CCI calculation.

4.4 Statistical Analysis

Pre and postoperative measures were compared using paired samples *t*-tests. Standardized response means were calculated, where a value of 0.2 to 0.5 indicates a low effect size, 0.5-0.8 moderate, and >0.8 large (Cornett et al., 2020). Associations between the changes in outcome measures were measured using Pearson's correlations (r). Statistical significance was set to $p<0.05$.

4.5 Results

A total of 29 patients participated. Of those, two patients were excluded after following previously described OpenSim best practices (Hicks et al., 2015). Specifically. marker errors were reviewed, and two patients were excluded as they exceeded a total square error over 2cm (included patients' mean ± SD total square error = 0.5 ±0.7cm) and maximum marker error RMS over 4cm (included patients' mean ± SD maximum marker error RMS = 1.5 ±0.8cm).

The mean time between pre and postoperative assessments was 17 ± 7 months. Patient demographic and clinical characteristics are presented in Table 4.1.

Table 4.1 Patient Demographic and Clinical Characteristics (n=29)

Age (years)	53 ± 5
Sex (male/female, N of patients)	20/9
Body Mass Index (kg/m^2)	29.8 ± 4.2
MAA*	
Preoperative	-6.5 ± 1.8
Postoperative	-1.4 ± 2.0
Kellgren and Lawrence Grade (N)	
1	4
2	13
3	12
4	0
Pain (0-100)**	

Preoperative	50 ± 14
Postoperative	71 ± 18
Other Symptoms (0-100)**	
Preoperative	51 ± 15
Postoperative	72 ± 16
Function in Activities of Daily Living (0-100)**	
Preoperative	64 ± 17
Postoperative	81 ± 14
Function in Sport and Recreation (0-100)**	
Preoperative	27 ± 19
Postoperative	59 ± 28
Knee Related Quality of Life (0-100)**	
Preoperative	22 ± 16

Postoperative	50 ± 28

Values are mean ± SD unless otherwise stated.

*MAA = mechanical axis angle. Negative values indicate varus.

**Knee Injury and Osteoarthritis Outcomes Score (KOOS) subscales. Higher scores represent less pain and greater function.

4.5.1 Knee Joint Loads

Ensemble average KJCF waveforms before and after MOWHTO are presented in Figure 4.3. Results indicated a moderate (SRMs>0.60) statistically significant decrease in the first (p=0.002) and second (p=0.003) peak medial compartment KJCF after MOWHTO (Figure 4.3, Table 4.2). Although not statistically significant, there was a small (SRM >0.10) increase in the first (p=0.21) and second (p=0.63) peaks of the lateral compartment KJCF, resulting in a small decrease (SRMs>0.20) in the overall knee contact force (Figure 4.3, Table 4.2). There was a large (SRMs>0.90) statistically significant decrease in the first (p=0.001) and second (p=0.001) peak of the EKAM (Table 4.4).

a.

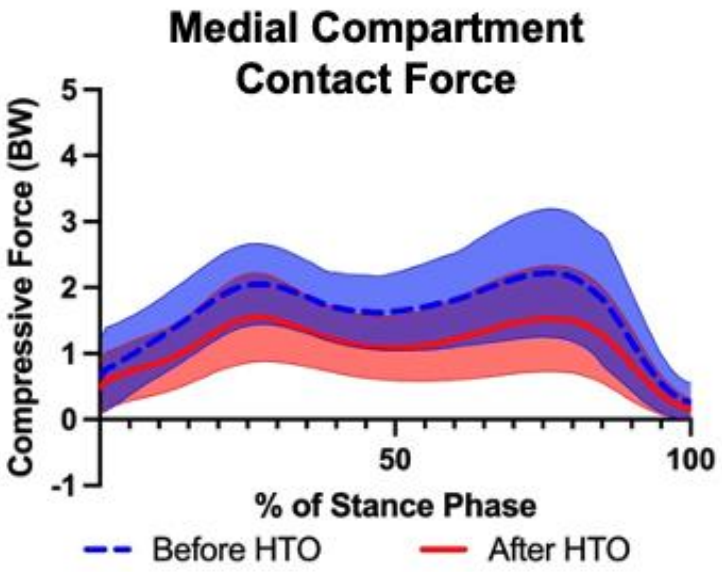
Medial Compartment
Contact Force
Compressive Force (BW)
5
4
3
2
1
0
-1
50
100
% of Stance Phase
Before HTO
After HTO

b.

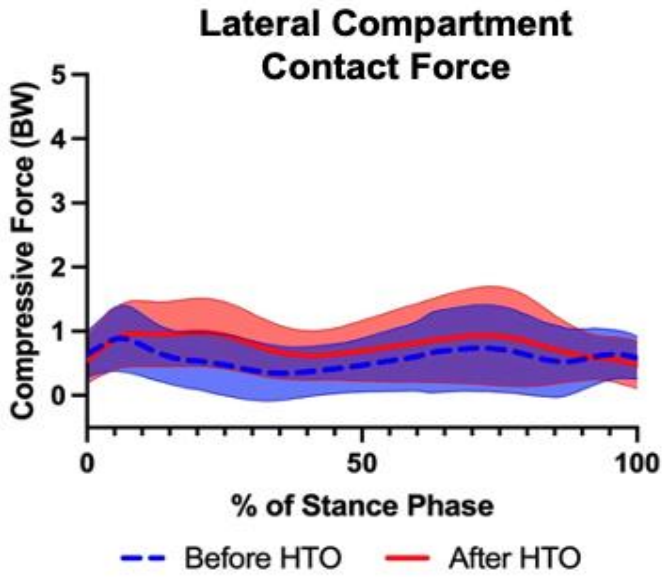
Lateral Compartment
Contact Force
Compressive Force (BW)
5
4
3
2
1
0
0
50
100
% of Stance Phase
Before HTO
After HTO

c.

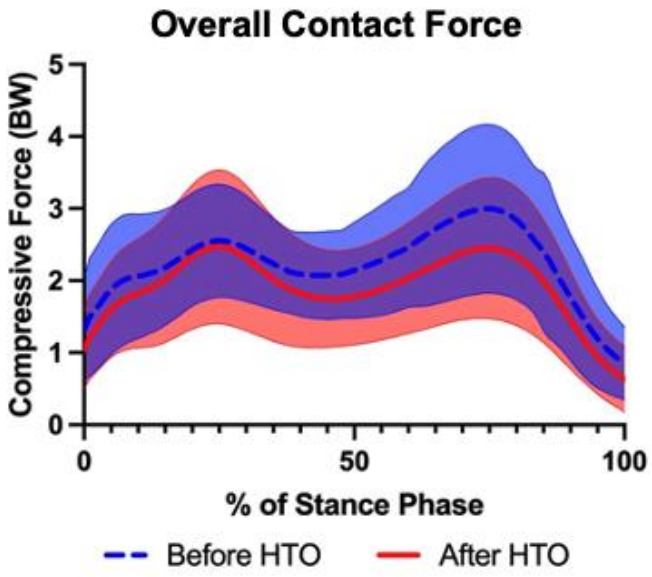

Figure 4.4 Ensemble mean (±SD) waveforms for a. Medial compartment contact force, b. Lateral compartment contact force, and c. Overall contact force before (solid line) and after (dashed line) MOWHTO with contact force (BW) on the y-axis and % of stance phase on the x-axis.

Table 4.2 Medial Compartment, Lateral Compartment, and Overall Contact Forces Before and After MOWHTO.

	Preoperative, mean ±SD	Postoperative, mean ±SD	Mean Difference, [95% CI]	*p*-value	SRM
Medial Compartment Contact Force					
First Peak (BW)	2.1 (± 0.6)	1.6 (± 0.7)	-0.5 [-0.9 to -0.2]	0.002	0.67
Second Peak (BW)	2.3 (± 1.1)	1.6 (± 0.8)	-0.7 [-1.1 to -0.3]	0.003	0.63
Lateral Compartment Contact Force					
First Peak (BW)	0.9 (± 0.5)	1.1 (± 0.6)	0.2 [-0.1 to 0.5)]	0.21	0.25
Second Peak (BW)	1.0 (± 0.6)	1.1 (± 0.7)	0.1 [-0.3 to 0.4)]	0.63	0.10
Overall Contact Force					

First Peak (BW)	2.7 (± 0.9)	2.5 (± 1.1)	-0.2 [-0.6 to 0.3]	0.33	0.20
Second Peak (BW)	3.0 (± 1.2)	2.5 (± 1.0)	-0.5 [-0.1 to 0.1]	0.06	0.52
External Knee Adduction Moment					
First Peak (%BW*Ht)	3.1 (± 0.8)	2.2 (± 0.7)	-1.0 [-0.6 to -1.3)]	0.001	0.97
Second Peak (%BW*Ht)	2.8 (± 0.9)	1.9 (± 0.7)	-0.9 [-0.6 to -1.3]	0.001	0.92

Values are presented as mean (±SD) and mean [95%CI], *p*-value.

4.5.2 Co-Contraction Indices

Changes in CCIs are reported in Table 4. There was a statistically significant reduction in the VL-LG muscle pair after MOWHTO (-12.3 [95%CI -20-4.6]). There were no statistically significant changes among the remaining muscle pairs (Table 4.3).

Table 4.3 Changes in Co-contraction Indices After MOWHTO.

	Preoperative, Mean ±SD	Postoperative, Mean ±SD	Mean Difference [95% CI]	*p*-value	SRM
VM-MG	27.5 (±18.0)	22.0 (±22.8)	-5.4 [-16.4 to 5.5]	0.32	0.20
VL-LG	23.9 (± 17.5)	11.6 (± 11.1)	-12.3 [-20.0 to -4.6]	0.003	0.63
VM-MH	29.8 (± 22.6)	22.3 (± 19.8)	-7.5 [-11.8 to 4.2]	0.20	0.25
VL-LH	18.9 (± 11.7)	13.6 (± 12.0)	-5.3 [-19.2 to 1.2]	0.11	0.32

Values are presented as mean (±SD) and mean [95%CI], *p*-value.

4.5.3 Associations

Correlations between the change in medial compartment KJCFs and change in EKAM and CCIs are reported in Table 4.4. There was a moderate positive correlation between KJCF and EKAM first peak (0.56, p=0.002) and second peak (0.53, p=0.004). Correlations between changes in KJCFs and CCIs were very low and not statistically significant.

Table 4.4 Associations with the Change in Medial Compartment KJCF after MOWHTO.

	Association			
	Peak 1		Peak 2	
	r [95% CI]	*p*-value	r [95% CI]	*p*-value
EKAM	0.56 [0.23 to 0.77]	0.002	0.53 [0.19 to 0.76]	0.004
VM-MG CCI	-0.03 [-0.41 to 0.36]	0.88	-0.04 [-0.41 to 0.35]	0.84
VL-LG CCI	0.27 [-0.13 to 0.59]	0.18	0.06 [-0.33 to 0.43]	0.77
VM-MH CCI	-0.06 [-0.43 to 0.32]	0.75	-0.14 [-0.49 to 0.26]	0.50
VL-LH CCI	0.22 [-0.17 to 0.56]	0.27	-0.01 [-0.39 to 0.37]	0.97

Values are presented as mean (±SD) and mean [95%CI], *p*-value.

4.6 Discussion

The main objective of this study was to investigate the effect and provide evidence for achieving biomechanical goals of MOWHTO on medial and lateral tibiofemoral compartment KJCFs during walking using a patient-specific EMG-assisted modelling framework. Secondary objectives were to investigate changes in the EKAM and CCIs, and their associations with changes in medial KJCFs. There were moderate decreases in

the medial compartment KJCF during the stance phase of gait (Table 4.2). These decreases were accompanied by larger decreases in the first and second peak of the EKAM and a moderate reduction in the VL-LG CCI (Table 4.3).

The present results suggest MOWHTO effectively reduced the medial compartment KJCF during walking (Table 4.2). Although not statistically significant, there was also a small increase in the lateral compartment KJCF, resulting in a decrease in the overall KJCF after MOWHTO.

Overall, these results suggest MOWHTO substantially decreases knee medial compartment load during walking and support the biomechanical rationale for the surgery. The present decrease in KJCF after MOWHTO (Table 4.2) was comparable to the decrease in KJCF using a contact modelling framework previously reported by Di Pieri et al. (2023) (approximate change in medial KJCF first peak=-0.6BW, second peak=-0.7BW; approximate change in lateral KJCF first peak=0.3BW and second peak=0.4BW). The present changes are larger than those reported by Bowd et al. (2022) who modelled a change in medial KJCF first peak=-0.2BW, second peak=-0.1BW; approximate change in lateral KJCF first peak=0.1BW and second peak=0.1BW.

The present decreases in the EKAM (Table 4.3) were generally comparable with previous studies (Bhatnagar and Jenkyn, 2010; Birmingham et al., 2009; Briem et al., 2007; De Pieri et al., 2023; Leitch et al., 2015; Marriott et al., 2015; Whatling et al., 2020). Importantly, the associations between the reductions in the EKAM and KJCF were moderate (r=0.56) suggesting only 31% of the variance in the change in KJCF can be explained by its association with change in the EKAM.

There were also reductions in muscle pair CCIs after MOWHTO (Table 4.4). The largest decrease was observed in the VL-LG muscle pair. Because previous studies have reported excessive co-contraction in the lateral muscle pairs of patients with knee OA (Hubley-Kozey et al., 2009), the present decreases may be viewed as a positive finding. Although speculative, the decrease in co-contraction could be the result of decreased pain or improved joint stability after MOWHTO. We are aware of two other studies evaluating muscle pair CCIs after MOWHTO (Briem et al., 2007; Ramsey et al., 2007). Interestingly, Ramsey et al. reported a reduction in VM-MG CCIs 12 months after MOWHTO (Ramsey et al., 2007). Additionally, Briem et al. reported a change in VM-MG CCIs to be positively correlated ($r = 0.5$) with the degree of correction after 12 months where patients with a correction close to neutral presented with decreased co-contraction. Notably, the present associations between changes in CCIs and medial KJCF were very low (r values between 0.01 and 0.27). The low-to-moderate correlations between changes in KJCF and EKAM and muscle pair CCI highlight the fact that these measures quantify different biomechanical parameters relevant to knee OA.

Limitations of this study include generalizability, as all surgeries were completed in a single tertiary care center by one surgeon with specialty training in limb realignment. Additionally, our results are modelled predictions as we were unable to directly measure KJCFs. Thus, our baseline KJCFs are similar to previous studies verified by instrumented knee implant data in the same target population (Hall et al., 2019; S. Starkey et al., 2022; S. C. Starkey et al., 2022). In addition, although corrections in patient reported outcome measures were beyond the minimal detectible value identified previously (Roos and Lohmander, 2003), comparing the clinical relevance of modelled measures versus

surrogates should be further measured. Finally, although condylar liftoff that was previously described as unphysiological findings within modelling analyses of healthy participants, the 95% CIs of this current study displayed this motion before MOWHTO. Previous studies have stated that people with medial dominant knee OA might display condylar liftoff (presented as varus knee thrust) if they are not able to counter increased external adduction moments at the knee. Furthermore, this type of knee mechanism can occur to increase stability in the knee in the presence of decreased quadriceps strength (Kumar et al., 2013; Schipplein & Andriacchi, 1991).

4.7 Conclusion

To our knowledge, this is the first study to report changes in KJCFs after MOWHTO using an EMG-assisted modelling framework. Results suggest a moderate decrease in medial compartment KJCF and lateral knee muscle CCI. Low correlations between changes in KJCF and EKAM and CCIs suggest these measures quantify substantially different biomechanical parameters that may provide different information for planning and evaluating MOWHTO.

4.8 References

Akhundov, R., Saxby, D.J., Edwards, S., Snodgrass, S., Clausen, P., Diamond, L.E., 2019. Development of a deep neural network for automated electromyographic pattern classification. J. Exp. Biol. 222, 1–5. https://doi.org/10.1242/jeb.198101

Amendola, A., Panarella, L., 2005. High tibial osteotomy for the treatment of unicompartmental arthritis of the knee. Orthop. Clin. North Am. 36, 497–504. https://doi.org/10.1016/j.ocl.2005.05.009

Andriacchi, T.P., 1994. Dynamics of knee malalignment. Orthop Clin North Am 25, 395–403.

Andriacchi, T.P., Mündermann, A., 2006. The role of ambulatory mechanics in the initiation and progression of knee osteoarthritis. Curr. Opin. Rheumatol. 18, 514–518. https://doi.org/10.1097/01.bor.0000240365.16842.4e

Bhatnagar, T., Jenkyn, T.R., 2010. Internal kinetic changes in the knee due to high tibial osteotomy are well-correlated with change in external adduction moment: An osteoarthritic knee model. J. Biomech. 43, 2261–2266. https://doi.org/10.1016/j.jbiomech.2010.05.001

Birmingham, T.B., Giffin, J.R., Chesworth, B.M., Bryant, D.M., Litchfield, R.B., Willits, K., Jenkyn, T.R., Fowler, P.J., 2009. Medial opening wedge high tibial osteotomy: A prospective cohort study of gait, radiographic, and patient-reported outcomes. Arthritis Care Res. 61, 648–657. https://doi.org/10.1002/art.24466

Birmingham, T.B., Hunt, M.A., Jones, I.C., Jenkyn, T.R., Giffin, J.R., 2007. Test-retest reliability of the peak knee adduction moment during walking in patients with medial compartment knee osteoarthritis. Arthritis Care Res. 57, 1012–1017. https://doi.org/10.1002/art.22899

Bowd, J., Van Rossom, S., Williams, D., Elson, D., Wilson, C., Whatling, G., Holt, C., Jonkers, I., 2023. Using musculoskeletal modelling to estimate knee joint loading pre and post high tibial osteotomy. Clin. Biomech. 101, 105855. https://doi.org/10.1016/j.clinbiomech.2022.105855

Briem, K., Ramsey, D.K., Newcomb, W., Rudolph, K.S., Snyder-mackler, L., 2007. Effects of the amount of valgus correction for medial compartment knee osteoarthritis on clinical outcome, knee kinetics and muscle co-contraction after opening wedge high tibial osteotomy 311–318. https://doi.org/10.1002/jor

Brouwer, R.W., Huizinga, M.R., Duivenvoorden, T., van Raaij, T.M., Verhagen, A.P., Bierma-Zeinstra, S.M., Verhaar, J.A., 2014. Osteotomy for treating knee osteoarthritis. Cochrane Database Syst. Rev. https://doi.org/10.1002/14651858.CD004019.pub4

Cava, D., Birmingham, T., Willing, R., 2023. The effect of reducing sampling rate on electromyography parameters during gait in patients with knee osteoarthritis. Osteoarthritis Cartilage 31, S136–S137. https://doi.org/10.1016/j.joca.2023.01.094

Ceseracciu, E., Reggiani, M., 2015. CEINMS user guide documentation 1–58.

Cornett, K.M.D., Menezes, M.P., Bray, P., Shy, R.R., Moroni, I., Pagliano, E., Pareyson, D., Estilow, T., Yum, S.W., Bhandari, T., Muntoni, F., Laura, M., Reilly, M.M., Finkel, R.S., Eichinger, K.J., Herrmann, D.N., Shy, M.E., Burns, J., CMTPedS Study Group, 2020. Refining clinical trial inclusion criteria to optimize the standardized response mean of the CMTPedS. Ann. Clin. Transl. Neurol. 7, 1713–1715. https://doi.org/10.1002/acn3.51145

De Luca, C.J., Donald Gilmore, L., Kuznetsov, M., Roy, S.H., 2010. Filtering the surface EMG signal: Movement artifact and baseline noise contamination. J. Biomech. 43, 1573–1579. https://doi.org/10.1016/j.jbiomech.2010.01.027

De Pieri, E., Nüesch, C., Pagenstert, G., Viehweger, E., Egloff, C., Mündermann, A., 2023. High tibial osteotomy effectively redistributes compressive knee loads during walking. J. Orthop. Res. 41, 591–600. https://doi.org/10.1002/jor.25403

Delp, S.L., Anderson, F.C., Arnold, A.S., Loan, P., Habib, A., John, C.T., Guendelman, E., Thelen, D.G., 2007. OpenSim: Open-source software to create and analyze dynamic simulations of movement. IEEE Trans. Biomed. Eng. 54, 1940–1950. https://doi.org/10.1109/TBME.2007.901024

DeMeo, P.J., Johnson, E.M., Chiang, P.P., Flamm, A.M., Miller, M.C., 2010. Midterm follow-up of opening-wedge high tibial osteotomy. Am. J. Sports Med. 38, 2077–2084. https://doi.org/10.1177/0363546510371371

Dhand, N.K., Khatkar, M.S., 2014. Statulator: An online statistical calculator. Sample Size Calculator for Comparing Two Paired Means.

Dougdale, T.W., Noyes, F.R., Styer, D., 1992. Preoperative planning for high tibial osteotomy. The effect of lateral tibiofemoral separation and tibiofemoral length. Clin. Orthop. 1992, 248–268.

Fowler, P.J., Tan, J.L., Brown, G.A., 2012. Medial opening wedge high tibial osteotomy: How I do it. Oper. Tech. Sports Med. 20, 87–92. https://doi.org/10.1053/j.otsm.2012.03.010

Gerus, P., Sartori, M., Besier, T.F., Fregly, B.J., Delp, S.L., Banks, S.A., Pandy, M.G., D'Lima, D.D., Lloyd, D.G., 2013. Subject-specific knee joint geometry improves predictions of medial tibiofemoral contact forces. J. Biomech. 46, 2778–2786. https://doi.org/10.1016/j.jbiomech.2013.09.005

Hall, M., Diamond, L.E., Lenton, G.K., Pizzolato, C., Saxby, D.J., 2019. Immediate effects of valgus knee bracing on tibiofemoral contact forces and knee muscle forces. Gait Posture 68, 55–62. https://doi.org/10.1016/j.gaitpost.2018.11.009

Hamner, S.R., Seth, A., Delp, S.L., 2010. Muscle contributions to propulsion and support during running. J. Biomech. 43, 2709–2716. https://doi.org/10.1016/j.jbiomech.2010.06.025

Heiden, T.L., Lloyd, D.G., Ackland, T.R., 2009. Knee joint kinematics, kinetics and muscle co-contraction in knee osteoarthritis patient gait. Clin. Biomech. 24, 833–841. https://doi.org/10.1016/j.clinbiomech.2009.08.005

Hicks, J.L., Uchida, T.K., Seth, A., Rajagopal, A., Delp, S.L., 2015. Is my model good enough? Best practices for verification and validation of musculoskeletal models

and simulations of movement. J. Biomech. Eng. 137, 1–24. https://doi.org/10.1115/1.4029304

Hubley-Kozey, C.L., Hill, N.A., Rutherford, D.J., Dunbar, M.J., Stanish, W.D., 2009. Co-activation differences in lower limb muscles between asymptomatic controls and those with varying degrees of knee osteoarthritis during walking. Clin. Biomech. 24, 407–414. https://doi.org/10.1016/j.clinbiomech.2009.02.005

Hunter, D.J., Bierma-Zeinstra, S., 2019. Osteoarthritis. The Lancet 393, 1745–1759. https://doi.org/10.1016/S0140-6736(19)30417-9

Kumar, D., Manal, K. T., & Rudolph, K. S. (2013). Knee joint loading during gait in healthy controls and individuals with knee osteoarthritis. *Osteoarthritis and Cartilage*, *21*(2), 298–305. https://doi.org/10.1016/j.joca.2012.11.008

Leitch, K.M., Birmingham, T.B., Dunning, C.E., Giffin, J.R., 2015. Medial opening wedge high tibial osteotomy alters knee moments in multiple planes during walking and stair ascent. Gait Posture 42, 165–171. https://doi.org/10.1016/j.gaitpost.2015.05.005

Lloyd, D.G., Besier, T.F., 2003. An EMG-driven musculoskeletal model to estimate muscle forces and knee joint moments in vivo. J. Biomech. 36, 765–776. https://doi.org/10.1016/S0021-9290(03)00010-1

Lloyd, D.G., Buchanan, T.S., 2001. Strategies of muscular support of varus and valgus isometric loads at the human knee. J. Biomech. 34, 1257–1267. https://doi.org/10.1016/S0021-9290(01)00095-1

Lloyd, D.G., Buchanan, T.S., 1996. A model of load sharing between muscles and soft tissues at the human knee during static tasks. J. Biomech. Eng. 118, 367–376. https://doi.org/10.1115/1.2796019

Lorbergs, A.L., Birmingham, T.B., Primeau, C.A., Atkinson, H.F., Marriott, K.A., Giffin, J.R., 2019. Improved methods to measure outcomes after high tibial osteotomy. Clin. Sports Med. 38, 317–329. https://doi.org/10.1016/j.csm.2019.02.001

Mantoan, A., Pizzolato, C., Sartori, M., Sawacha, Z., Cobelli, C., Reggiani, M., 2015. MOtoNMS: A MATLAB toolbox to process motion data for neuromusculoskeletal modeling and simulation. Source Code Biol. Med. 10, 1–14. https://doi.org/10.1186/s13029-015-0044-4

Marriott, K., Birmingham, T.B., Kean, C.O., Hui, C., Jenkyn, T.R., Giffin, J.R., 2015. Five-year changes in gait biomechanics after concomitant high tibial osteotomy and ACL reconstruction in patients with medial knee osteoarthritis. Am. J. Sports Med. 43, 2277–2285. https://doi.org/10.1177/0363546515591995

Moyer, R.F., Birmingham, T.B., Dombroski, C.E., Walsh, R.F., Leitch, K.M., Jenkyn, T.R., Giffin, J.R., 2013. Combined effects of a valgus knee brace and lateral wedge foot orthotic on the external knee adduction moment in patients with Varus gonarthrosis. Arch. Phys. Med. Rehabil. 94, 103–112. https://doi.org/10.1016/j.apmr.2012.09.004

Moyer, R.F., Ratneswaran, A., Beier, F., Birmingham, T.B., 2014. Osteoarthritis year in review 2014: mechanics – basic and clinical studies in osteoarthritis. Osteoarthritis Cartilage 22, 1989–2002. https://doi.org/10.1016/j.joca.2014.06.034

Pandy, M.G., Andriacchi, T.P., 2010. Muscle and joint function in human locomotion. Annu. Rev. Biomed. Eng. 12, 401–433. https://doi.org/10.1146/annurev-bioeng-070909-105259

Pizzolato, C., Lloyd, D.G., Sartori, M., Ceseracciu, E., Besier, T.F., Fregly, B.J., Reggiani, M., 2015. CEINMS: A toolbox to investigate the influence of different neural control solutions on the prediction of muscle excitation and joint moments during dynamic motor tasks. J. Biomech. 48, 3929–3936. https://doi.org/10.1016/j.jbiomech.2015.09.021

Primeau, C.A., Birmingham, T.B., Appleton, C.T., Leitch, K.M., Fowler, P.J., Marsh, J.D., Giffin, J.R., 2023. Responders to medial opening wedge high tibial osteotomy for knee osteoarthritis. J. Rheumatol. 50, 809–816. https://doi.org/10.3899/jrheum.220956

Ramsey, D.K., Snyder-Mackler, L., Lewek, M., Newcomb, W., Rudolph, K.S., 2007. Effect of anatomic realignment on muscle function during gait in patients with medial compartment knee osteoarthritis. Arthritis Care Res. 57, 389–397. https://doi.org/10.1002/art.22608

Roos, E.M., Lohmander, L.S., 2003. The Knee injury and osteoarthritis outcome score (KOOS): from joint injury to osteoarthritis. Health Qual. Life Outcomes.

Rueterbories, J., Spaich, E.G., Larsen, B., Andersen, O.K., 2010. Methods for gait event detection and analysis in ambulatory systems. Med. Eng. Phys. 32, 545–552. https://doi.org/10.1016/j.medengphy.2010.03.007

Sartori, M., Farina, D., Lloyd, D.G., 2014. Hybrid neuromusculoskeletal modeling to best track joint moments using a balance between muscle excitations derived from electromyograms and optimization. J. Biomech. 47, 3613–3621. https://doi.org/10.1016/j.jbiomech.2014.10.009

Saxby, D.J., Modenese, L., Bryant, A.L., Gerus, P., Killen, B., Fortin, K., Wrigley, T.V., Bennell, K.L., Cicuttini, F.M., Lloyd, D.G., 2016. Tibiofemoral contact forces during walking, running and sidestepping. Gait Posture 49, 78–85. https://doi.org/10.1016/j.gaitpost.2016.06.014

Schipplein, O. D., & Andriacchi, T. P. (1991). Interaction between active and passive knee stabilizers during level walking. *Journal of Orthopaedic Research*, *9*(1), 113–119. https://doi.org/10.1002/jor.1100090114

Sharma, L., 2001. The role of knee alignment in disease progression and functional decline in knee osteoarthritis. JAMA 286, 188. https://doi.org/10.1001/jama.286.2.188

Specogna, A., Birmingham, T., DaSilva, J., Milner, J., Kerr, J., Hunt, M., Jones, I., Jenkyn, T., Fowler, P., Giffin, J., 2004. Reliability of lower limb frontal plane alignment measurements using plain radiographs and digitized images. J. Knee Surg. 17, 203–210. https://doi.org/10.1055/s-0030-1248222

Starkey, S., Hinman, R., Paterson, K., Saxby, D., Knox, G., Hall, M., 2022. Tibiofemoral contact force differences between flat flexible and stable supportive walking shoes in people with varus-malaligned medial knee osteoarthritis: A randomized cross-over study. PLoS ONE 17, 1–20. https://doi.org/10.1371/journal.pone.0269331

Starkey, S.C., Diamond, L.E., Hinman, R.S., Saxby, D.J., Knox, G., Hall, M., 2022. Muscle forces during weight-bearing exercises in medial knee osteoarthritis and varus malalignment: A cross-sectional study. Med. Sci. Sports Exerc. 54, 1448–1458. https://doi.org/10.1249/MSS.0000000000002943

Vos, T. et al., 2016. Global, regional, and national incidence, prevalence, and years lived with disability for 310 diseases and injuries, 1990–2015: a systematic analysis for the Global Burden of Disease Study 2015. The Lancet 388, 1545–1602. https://doi.org/10.1016/S0140-6736(16)31678-6

Whatling, G.M., Biggs, P.R., Elson, D.W., Metcalfe, A., Wilson, C., Holt, C., 2020. High tibial osteotomy results in improved frontal plane knee moments, gait patterns and patient-reported outcomes. Knee Surg. Sports Traumatol. Arthrosc. 28, 2872–2882. https://doi.org/10.1007/s00167-019-05644-7

Winby, C.R., Lloyd, D.G., Besier, T.F., Kirk, T.B., 2009. Muscle and external load contribution to knee joint contact loads during normal gait. J. Biomech. 42, 2294–2300. https://doi.org/10.1016/j.jbiomech.2009.06.019

Zeni, J.A., Rudolph, K., Hihhinson, J.S., 2012. Alterations in quadriceps and hamstrings coordination in persons with medial compartment knee osteoarthritis. Bone 23, 1–7. https://doi.org/10.1038/jid.2014.371

Chapter 5

5 Summary and General Discussion

The purpose of this chapter is to summarize and provide an overall understanding of the main findings of this thesis. Strengths, limitations, future directions, clinical considerations, and potential impact of findings are also reviewed and discussed.

5.1 Summary

The objectives of this thesis were to: 1) develop an EMG-informed neuromusculoskeletal (NMSK) modelling framework to predict tibiofemoral medial and lateral compartment knee joint contact forces (KJCFs) during walking in patients with medial dominant knee OA and varus alignment, and 2) evaluate the effect of medial opening wedge high tibial osteotomy (MOWHTO) on KJCFs during walking.

These research objectives were realized through three distinct studies. The first study (Chapter 2) aimed to evaluate and compare results from patient-specific computational NMSK models using two simulated NMSK control modes in patients with medial dominant knee OA. As EMG-assisted NMSK modelling requires increased processing times, the objective was to determine the most appropriate control mode to use for our selected population. The second study (Chapter 3) aimed to compare results in patients with varus alignment and medial dominant knee OA based on two different patient-specific EMG assisted NMSK models where the first was scaled to an assumed varus angle of 0 and the second to a patient-specific varus angle in patients with varus alignment and medial dominant knee OA. Finally, the third study (Chapter 4) aimed to investigate: 1) the effect of MOWHTO on medial and lateral tibiofemoral compartment

KJCFs during walking using a patient-specific EMG-assisted modelling framework, 2) changes in the external knee adduction moment (EKAM) and muscle co-contraction indices (CCIs), and 3) the associations between changes in medial compartment KJCF, EKAM, and CCIs.

5.2 Overview

Knee OA is a complex disease that is not yet completely understood. Common risk factors have been identified in the literature and include abnormal frontal plane alignment and increased KJCFs (Andriacchi and Mündermann, 2006). As there is no way to directly measure KJCFs in the intact knee, musculoskeletal (MSK) models can be used to provide estimates of these loads. MSK models use optimization algorithms to generate muscle activations, yet research has indicated these activations are aberrant in patients with knee OA. Further, NMSK models utilize patient specific muscle activations that can provide better estimates of KJCFs (Sartori et al., 2014). Thus, NMSK modelling frameworks must first be evaluated and made as patient-specific as possible before interpreting the results after an intervention.

To evaluate our modelling framework, Chapter 2 (Study 1) evaluated patient-specific EMG-driven and EMG-assisted NMSK control modes in patients with medial dominant knee OA. These are two NMSK control modes that are commonly used in the literature, but it is unclear which control mode produces the most accurate KJCF predictions in patients with medial dominant knee OA. Both control modes were assessed by comparing external knee flexion/extension torques that were provided as inputs to each NMSK modelling framework to internal knee flexion/extension torques that were computed by each NMSK model. Differences in KJCFs predicted using both NMSK modes were

identified. The EMG-assisted NMSK control mode's internal knee flexion/extension torque results more closely matched Open-Sim's external knee flexion/extension torques when compared to the EMG-driven mode. As patients with knee OA walk with altered muscle activity (Heiden et al., 2009; Hubley-Kozey et al., 2009; Ramsey et al., 2007), NMSK modelling frameworks can better model these alterations in comparison to optimization approaches. Yet, it is possible that solely relying on the muscle activity can introduce errors associated with data collection and the muscle activation patterns themselves. Because the EMG-assisted mode also incorporates sagittal plane knee torques in the optimization algorithm, it may provide a more accurate representation of the patient's KJCFs.

After establishing the EMG-assisted NMSK control mode was more appropriate to use within our selected population, Chapter 3 (Study 2) examined a patient-specific parameter of frontal plane alignment that is related to disease progression (Andriacchi and Mündermann, 2006). Patients with medial dominant knee OA commonly present with varus frontal plane alignment (Andriacchi and Mündermann, 2006; Sharma, 2001). Therefore, this study examined the effect of assuming a neutral (0^o) versus patient-specific knee varus (PSV) angle when using EMG-assisted NMSK models to estimate knee joint contact forces. Findings identified statistically significant differences in scaled model poses where the neutral model was scaled with a decrease in hip abduction angle and increase in subtalar angle. There were no statistically significant differences in model prediction accuracy and KJCFs, yet the PSV model predicted increased KJCFs among the medial and lateral compartments and the overall knee force. Although there were only

slight differences in the modelled results, there was an obvious static compensation with other DOFs to match the frontal plane alignment.

Once an evaluation of important parameters that might affect our modelling framework was obtained, we were prepared to answer our final research question in Chapter 4 (Study 3). KJCFs were evaluated during walking before and after MOWHTO in patients with varus alignment and medial dominant knee OA using patient-specific NMSK modelling. Previous studies have identified changes to proxy measures of medial KJCFs after surgery (Birmingham et al., 2009, 2007; De Pieri et al., 2023; DeMeo et al., 2010; Leitch et al., 2015; Marriott et al., 2015), but little is known about the direct effect on these loads. Findings identified statistically significant decreases in medial compartment KJCFs, EKAM, and CCIs for the VL-LG muscle pair after MOWHTO. These results suggest that MOWHTO is largely meeting the biomechanical goals of the surgery. Importantly, low to moderate correlations between changes in the KJCF and changes in the EKAM and CCIs suggest these measures quantify substantially different biomechanical parameters, and that EMG-assisted modelling adds value when investigating the effects of MOWHTO.

5.3 EMG-Assisted NMSK Models in Rehabilitation (Strengths)

This collection of studies includes a novel method to compute KJCFs using an EMG-assisted NMSK model in medial and lateral compartments of the knee before and after MOWHTO. Current models can compute internal KJCFs using the patient-specific knee torques but neglect patient-specific muscle activity. We know, however, that patients with knee OA may walk with altered muscle activity and joint torques.

This research bridges a gap between health sciences and engineering disciplines by providing knowledge of lower extremity anatomy and knee OA disease pathology, as well as the technical computational modelling components required to accurately model these data. Ultimately, we plan for this research to bridge an even larger gap between research and clinical practice to provide data for clinicians to efficiently create and plan interventions intended to alter knee loading with the aim of delaying disease progression for patients.

5.4 Limitations

This research has limitations. Participants were recruited from patients referred to a tertiary care center for potential MOWHTO. As such, the sample consisted mostly of men. It is possible that results are different for women. Additionally, although the sample size was sufficient to detect changes, it was not large enough to statistically adjust for other factors that may affect changes after MOWHTO, such as OA severity.

5.5 Future Applications of EMG-Assisted Modelling in Patients with Medial Dominant Knee OA

5.5.1 Increasing Patient-Specificity of Models

Future applications of the developed EMG-assisted modelling framework can be described in three objectives. The first objective would be to continue from Chapter 3 and work on developing a patient-specific model that also includes patient specific geometry and a prescribed frontal plane alignment obtained via the patient's radiograph. As slight differences occurred in the scaled model pose when adjusting for patient-specific frontal plane alignment, a sensitivity analysis including a variety of patient-specific measures could aid in determining the parameters that require adjustment. In addition, increasing

the sample size would enable stratification of modelled results. Doing so can increase knowledge of differences that may occur in patients based on factors such as sex and OA severity.

5.5.2 Improving Model Framework Automation

The second objective would be to automate the framework as much as possible to create a seamless, easy-to-use framework. This goal would help identify where in the framework we are able to cut down on computation costs. By doing so, we would be able to process larger data sets and work towards utilizing NMSK modelling in a clinical setting.

5.5.3 Optimizing Patient Care

Finally, future research using this modelling framework may bridge the gap between biomechanics and clinical practice by providing surgeons with patient specific KJCFs that may help optimize patient care. In addition to promising data that indicates MOWHTO may delay conversion to TKR, research has also identified low complication rates and large clinically important improvements in gait biomechanics and patient-reported outcome measures that are sustained after surgery (Birmingham et al., 2017; Martin et al., 2014; Primeau et al., 2021). Therefore, future research may also benefit from investigating how changes in KJCFs are associated with clinically important endpoints for MOWHTO, including long-term changes in patient-reported outcome, performance-based measures of function, and the time to total knee replacement (TKR).

5.6 Conclusion

An EMG-assisted NMSK modelling framework was developed to predict tibiofemoral medial and lateral compartment KJCFs during walking in patients with medial dominant knee OA and varus alignment. Results supported an EMG-assisted versus EMG-driven NMSK control mode. Similar estimates for KJCF were obtained with and without using patient-specific alignment which warrant future research that explores patient-specific parameters in greater detail. Finally, using the developed model, moderate reductions in knee medial compartment KJCF were observed after MOWHTO to support the biomechanical rationale for surgery.

5.7 References

Andriacchi, T.P., Mündermann, A., 2006. The role of ambulatory mechanics in the initiation and progression of knee osteoarthritis. Curr. Opin. Rheumatol. 18, 514–518. https://doi.org/10.1097/01.bor.0000240365.16842.4e

Birmingham, T.B., Moyer, R., Leitch, K., Chesworth, B., Bryant, D., Willits, K., Litchfield, R., Fowler, P.J., Giffin, J.R., 2017. Changes in biomechanical risk factors for knee osteoarthritis and their association with 5-year clinically important improvement after limb realignment surgery. Osteoarthritis Cartilage 25, 1999–2006. https://doi.org/10.1016/j.joca.2017.08.017

Heiden, T.L., Lloyd, D.G., Ackland, T.R., 2009. Knee joint kinematics, kinetics and muscle co-contraction in knee osteoarthritis patient gait. Clin. Biomech. 24, 833–841. https://doi.org/10.1016/j.clinbiomech.2009.08.005

Holder, J., Van Drongelen, S., Uhlrich, S.D., Herrmann, E., Meurer, A., Stief, F., 2023. Peak knee joint moments accurately predict medial and lateral knee contact forces in patients with valgus malalignment. Sci. Rep. 13, 2870. https://doi.org/10.1038/s41598-023-30058-4

Hubley-Kozey, C.L., Hill, N.A., Rutherford, D.J., Dunbar, M.J., Stanish, W.D., 2009. Co-activation differences in lower limb muscles between asymptomatic controls and those with varying degrees of knee osteoarthritis during walking. Clin. Biomech. 24, 407–414. https://doi.org/10.1016/j.clinbiomech.2009.02.005

Kutzner, I., Trepczynski, A., Heller, M.O., Bergmann, G., 2013. Knee adduction moment and medial contact force-facts about their correlation during gait. PLoS ONE 8, 8–15. https://doi.org/10.1371/journal.pone.0081036

Martin, R., Birmingham, T.B., Willits, K., Litchfield, R., LeBel, M.-E., Giffin, J.R., 2014. Adverse event rates and classifications in medial opening wedge high tibial osteotomy. Am. J. Sports Med. 42, 1118–1126. https://doi.org/10.1177/0363546514525929

Miyazaki, T., Wada, M., Kawahara, H., Sato, M., Baba, H., Shimada, S., 2002. Dynamic load at baseline can predict radiographic disease progression in medial compartment knee osteoarthritis. Ann. Rheum. Dis. 61, 617–622. https://doi.org/10.1136/ard.61.7.617

Primeau, C.A., Birmingham, T.B., Leitch, K.M., Willits, K.R., Litchfield, R.B., Fowler, P.J., Marsh, J.D., Chesworth, B.M., Dixon, S.N., Bryant, D.M., Giffin, J.R., 2021. Total knee replacement after high tibial osteotomy: time-to-event analysis and predictors. Can. Med. Assoc. J. 193, E158–E166. https://doi.org/10.1503/cmaj.200934

Ramsey, D.K., Snyder-Mackler, L., Lewek, M., Newcomb, W., Rudolph, K.S., 2007. Effect of anatomic realignment on muscle function during gait in patients with medial compartment knee osteoarthritis. Arthritis Care Res. 57, 389–397. https://doi.org/10.1002/art.22608

Sartori, M., Farina, D., Lloyd, D.G., 2014. Hybrid neuromusculoskeletal modeling to best track joint moments using a balance between muscle excitations derived from electromyograms and optimization. J. Biomech. 47, 3613–3621. https://doi.org/10.1016/j.jbiomech.2014.10.009

Sharma, L., 2001. The role of knee alignment in disease progression and functional decline in knee osteoarthritis. JAMA 286, 188. https://doi.org/10.1001/jama.286.2.188

Walter, J.P., D'Lima, D.D., Colwell, C.W., Fregly, B.J., 2010. Decreased knee adduction moment does not guarantee decreased medial contact force during gait. J. Orthop. Res. 28, 1348–1354. https://doi.org/10.1002/jor.21142

Zhao, D., Banks, S.A., Mitchell, K.H., D'Lima, D.D., Colwell, C.W., Fregly, B.J., 2007. Correlation between the knee adduction torque and medial contact force for a variety of gait patterns. J. Orthop. Res. 25, 789–797. https://doi.org/10.1002/jor.20379

Curriculum Vitae

Name:	Dominique Cava
Post-secondary Education and Degrees:	Lakehead University Thunder Bay, Ontario, Canada 2013-2017 H.B.K. Lakehead University Thunder Bay, Ontario, Canada 2017-2019 M.Sc. The University of Western Ontario London, Ontario, Canada 2019-2023 Ph.D.
Honours and Awards:	Graduate Student Representative, Lakehead University 2017-2019 Dr. John Porter Sports Medicine Graduate Scholarship 2019 John & Rheta Andrews Grad Bursary 2019 Graduate Student Representative, The University of Western Ontario 2020-2022
Related Work Experience	Research Assistant Lakehead University 2015-2016 Teaching Assistant Lakehead University 2016-2019 Teaching Assistant The University of Western Ontario 2019-2023 Research Assistant The University of Western Ontario 2019-2023

Publication:

Cava, D., Sanzo, P., Kivi, D., Zerpa, C. (July 2021). The effect of ankle taping on the kinematics of the lower extremity while running on level, inclined, and declined slopes. *Topics of Exercise Science and Kinesiology, 2*(1), 8.